RECOVERY OF COPPER & GOLD FROM WASTE ELECTRICAL & ELECTRONIC EQUIPMENT

A Technical Paper submitted to the Department of Chemical Engineering
In Partial Fulfillment of the Requirements for the Degree
Bachelor of Science in Chemical Engineering

By
Rachel L. Ho

April 28, 2020

Technical Project Team Members
Matt Denecke
Caitlin Rudy
Jonathan Zheng

On my honor as a University student, I have neither given nor received unauthorized aid on this assignment as defined by the Honor Guidelines for Thesis-Related Assignments.

ADVISOR
Eric W. Anderson, Department of Chemical Engineering

TABLE OF CONTENTS

SUMMARY

This process is designed to recover copper and gold from waste electrical and electronic equipment (WEEE). Increasing demands for technology has made WEEE a major waste stream that is often not recycled properly and is discarded in landfills. This proposed process aims both to reduce waste and to recover nonrenewable, precious metals. Four major blocks make up this process: Block A involves the steam gasification of plastic in WEEE into syngas and the removal and pretreatment of leftover metals for downstream recovery; Block B involves copper recovery via agitated leaching, solvent extraction, stripping, and electrowinning; Block C involves gold recovery via agitated leaching, adsorption and elution of gold on activated carbon, and electrowinning; finally, Block D involves the conversion of syngas into power.

The process treats 181.5 kt/a WEEE and recovers 31.9 kt/a copper and 0.151 kt/a gold. The syngas generates 27,000 kW of thermal power used in Block A and 9,700 kW of electrical power. The process requires an additional 1,160 kW.

The startup costs total more than $17 million, but the plant has an non-discounted yearly cash flow of about $3.4 billion and could return a profit within as little as one year after construction. This process' revenue yields a high internal rate of return of over 9,500%.

This process poses environmental and safety considerations. For instance, the molten salt reactor in Block A operates at high temperatures and poses safety hazards to workers. Also, many of the chemicals used are corrosive or toxic, and so exposure to employees and the environment must be mitigated. However, this plant is an opportunistic investment and may serve an environmental benefit by reducing landfill waste.

I. INTRODUCTION

Electronic technology has brought about a myriad of benefits including instantaneous communication via phones and computers, automation via robots, industrialization, and more. Technology has pervaded society and is one source of the world's fastest-growing trash streams. Waste electrical & electronic equipment, also known as WEEE or e-waste, includes discarded computers, cell phones, and other electronic devices. In a global e-waste monitor report from 2017, researchers from the United Nations University estimated that 49.3 million tons of WEEE were generated globally in 2016, which is projected to increase to 57.5 million tons by 2021 (Baldé et al., 2017). Apparently, only 20% of WEEE is collected and properly recycled, and the other 80% is improperly discarded, i.e., thrown away with residual waste, dumped, traded, or recycled under substandard conditions.

WEEE's growth stems from several factors. *Time* reporter Semuels explains that inadequate regulation is problematic. The U.S. is a leading producer of WEEE, yet only 19 states ban the disposal of electronics with regular trash (Semuels, 2019, para. 1). Another issue is the rapid development of new electronics with a high turnover, for example, those developed for the new 5G network.

Several components of WEEE, including cadmium, chromium, brominated flame retardants, and polychlorinated biphenyl, are toxic and pose major health and environmental concerns through the "inhalation of toxic fumes" and possible exposure through "accumulation of chemicals in soil, water and food" (*World Health Organization,* n.d., para. 1). These threaten the quality of life worldwide, but are especially hazardous to third-world countries in Asia and Africa where the U.S. exports the majority of its WEEE (Larmer, 2018, para. 5). In third-world countries, small-scale mining efforts to recover precious metals from WEEE by bathing circuit boards in acid and cooking them on stoves offer communities a quick way to make money but poison waterways and increase chemical emissions (Larmer, 2018, para. 9). Thus, environmental and health concerns are exacerbated by unregulated mining efforts and afflict struggling communities.

Interest in recycling WEEE is growing. For example, for the 2021 Summer Olympic Games in Tokyo (originally slated for 2020 but delayed due to the coronavirus pandemic), five-thousand olympic medals were made from 78,985 tons of discarded electronic devices donated by citizens and companies. The Organising Committee (TOCOG) recovered 30.3 kg of gold, 4,100 kg of silver and 2,700 kg of bronze from the devices (Olympic Games, 2019). Still, WEEE continues to be a global problem that requires technological innovation.

We propose a novel process to more safely treat WEEE, recover precious metals, and produce power from syngas. WEEE contains precious metals which constitute less than 1 wt% of the waste, but up to 80% of WEEE's monetary value, assuming that each component of WEEE could be recovered and sold (Park & Fray, 2009). The plastics in WEEE can be gasified into syngas, which can generate power or be a chemical intermediate. This process treats an underutilized resource, traditionally a source of waste, while minimizing health risks, which may improve the wellbeing of people worldwide.

II. PREVIOUS WORK

II.A. Current State of WEEE Treatment

Lu and Xu (2016) summarized the current state of precious metal recovery from waste printed circuit boards (PCBs) and made future recommendations for metal recycling. For example, to recover metals from WEEE, they suggested that hydro-metallurgical treatment processes may be preferable over pyro-metallurgy because of lower waste gas emissions, lower energy consumption, higher recovery rate, less slag production, and easier working conditions. They did not mention the use of molten salt to gasify WEEE; however, they summarized other methods of WEEE pretreatment (gasifying, crushing, etc.), leaching, and refining, which includes ion exchange, adsorption, electrowinning, and extraction. Y. Zhang et al. (2012) detailed the current state of leaching precious metals out of WEEE, including cyanide, thiourea, thiosulfate, and halide leaching.

II.B. Gasification of WEEE and Molten Salt Reactors

A 2015 University of Virginia capstone report, *Recycling of Printed Circuit Boards from Electronic Waste: A Hydrometallurgical Process*, outlines WEEE gasification and metallurgical recovery via common industrial techniques to treat PCBs (Diplas et al., 2015). Diplas et al.'s design treats 3.03 million units of personal computer and mobile phone electronics per year, i.e., 8,000 units per day, and recovers 63.7 kg/day of copper, 0.26 kg/day of gold, 0.72 kg/day of silver, and 1.76 kg/day of palladium (2015, p. 51). Brems et al. (2013) reported that the traditional gasification of plastic waste is a first order reaction. S. Zhang et al. (2013) modeled the gasification kinetics of PCBs in an eutectic mixture of molten lithium carbonate, sodium carbonate, and potassium carbonate salts (LNK) and steam. They found that the steam gasification of WEEE in molten salt can produce clean hydrogen gas. Salbidegoitia et al. (2015) also studied steam gasification of WEEE in LNK and discovered that adding nickel powder to the molten salt catalyzed the reaction and that the metals were recoverable afterwards. Riedewald and Sousa-Gallagher (2015) used a novel U-shaped molten salt reactor (MSR) to facilitate the recovery of metals after the gasification of WEEE in molten LiCl–KCl. Riedewald et al. (2016) used the same U-shaped MSR to gasify tyres, another large waste stream, in molten zinc.

II.C. Copper and Gold Recovery

An overview of hydrometallurgical processes, including leaching and precipitation, for numerous metals is given in *Extractive Metallurgy 2: Metallurgical Reaction Processes: Metallurgical Reaction Processes* by Vignes (2013). Copper recovery is a well established process. *Extractive Metallurgy of Copper* by Schlesinger et al. (2011) summarizes in depth the complete copper production process, including copper leaching, extraction, and electrowinning. Jergensen II (1999) also summarizes the copper recovery process and the optimization of mixer-settlers.

Torres and Lapidus (2016) studied the leaching of copper from crushed PCBs in HCl, HNO_3, H_2SO_4, EDTA and citrate, with and without air sparging, to improve gold recovery. To recover gold, they recommended pretreating crushed PCBs in HCl with air sparging, and then leaching gold from the leftover solid residue with thiourea. Jadhav and Hocheng (2015) found

that all metals in PCBs will completely leach after pretreatment with sodium hydroxide and agitation for 24 hours in 1 M HCl. Mishra and Devi (2011) modeled the extraction of cupric ions out of HCl solution into Cyanex 921 and also found that 99.7% of the copper can be stripped from the organic extractant into sulfuric acid.

Hiskey (1984) explored the viability of thiourea as a reagent to leach silver and gold. Ubaldini et al. (1998) reported thiourea's leaching kinetics and recovered 80% of gold from crushed ore by leaching with thiourea and ferric sulfate in acidic conditions, adsorbing and eluting the gold on activated carbon, and electrowinning. Both Torres and Lapidus (2016) and Zatko and Kratochvil (1968) reported that copper consumes thiourea. Rogans (2012) and McDougall and Hancock (1981) discussed the industrial norms for gold adsorption onto activated carbon, including the use of carbon-in-pulp (CIP) or carbon-in-leach (CIL) processes. H. Zhang et al. (2004) studied the adsorption isotherms of gold-thiourea complexes onto activated carbon.

III. DISCUSSION

III.A. Overall Design Basis

Our process has four major sections: WEEE treatment, copper recovery, gold recovery, and syngas processing. In Block A, pretreated WEEE is gasified in a molten salt reactor (MSR). The organic, plastic components generate syngas, and the solid metals are recovered, cooled, washed, dried, and crushed before being sent to Block B. In Block B, copper is recovered from crushed WEEE via agitated leaching, solvent extraction, stripping, and electrowinning. The solid, leach residue out of Block B is sent to Block C where gold is recovered via agitated leaching, adsorption and elution on activated carbon, and electrowinning. Block D involves burning the syngas to generate power.

A total of 181.5 kt/a (18,800 kg/h) WEEE is fed to the process, and 31.9 kt/a Cu and 0.151 kt/a Au are recovered. These flowrates were chosen to meet a target Cu output. In order to design a plant with a realistic and reasonable scale, we designed Block B, Cu recovery, first based on real, copper recovery plants described by Schlesinger et al. (2011). The required WEEE input and resultant gold output result from designing around copper recovery.

The process requires upwards of 1,160 kW of input energy. The major waste streams include the used Rinse Bath water from X-101, the metal-pregnant purge streams in Block B and Block C, and the solid leach residue out of the Au leaching agitation tank, R-301. The overall process flow diagram (PFD) is given in Figure III.A.1-1.

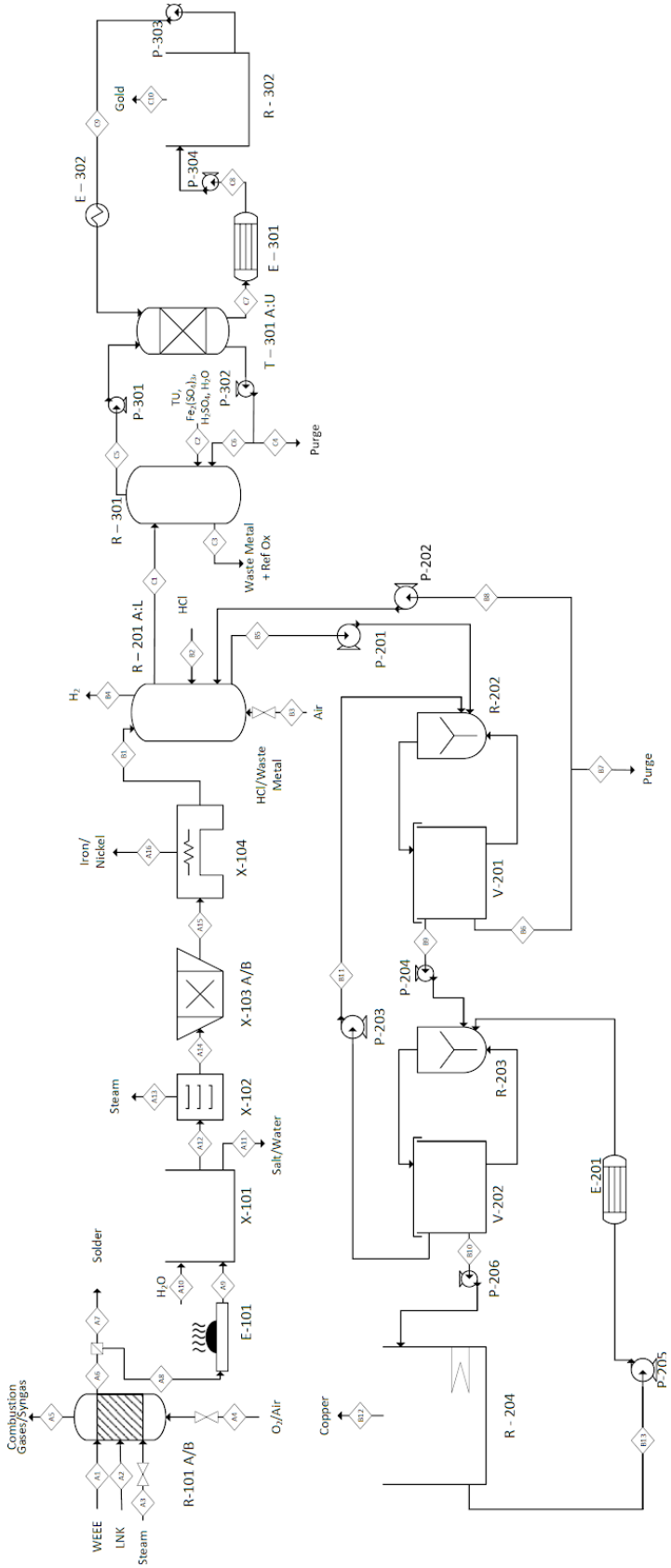

Figure III.A.1-1. PFD of entire process.

III.B. Block A: Molten Salt Reactor, R-101, and Preliminary Metal Processing

III.B.1. Reactor Block Overview

Block A separates the plastic and metal components of WEEE and prepares the metals for downstream processing. The organic components are gasified in a molten salt reactor (MSR) and converted into syngas. The recovered metals and residual solids are cooled, washed, dried, crushed, and magnetically separated before being sent to Block B for Cu recovery. The overall block flow diagram (BFD) for Block A is given in Figure III.B.1-1.

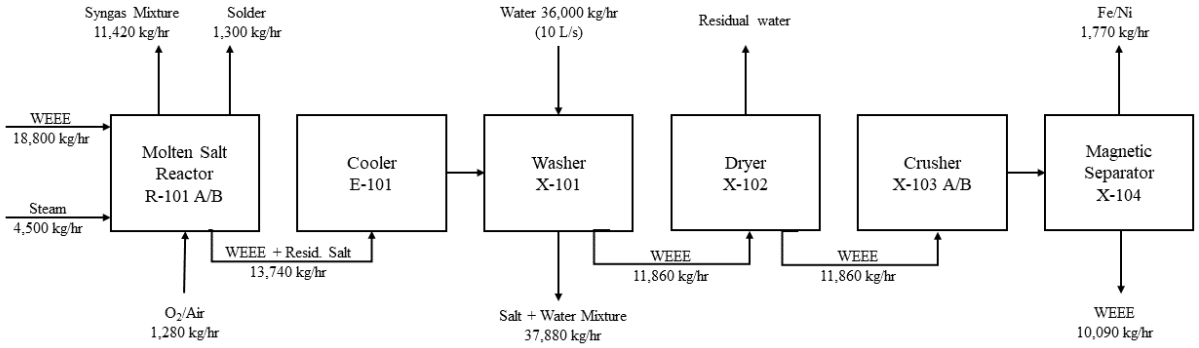

Figure III.B.1-1. Block A BFD.

The composition of WEEE used for the design basis was chosen based on estimates cited in academic literature, and is shown in Table III.B.1-1 (Salbidegoitia et al., 2015). In practice, feed composition will vary over time. However, accounting for this variation requires enormous amounts of real-world data and advanced process design and is outside the scope of this project.

Table III.B.1-1. Input WEEE Composition

Component	Weight Percentage of WEEE (%)
Copper (Cu)	20
Iron (Fe)	8
Tin (Sn)	4
Nickel (Ni)	2
Lead (Pb)	2
Zinc (Zn)	1
Silver (Ag)	0.2
Gold (Au)	0.1
Palladium (Pd)	0.005
Misc. metals	2.69
High impact polystyrene (HIPS)	12.6
Acrylonitrile–butadiene–styrene copolymer (ABS)	11.4
Polypropylene (PP)	3
Other plastics (polycarbonate, PVC, polyamide)	3
Refractory oxides (ceramics, glass, and brominated fire retardants etc.)	30

III.B.2. Pretreatment of WEEE

Moisture should be avoided in the MSR, R-101, because water vaporizes and expands explosively at molten salt's high temperatures. OSHA reported a case in which a worker was killed and two others injured after a towing bar, filled with residual water, was dipped into molten salt, exploded, and ruptured the tip tank (OSHA, 2010). Therefore, dehydrating the input WEEE is a critical safety concern.

Batteries also must be removed to avoid the risk of explosion. Capacitors may be removed to recover small amounts of tantalum, which is priced around $140,000 per short ton as of 2018 ("Tantalum Price 2020 [Updated Daily]," n.d.). We did not design these pretreatment steps, but they should be done to maximize process safety.

III.B.3. Molten Salt Reactor, R-101

Molten salt background.

Molten salt is used in nuclear and solar energy plants for its excellent heat transfer and energy storage properties (Reddy, 2011). Molten salt reactors (MSRs) use an eutectic mixture of salts which melt at a lower temperature than the pure components. Molten salt has a low vapor pressure, high boiling point, large specific heat and thermal conductivity, and high density at low pressures (Piyush Sabharwall et al., 2010). Salt mixtures are chosen to minimize the melting point while maintaining thermal stability at the operating conditions. Molten salt is an extremely efficient heat-transfer fluid for high energy processes (Piyush Sabharwall et al., 2010).

The MSR, R-101, uses an equal weight ratio of lithium carbonate, sodium carbonate, and potassium carbonate, i.e., LNK-carbonate or simply LNK. We chose LNK because we have data on the gasification of PCBs in LNK provided by S. Zhang et al. (2013). LNK is, at worst, only slightly corrosive with common steel alloys and does not react with the target metals; LNK acts as a catalyst for the steam gasification of organics, and may retain carbon dioxide, acid gases, and halogen compounds as safe, stable salts (Flandinet et al., 2012; S. Zhang et al., 2013). Due to a lack of data, we did not model the retention of gases as stable salts in our design.

The benefits of oxidizing WEEE via molten salt versus incineration include no formation of dioxin or furan, flameless oxidation, reduced volumes with no effluents, self-heating, exothermic oxidation, and the ability to form syngas (Flandinet et al., 2012). Drawbacks are that the salt requires high temperatures at low pressures to stay liquid and can freeze and plug parts of the reactor if cooled, such as during cleaning or heating failure.

The properties of LNK salt are given in Table III.B.3-1 (Kanai et al., 2013; Liu et al., 2019).

Table III.B.3-1 Properties of Equal Weight Ratio LNK Salt at 693 K

Property	Value
Density (kg / m^3)	2081
Viscosity (Pa s)	3.27×10^{-2}
Surface tension (N/m)	0.226
Melting point (K)	673.15
Thermal stable temperature (K)	933.15-983.15
Thermal conductivity (W / m K)	~0.5
Heat Capacity (J / g K)	1.6

The ternary phase diagram of LNK melting-point versus salt composition is given in Figure III.B.2-1. The diagram shows that the eutectic point of LNK is at 397 ± 1 °C (670.15 ± 1 K) at 43.5 : 31.5 : 25.0 mol% Li_2CO_3 : Na_2CO_3 : K_2CO_3 respectively.

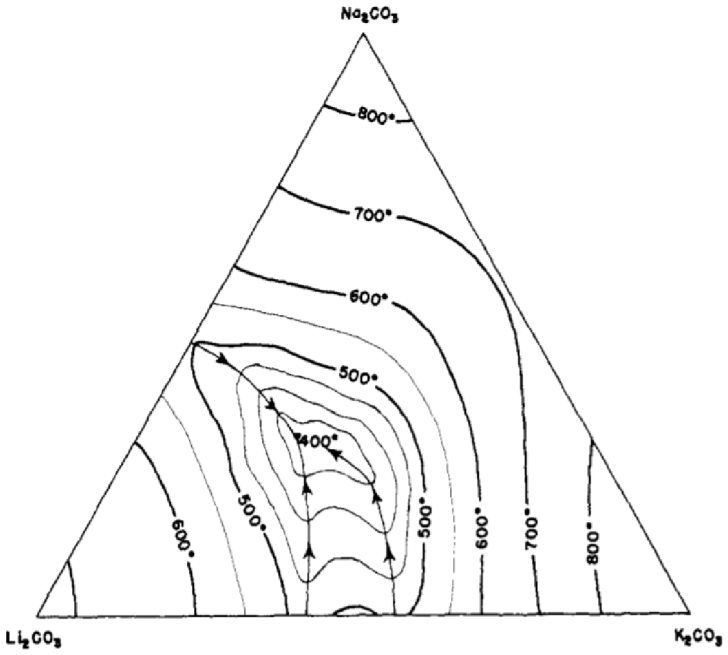

Figure III.B.2-1. "Temperature isotherms for liquid-solid equilibria in ternary Li_2CO_3-Na_2CO_3-K_2CO_3 system" (Janz & Lorenz, 1961, p. 323). Reprinted from *Solid-Liquid Phase Equilibria for Mixtures of Lithium, Sodium, and Potassium Carbonates*, by G.J. Janz and M.R. Lorenz, 1961, Journal of Chemical & Engineering Data. Copyright 1961, American Chemical Society. Reprinted with permission.

MSR design, R-101.

Pretreated WEEE is fed to the MSR, R-101, via a lock hopper to maintain pressure in the reactor. Plastics from the WEEE are gasified and combusted in the molten LNK salt. Combustion is controlled by feeding a limited amount of oxygen. Metals and refractory oxides settle as separate phases at the bottom of the reactor. Sludge pans are commonly used to remove material from molten salt baths. For this process, solids are collected in a sieve tray which sits right above

the sludge pan, and the liquid solder passes through the sieve tray, sinks to the bottom, and is collected in the sludge pan. Solids removal is a challenge because the MSR is pressurized. Two possible designs are, first, to periodically depressurize the MSR and remove the solids via the sieve tray, and second, to use two chambers so that the solids continuously drain into a high-pressure chamber while the low-pressure chamber is cleaned, and then to swap the pressure and cleaning between the chambers. This design is beyond the scope of our project. We modeled the MSR, R-101, as one unit with 100% removal of solids.

The MSR, R-101, operates at 675 ℃ and 2 bar to melt the LNK and allow for rapid gasification of plastic. The MSR's energy consumption includes the energy required to heat the input LNK and WEEE, fed at room temperature, the energy change of reactions, including the breaking of polymer bonds and formation of syngas, and the energy recovered by partially combusting the WEEE. We considered the reactor to be isothermal.

Combustion of WEEE is exothermic and would be more energy-efficient than generating and burning syngas for the reactor, but the high temperatures and volumes of waste involved are safety concerns. Furthermore, full combustion is kinetically slow and would hinder the process. Therefore, the input flowrate of oxygen gas is controlled for partial combustion of WEEE.

Quan et al. (2013) found that the combustion of PCBs can be represented in two, distinct, first-order reaction stages: pyrolytic decomposition with char formation and char combustion. Char combustion appears to be the rate-limiting step, which we assumed to determine an appropriate amount of combustion for the MSR, R-101. Equation III.B.3.1 combines the kinetic parameters from Quan et al.'s work with the Arrhenius rate equation.

$$k = A\, exp\left(\frac{-E}{RT}\right) \qquad (III.B.3.1)$$

where k is the reaction rate constant in min^{-1}, A is the pre-exponential factor in min^{-1}, E is the activation energy in J/mol, R is the gas constant in J/(mol K), and T is the temperature in K. Multiple iterations were done in Aspen to achieve an 80% conversion; combusting 80% of the PCB char takes 27.4 min, which was rounded to a 30 min residence time. Steam was fed to consume the remaining char because steam gasification is kinetically faster than combustion and reduces the amount of underutilized char.

Aspen Plus modeled the MSR, R-101, as a RGibbs reactor block. The Wilson model was used because of the presence of polar compounds and because the MSR operates near supercritical conditions. The heat duty from the optimized simulation was 18,650 kW and includes the fusion of LNK and the combination of pyrolysis, combustion, and steam gasification of the WEEE. The total heat duty of the MSR is given by Equation III.B.3.2.

$$Q_{tot} = Q_1 + \sum_{i=1}^{n} \dot{m}_i\, C_{P,i,avg} \Delta T + \sum_{i=1}^{k} \dot{m}_i \Delta H_{fus,i} \qquad (III.B.3.2)$$

where Q is the heat duty in Watts calculated with Aspen Plus, C_p is the heat capacity of each component in J/(mol K), ΔT is the temperature difference from heating the waste up from ambient conditions in K, ΔH_{fus} is the enthalpy of fusion for each melted component, $\dot{m}_i$ is the mass flow rate of each component, n is the number of components heated, and k is the number of

components that melt in the reactor. The total heat duty of the reactor was estimated to be about 27,460 kW. To meet this energy requirement, we could burn the syngas at an 80% efficiency and recover about 59,580 kW. This is more than enough energy to power the reactor, and so we will convert the excess energy into electrical power at a 30% efficiency to power other utilities.

The MSR, R-101, is 4 ft x 20 ft x 6 ft (i.e., 480 ft^3 or 13.6 m^3). This is based on the largest, industrial MSR we found, which is a nitrate MSR tank made by McDonnel Douglas and has ceramic insulation and an inner liner of ¾ inch carbon steel (Carling & Mar, 1981, p.24). The MOC is Hastelloy C276, a solid solution made primarily of nickel, chromium, and molybdenum, strengthened with iron, cobalt, tungsten, and vanadium, because of its superior corrosion resistance to molten LNK-carbonate salts compared to other common materials such as stainless steel and nickel-based alloys (Liu et al., 2019). Another candidate was SAE 310S stainless steel but was rejected because of a lack of corrosion data in the presence of molten salts.

III.B.4. WEEE Heap, E-101

Conventional heat transfer equipment would ineffectively cool the metals leaving the MSR, R-101, because of the metals' extreme temperature and solid phase. This solid output has residual LNK which solidifies upon cooling. Original considerations included a conveyor belt with large fans which would direct air across the conveyor; however, preliminary calculations showed that the additional energy and equipment costs largely did not save more time than letting the metal cool from convection in open air. The MSR's, R-101, metal outlet temperature of 675 ℃ gives a large temperature driving force and promotes a larger heat transfer coefficient for free convection, i.e., 50 W/(m^2 K), which is an average value based on free convection with a large temperature difference from Welty et al. (2008).

The WEEE Heap, E-101, requires no special equipment, which is appealing. Hot solid output can cool on designated pads, or merely on the ground outdoors, reducing both capital and operating costs. The WEEE Heap allows for metal accumulation, which can buffer the downstream process in the event of MSR, R-101, downtime. The heat transfer rate was estimated by modeling the solids as a rectangular slab with a depth of 0.1 m. At this depth, the Biot number, i.e., the ratio of exterior thermal resistance to interior thermal resistance, is roughly 0.05 (Equation III.B.4.1). Therefore, heat transfer is convection limited, and thermal gradients within the cooling waste are minimal.

$$Bi = (h / \lambda) L \qquad \textit{(III.B.4.1)}$$

A mass-weighted, average heat capacity of 912.6 J/(kg K) was calculated with the mass composition of the output solid stream and the individual heat capacities of the individual components. Component heat capacities were obtained from the NIST website at 350℃, the median of the temperature range experienced by the solids. Assuming ambient air is about 20℃, it takes two to three hours for the solids to cool to 25℃, which was deemed an acceptable final temperature (Equations III.B.4.2 and III.B.4.3). We assumed that any heat introduced in the solid crushing and magnetic metal separation steps is negligible and dissipated convectively during transport between unit operations.

$$\dot{Q} = Cp\ \dot{m}(T_i - T_f) = A\ h(T_i - T_\infty) \qquad (III.B.4.2)$$

$$t = \frac{d\ \rho\ Cp(T_i - T_f)}{h(T_i - T_\infty)}\ ;\ d = depth\ of\ solids\ [m] \qquad (III.B.4.3)$$

III.B.5. Rinse Bath, X-101, and Dryer, X-102

Some amount of LNK leaves with the solid output out of the MSR, R-101 and is called "dragout." This dragout needs to be removed to avoid complications between the carbonate salts and downstream processes and to avoid equipment corrosion. The LNK salt is washed away in a Rinse Bath, X-101.

The solubilities of lithium carbonate, sodium carbonate, and potassium carbonate in water at 25℃ are 0.0129 kg/L, 0.3407 kg/L, and 1.12 kg/L respectively (*PubChem*, 2020). An estimate of 5 wt% of the output solid stream from the MSR, R-101, i.e., 1,880 kg/h LNK, will be dragout LNK salt. At this flowrate, 10 L/s of wash water will fully dissolve the salt at equilibrium. Kinetic data was found for lithium carbonate only, which requires 30 minutes to fully dissolve (Wall et al., 1985).

The Rinse Bath, X-101, is a water storage tank with an open top for easy removal of the solids and is made from high density polyethylene due to the saltwater's corrosiveness. The effective tank volume is 20,000 L based on a residence time of 30 minutes and a total volumetric flow rate of 10.6 L/s. A bucket conveyor carries the solids through and out of the washer and deposits the solids onto a belt conveyor which passes through an industrial conveyor oven, X-102, to briefly dry the solids. The oven is an off-the-shelf 12-ft (3.6 m) long unit operating at 250℃, which temperature is only an estimate and needs onsite experimentation to determine the operating conditions that best remove moisture.

III.B.6. Solid Crushing, X-103A/B

After washing away residual LNK, the solids need to be crushed and the particles' size homogenized both for magnetic separation and for agitated leaching. Particles of 5 mm diameter are recommended for high levels of magnetic separation (Yoo et al., 2009). Additionally, particles larger than 1.5 mm are difficult to keep suspended in agitated leaching (Marsden & House, 2006). Two crushers are used in series to achieve the target particle size. Firstly, a low-speed, high-torque shear shredder, X-103A, ideal for the initial crushing, reduces the median particle size to about 10 mm. Secondly, a swing hammer type crusher, X-103B, reduces the particle size to 5 mm and is the industry standard for creating particles of this size (Magdi Abadir, n.d.)

III.B.7. Magnetic Separation, X-104

Iron and nickel are removed first from the crushed WEEE via magnetic separation. Typical methods are either drum magnet type separators or electro cross-belt separators. An electro cross-belt separator was chosen because they are typically used for high throughput in industry. About 94% of the iron and nickel is removed by two cross-belt separators run in series, the first of which is operated at 700 Gauss and the second at 3,000 Gauss (*Bunting Electro Crossbelt Magnets*, n.d.). The typical capacity of industrial cross-belt separators is between 10 to 15 tons per hour, necessitating two parallel trains, or four total separators.

III.B.8. Alternative Designs & Considerations

Steam generation.

We considered generating steam by feeding the molten salt exiting the MSR, R-101, directly to a heat exchanger with liquid water, but discarded this idea because the salt would freeze and cause plugs.

Cooling solid MSR output.

We considered cooling the solid output from the MSR, R-101, on conveyor belts with fans, or dumping it out and letting it cool naturally (2-3 hours). We decided on dumping the solids onto a flat surface and allowing them to cool with ambient air.

LNK recovery.

We considered evaporating the wash water from the Rinse Bath, X-101, to recycle the LNK salt. However, evaporating the wash water was too energy intensive and unfeasible. We recommend salt recovery as an area of future improvement to reduce raw material costs and environmental footprint.

III.C. Block B: Copper Recovery

III.C.1. Copper Recovery Overview

Block B focuses on Cu recovery via leaching, solvent extraction, stripping, and electrowinning. Cu comprises about 20 wt% of WEEE and represents about 9.7% of a PCB's intrinsic value (Park & Fray, 2009). Cu must be removed before Au leaching because it complexes with the thiourea (TU) (Torres & Lapidus, 2016). Crushed WEEE is leached in a 5 M HCl solution sparged with air in a leaching agitation tank. The *pregnant leach solution* (PLS) is sent to a mixer-settler which selectively extracts cupric ions from the aqueous solution into an organic solvent, 0.28 M Cyanex 921 in kerosene. The aqueous *raffinate* is sent back to the leaching agitation tank and the *loaded organic* is sent to another mixer-settler where Cu is stripped from the organic phase into an aqueous, 180 g/L H_2SO_4 electrolyte solution. The *stripped organic* is recycled back to the extraction mixer-settler. The *advance electrolyte* is sent to electrowinning cells (EW), where an electric current causes the Cu to deposit on stainless steel cathodes. The copper-gilded cathodes are harvested and sold directly. The *spent electrolyte* returns to the stripping mixer-settler to be reloaded. The overall BFD for Block B is shown in Figure III.C.1-1. The mass flowrates represent the components of WEEE and do not include any solvents' mass flowrate. The volumetric flowrates represent the solvents.

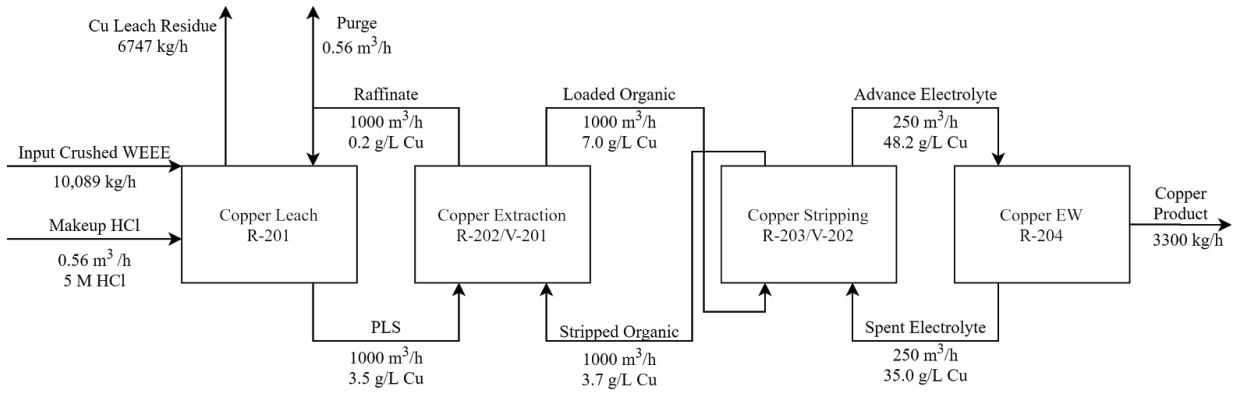

Figure III.C.1-1 Block B BFD.

III.C.2. Copper Leaching

Copper leaching background.

In hydrometallurgical Cu extraction, Cu ore is often heap leached with a sulfuric acid (H_2SO_4) lixiviant. Heap leaching is when the lixiviant is trickled by gravity through the crushed ore's pores at atmospheric conditions and without oxidation (Schlesinger et al., 2011). Heap leaching is used for particles 12 - 50 mm in diameter, is diffusion controlled, and is slow; leach cycles require 90 to 120 days (Schlesinger et al., 2011). Agitation leaching is used on smaller particles (<1 mm) that leach easily, such as oxides, and is done in stirred tanks as opposed to outdoor heaps. Particles larger than 1.5 mm are difficult to keep suspended (Marsden & House, 2006). Agitation leaching is capital-intensive but kinetically fast (on the order of hours versus months) and can achieve nearly 100% Cu recovery (Schlesinger et al., 2011). The heat of solution for leaching is considered negligible (Wankat, 2016).

Lixiviant selection: hydrochloric acid vs. sulfuric acid.

We chose agitation leaching in HCl lixiviant because WEEE contains pure metals, not ores, which can be crushed and oxidized. Agitation leaching in HCl occurs faster than either agitation or heap leaching in H_2SO_4. Also, the Cu^{2+}/Cu^{+} redox couple is stable in hydrochloric acid media and can oxidize solid copper, and so has additional oxidizing potential that it lacks in H_2SO_4 solution. Additionally, cupric is regenerated by dissolved oxygen (Torres & Lapidus, 2016).

Torres and Lapidus (2016) observed that about 88% of the crushed Cu from WEEE leached within 6 hours when sparged with air in 0.5 M HCl. After 24 hours of adequate agitation, nearly 100% of the Cu and other metals leached (Jadhav & Hocheng, 2015). We modeled our process on Torres and Lapidus' study, which examined Au leaching in thiourea after pretreatment in HCl. Our process uses 5 M HCl instead of the 0.5 M HCl used by Torres and Lapidus in order to match available data for cupric ion extraction from 5 M HCl into Cyanex 921 (Mishra & Devi, 2011). Increasing the HCl concentration is expected to shorten leaching time; therefore, using data for 0.5 M HCl is a conservative estimate (Torres & Lapidus, 2016). Moreover, in a real process, Cu concentration is difficult to control, especially because the feed WEEE composition would not be constant (Jergensen II, 1999).

HCl and H_2SO_4 have relatively similar safety concerns. Both are corrosive, strong acids that need to be neutralized before disposal. Both require appropriate PPE (e.g. resistant boots, gloves, neutralization kits on-site, goggles) and equipment that can resist corrosion (e.g. rubber lining). HCl vapor is corrosive and toxic, and so the gas coming out of R-201 needs to be scrubbed. Besides the HCl vapor, HCl is not a more dangerous lixiviant choice than H_2SO_4.

Copper leaching data and kinetics.

The leaching of Cu in the presence of air sparging and acid occurs according to Equation III.C.2.1.

$$2Cu + O_2 + 4H^+ \rightarrow 2H_2O + 2Cu^{2+} \qquad (III.C.2.1)$$

where Cu is copper, O_2 is oxygen gas, H^+ is hydrogen cation, H_2O is liquid water, and Cu^{2+} is a cupric ion (Torres & Lapidus, 2016). The Cu can also react with chlorine anions, shown in Equation III.C.2.2.

$$4Cu + 8Cl^- + O_2 + 4H^+ \rightarrow 2H_2O + 4\ CuCl_2^- \qquad (III.C.2.2)$$

where Cl^- is a chloride ion and $CuCl_2^-$ is cupric chloride.

The kinetic data for Cu leaching was taken from Torres and Lapidus (2016) and is given in Figure III.C.2-1.

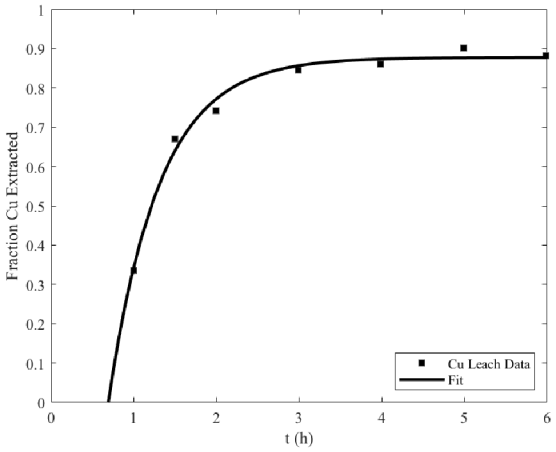

Figure III.C.2-1. Fraction of Cu Extracted (Leached) vs. Time with "air sparging (1 L/min) on copper leaching from EW-PCB for [0.5 M] hydrochloric acid leaching solution. . . at 25°C and 125 rpm stirring rate, with a constant solid-liquid ratio of 20 g EW-PCB per liter of leaching solution and particle size ⩾500 μm" (Torres & Lapidus, 2016, p. 4). Experimental data (squares); empirical fit (line).

Parameters for the Cu leaching data were empirically fit by minimizing the sum of squared errors (SSE) on the general expression $f(t) = a \exp(b\ t) + c$ (Equation III.C.2.3).

$$E_{Cu,B} = -2.7\ e^{(-1.62\ t)} + 0.88 \qquad (III.C.2.3)$$

where $E_{Cu,B}$ is the fraction of Cu leached in the leaching agitation tank, R-201, and t is the leach time in hours. For Ni, we used kinetic data for nickel oxide dissolution in HCl as an approximation, given by Equation III.C.2.4.

$$1 - (1 - E_{Ni,B})^{2/3} = 0.0011\ t - 0.023 \qquad (III.C.2.4)$$

where $E_{Ni,B}$ is the percentage of Ni leached in R-201, and t is the leach time in hours (Hosseini et al., 2012). This fit is based on shrinking-core model theory in which the leach is controlled at the particle's boundary layer. Therefore, "the reaction rate is controlled by shrinking sphere nickel oxide particles" (Hosseini et al., 2012, p. 732).

We lack both equilibrium and kinetic data for how the other metals leach in HCl with air sparging other than that nearly 100% of the metals will leach after 24 hours (Jadhav & Hocheng, 2015). For the other metals, we assumed a significant, arbitrarily-chosen fraction would leach. In practice, the concentrations of these metals would vary over time with the feedstock and would be hard to control, and so recognizing that each metal must be considered in waste stream treatment is more important than pinpointing the exact purge concentration. Moreover, the extraction of Cu^{2+} is selective over other cations, and so other metals' ion concentrations should not affect downstream copper recovery. The fraction of each metal leached is given in Table III.C.2-1, where Cu and Ni are calculated using Equations III.C.2.3 and III.C.2.4, and the rest are arbitrary (marked with †).

Table III.C.2-1. Fraction of Metal Leached in 5 M HCl Lixiviant after t = 6 h

Metal, *i*	Cu	Fe†	Sn†	Ni	Pb†	Zn†	Ag†	Au†	Pd†
Fraction Leached, $E_{i,B}$	0.88	0.30	1.0	0.015	1.0	1.0	0.015	0.015	0.015

Ag, Au, and Pd's leach fractions are small due to their resistance to oxidation (Jadhav & Hocheng, 2015). Also, Torres and Lapidus (2016) recovered most of the Au after HCl pretreatment, suggesting a small amount of Au leaches. However, Au does leach in HCl solution with air sparging (Vignes, 2013). As a conservative estimate, we assumed Ag, Au, and Pd would leach as much as Ni. Although we assumed the other metals' ion concentrations are negligible, kinetic leaching data for each metal in 5 M HCl with air sparging should be collected to optimize this design.

Copper PLS, raffinate, purge, and recycle stream design.

The volumetric flow rates of the PLS and raffinate, 1000 m^3/h, were chosen based on industrial standards for hydrometallurgical Cu extraction. We targeted 3.5 g/L Cu in the PLS based on industrial practice (Schlesinger et al., 2011). In reality, the PLS Cu concentration is difficult to control (Jergensen II, 1999). The purge stream prevents metal ion accumulation and was based on Ni accumulation because it is the only metal with leaching data besides Cu. The purge stream was designed using a mass balance around the leaching agitation tank, R-201, for Cu and around Block B for Ni. The mass balance for Cu is given by Equation III.C.2.5.

$$x_{Cu}m_{WEEE} + V_{R,B}C_{Cu,R,B} = x_{Cu}m_{WEEE}(1 - E_{Cu,B}) + V_{PLS,B}C_{Cu,PLS,B} \qquad (III.C.2.5)$$

where x_{Cu} is the weight fraction of Cu in WEEE, m_{WEEE} is the mass flowrate of input WEEE into the MSR, R-101, in g/h, $V_{R,B}$ is the volumetric flowrate of the recycle stream in Block B in L/h, $C_{Cu,R,B}$ is the concentration of Cu in the recycle stream in Block B in g/L, $E_{Cu,B}$ is the fraction of Cu leached in 6 hours in R-201, $V_{PLS,B}$ is the volumetric flowrate of the PLS stream in Block B in L/h, and $C_{Cu,PLS,B}$ is the concentration of Cu in the PLS stream in Block B in g/L.

The mass balance around Block B for Ni is given by Equation III.C.2.6.

$$x_{Ni}m_{WEEE}(1 - f_{Ni,mag}) = x_{Ni}m_{WEEE}(1 - f_{Ni,mag})(1 - E_{Ni,B}) + V_{P,B}C_{Ni,B} \qquad (III.C.2.6)$$

where x_{Ni} is the weight fraction of Ni in WEEE, $f_{Ni,mag}$ is the fraction of Ni removed by the magnetic separation, X-104, i.e., 0.94, $E_{Ni,B}$ is the fraction of Ni leached in 6 hours in R-201, $V_{P,B}$ is the volumetric flowrate of the purge stream in Block B in L/h, and $C_{Ni,B}$ is the concentration of Ni in all streams in Block B in g/L.

The balance around the purge stream is given by Equation III.C.2.7.

$$V_{PLS,B} = V_{Raff,B} = V_{R,B} + V_{P,B} \qquad (III.C.2.7)$$

Both Equations IIII.C.2.5 and III.C.2.6 can be solved for m_{WEEE} and then equated. Equation III.C.2.7 is used to substitute $V_{PLS,B}$ and $V_{P,B}$ for $V_{R,B}$. Next, $V_{P,B}$ is isolated to yield Equation III.C.2.8.

$$V_{P,B} = V_{PLS,B}(C_{Cu,PLS} - C_{Cu,R}) / [\,(C_{Ni,B}x_{Cu}E_{Cu} / (1 - f_{Ni,mag})x_{Ni}E_{Ni}) - C_{Cu,R,B}\,] \qquad (III.C.2.8)$$

The purge flowrate required to prevent accumulation depends on the purge stream's Ni concentration, shown in Figure III.C.2-2. At dilute Ni concentrations, the purge stream flowrate approaches infinity, and so Ni is allowed to accumulate to 0.60 g/L before tapping the purge stream at 0.56 m^3/h.

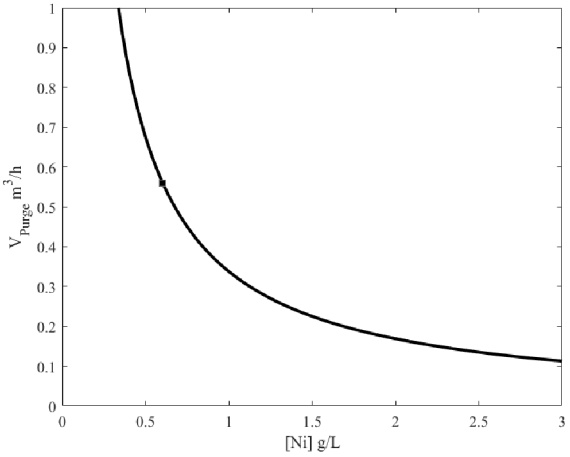

Figure III.C.2-2. Purge Volumetric Flowrate vs. Nickel Concentration. Black square indicates chosen $C_{Ni,P}$ and V_P.

The purge flowrate was originally calculated before accounting for the magnetic removal of Ni in X-104, and so the purge flowrate is likely an overestimate. However, a larger purge stream allows for the removal of other metal ions, especially Fe, which would accumulate. In practice, the purge flowrate must be flexible and accommodate the variable composition of the input WEEE.

The concentration of each metal in the purge stream required to prevent accumulation is given by Equation III.C.2.9.

$$C_{i,P,B} = m_{i,in,B} \times E_{i,B} / V_{P,B} \qquad (III.C.2.9)$$

where $C_{i,P,B}$ is the concentration of species *i* in the purge stream in Block B in g/L, $m_{i,in,B}$ is the input mass flowrate of species *i* into the agitated leach tank, R-201, in g/h, and $E_{i,,B}$ is the fraction of species *i* leached in R-201 after 6 h, given previously in Table III.C.2-1. Each metal's concentration in the purge stream required to prevent accumulation is given in Table III.C.2-2. Note that the Cu purge concentration is due to Cu extraction and was not found with Equation III.C.2.9.

Table III.C.2-2. Concentration Metal ions in Purge Stream in Block B, where V_P = 0.56 m³/h

Metal, *i*	Cu	Fe	Sn	Ni	Pb	Zn	Ag	Au	Pd
$C_{i,P,B}$ **(g/L)**	0.20	48.1	13.4	0.60	6.68	3.34	1.0	0.50	0.025

Copper leaching agitation tank design, R-201.

Crushed Cu is leached in a stirred tank, or leaching agitation tank, R-201. While designing R-201, we maintained the solid-liquid ratio used by Torres and Lapidus (2016), i.e., 20g crushed WEEE per 1 L lixiviant. Industrially, a slurry density of 35-50% is targeted for agitation leaching, depending on the solids' specific gravity, particle size, and solution viscosity (Marsden & House, 2006). About 6 hours worth of throughput will be leached at once. The effective volume of lixiviant required is given by Equation III.C.2.10.

$$V_{eff} = 6\ h \times (m_{WEEE}\ /\ 20\ g\ WEEE\ /L) \times 1\ m^3/1000\ L \qquad (III.C.2.10)$$

Therefore, 5,640 m³ of lixiviant is required to leach an input of 2.26×10^7 g Cu / 6 h (i.e., 1.13×10^8 g WEEE / 6h) into the MSR, R-101. The lixiviant volume was calculated before accounting for the removal of plastic, solder, iron, or nickel.

Our process uses leaching agitation tanks manufactured for Au leaching by Xinhai Mineral Processing EPC. The tank has two, rubber lined impellers and built-in air sparging capabilities. The largest tank produced has an effective volume of 480 m³, model SJ8.5X9.0 (Xinhai, n.d.). Thus, 12 agitation tanks in parallel are required to handle our lixiviant volume. The tank specifications are given in Table III.C.2-3 (Xinhai, n.d.).

Table III.C.2-3. Leaching Agitation Tank, SJ8.5X9.0, by Xinhai Mineral Processing EPC Specifications

Part	**Description**	**Value**
V_{eff}	Effective volume	480 m³
T_d	Tank diameter	8.5 m
Z	Tank height	9 m
d_i	Impeller diameter	3.3 m
N	Impeller speed	18.5 RPM
P	Motor power	30 kW

The liquid height is given by Equation III.C.2.11.

$$H = V_{R,eff} / (\pi\ (\ T_d / 2)^2) \qquad (III.C.2.11)$$

where H is the liquid height in m. If $V_{R,eff}$ = 480 m^3 and T_d = 8.5 m, then H = 8.5 m, which leaves a headspace of 0.50 m. The other tank dimensions were estimated via the geometric proportions suggested by Lepek et al. (2018) and are given in Table III.C.2-4.

Table III.C.2-4. Additional Au Leaching Agitation Tank (R-201) Dimensions

Part	Description	Geometric Proportion	Dimension
V_R	Reactor volume		510.7 m^3
H	Liquid height		8.5 m
C_{bot}	Bottom Impeller clearance	C / T_d = 1/3	2.8 m
C_{top}	Top Impeller clearance	C / T_d = 2/3	5.7 m
W	Impeller height	W / d_i = 1/5	0.66 m
J	Baffle width	J / T_d = 1/12	0.71 m

The agitated leaching tanks, R-201, are lined with cross-linked polyethylene (XLPE). Two, 45° pitched-blade turbines (PBT) with four blades impellers were chosen for axial flow and solid suspension (Hemrajani & Tatterson, 2003). The impellers are coated with rubber to prevent corrosion (Xinhai, n.d.).

The dimensionless, impeller Reynolds number is given by Equation III.C.2.12.

$$Re = d_i^2 N \rho / \mu \qquad (III.C.2.12)$$

where Re is the impeller Reynolds number, d_i is the impeller diameter in m, N is the impeller rotational speed in revolutions per second (RPS), ρ is the lixiviant density, and μ is the lixiviant viscosity (Wankat, 2016). The density of 15 wt% HCl solution is about 1.0776 kg/L (Sunga, n.d.). Due to a lack of data, we assumed the solution viscosity to be that of water, 1 cP. For an impeller speed of 18.5 RPM (0.31 RPS), Re = 3.62 × 10^6, which is in the turbulent regime.

The dimensionless power number is given by Equation III.C.2.13.

$$N_{Po} = (P g_c) / (\rho \ N^3 \ d_i^5) \qquad (III.C.2.13)$$

where N_{Po} is the power number, P is the power in watts, and g_c is a gravitation constant and is 1.0 m/s^2 in metric units (Wankat, 2016). The N_{Po} is estimated using correlations with Re and becomes constant in the turbulent regime. For a 45° PBT, with four blades with four standard baffles, N_{Po} = 1.27 in the turbulent regime (Hemrajani & Tatterson, 2003). Solving Equation III.C.2.13 yields a power of 15.7 kW.

Solid-liquid separation.

After leaching, the solid slurry must be separated from the PLS before entering Block C for gold recovery. Typically, this is done with a counter-current decantation (CCD) circuit (Schlesinger et al., 2011). CCD circuits use a series of thickeners to separate the solid slurry from the PLS. Due to the scope of our process, we did not design the CCD, but one is needed immediately after R-201. Designing the CCD would be a useful improvement to our process.

III.C.3. Copper Extraction

Copper extraction chemistry.

After Cu is leached, it is selectively extracted into an organic solvent to remove other metals that would otherwise deposit in electrowinning. This is crucial for producing high purity Cu cathodes (Schlesinger et al., 2011). Extraction is favored by low acid concentration because the reaction produces hydrogen ions (Schlesinger et al., 2011). The organic extractants complex selectively with Cu^{2+} in a process called *chelation*; a generalized extraction reaction is shown in Figure III.C.3-1, adapted from Schlesinger et al., (2011).

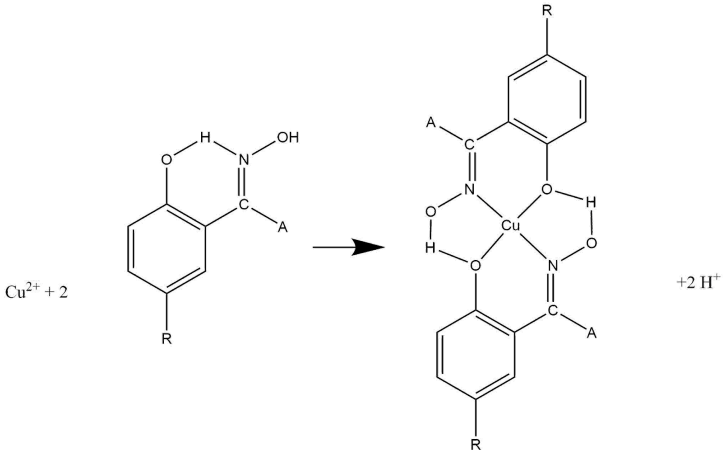

Figure III.C.3-1. "Structure of oxime extractant and Cu-oxime complex. The copper complex is formed from reaction of a Cu^{2+} cation with two oxime molecules, releasing two protons" (Schlesinger et al., 2011, p. 325)

The extractant must fulfill requirements including efficient extraction of Cu from the PLS and stripping into the electrolyte, rapid extraction and stripping kinetics, insolubility in the aqueous phases, preferential extraction of Cu over other metals, especially Fe, solubility in an inexpensive petroleum distillate diluent, inflammability, non-toxicity, and non-carcinginity (Schlesinger et al., 2011).

Cyanex 921 is a *solvating extractant*, which "can extract by solvation of electrically neutral inorganic species" according to the reaction in Equation III.C.3.1 (Vignes, 2013, p. 57).

$$(M^{n+} + nX^{-1})_{aq} + mL_{(org)} \rightarrow (MX_nL_m)_{org} \qquad (III.C.3.1)$$

where M^{n+} is a metal cation, X^{-1} is a counter anion (e.g. chloride), L_{org} is the solvating extractant, and $(MX_nL_m)_{org}$ is the chelate. We chose Cyanex 921 as the organic extractant because we have equilibrium data for cupric ion extraction from 5M HCl into Cyanex 921 in kerosene. Cyanex 921 is made by Solvay and is 99% trioctylphosphine oxide, i.e., TOPO ($(C_8H_{17})_3P = O$) (Dziwinski & Szymanowski, 1998). Based on the requirements for an extractant, we assumed that Cyanex 921 exclusively extracts Cu and that no other metals enter the organic phase. One extractant can selectively extract different metal cations depending on pH, and so we recommend that the pH of our PLS be optimized for Cu^{2+} selectivity with additional data (Vignes, 2013).

The extraction of cupric ions out of HCl solution into Cyanex 921 is given by Equation III.C.3.2.

$$Cu^{2+}_{(aq)} + 2H^{+}_{(aq)} + 4Cl^{-}_{(aq)} + 2L_{(org)} \rightleftharpoons H_2CuCl_4.2L_{(org)} \qquad (III.C.3.2)$$

where $L_{(org)}$ refers to Cyanex 921 and $H_2CuCl_4.2L_{(org)}$ is the copper-organic complex (Mishra & Devi, 2011). The equilibrium constant of the extraction is given by Equation III.C.3.3.

$$K = [H_2CuCl_4.2L]_{(org)} / ([Cu^{2+}]_{(aq)}[H^{+}]^2_{(aq)}[Cl^{-}]^4_{(aq)}[L]_{(org)}) \qquad (III.C.3.3)$$

where K is the equilibrium constant for the extraction (Mishra & Devi, 2011). The value of K is given by Equation III.C.3.4.

$$\ln(K) = 0.6633 \left(\frac{1000}{T}\right) - 4.497 \qquad (III.C.3.4)$$

where T is the temperature in Kelvin (Mishra & Devi, 2011).

The total Cyanex 921 concentration is given by Equation III.C.3.5.

$$[L]_T = [H_2CuCl_4.2L]_{(org)} + [L]_{(org)} \qquad (III.C.3.5)$$

where $[L]_T$ is the total molar concentration of Cyanex 921, $[H_2CuCl_4.2L]_{(org)}$ is the concentration of complexed Cyanex 921, and $[L]_{(org)}$ is the concentration of uncomplexed Cyanex 921 (Mishra & Devi, 2011). Equation IIII.C.3.3 can be rearranged to isolate $[L]_{(org)}$ and then plugged into Equation III.C.3.5. Next, $[H_2CuCl_4.2L]_{(org)}$ can be isolated to estimate the complexed Cyanex 921 concentration as a function of K and other species' concentrations (Equations III.C.3.6 and III.C.3.7) (Mishra & Devi, 2011).

$$[H_2CuCl_4.2L]_{(org)} = \tfrac{1}{8}(B - \sqrt{B^2 - 16([L]_T)^2}) \qquad (III.C.3.6)$$

where

$$B = 4[L]_T + (K \ [Cu^{2+}]_{(aq)}[H^{+}]^2_{(aq)}[Cl^{-}]^4_{(aq)})^{-1} \qquad (III.C.3.7)$$

We targeted 3.30×10^6 g/h Cu extracted with an extraction efficiency of 94.3%. The volumetric flowrates and target Cu concentrations in the aqueous and organic streams are given in Table III.C.3-1.

Table III.C.3-1. Copper Concentration in Aqueous and Organic Phases, where O/A = 1

Stream	PLS	Raffinate	Stripped Organic	Loaded Organic
Cu Concentration (g/L)	3.5	0.02	3.7	7
Volumetric Flowrate (m^3/h)	1000	1000	1000	1000

These streams were based on industrial values, with an organic-to-aqueous volumetric flowrate ratio (O/A) of 1 (Schlesinger et al., 2011). The O/A ratio affects how many theoretical stages are required for extraction and affects phase entrainment, discussed in the mixer-settler design.

Using MATLAB and Equations III.C.3.6 and III.C.3.7, we found that the loaded organic concentration, $[H_2CuCl_4.2L]_{(org)}$, is 7 g/L when $[L]_T = 0.285$ M given that $[Cu^{2+}]_{aq} = 3.5$ g/L, $[H^+] = [Cl^-] = 5$ M, and $K = 0.0085$. This corresponds to a 12.1 wt% Cyanex 921 in kerosene solution. The plot of $[H_2CuCl_4.2L]_{(org)}$ versus $[Cu^{2+}]$ at this Cyanex 921 concentration shows the extraction equilibrium. The extraction operating line passes through the set PLS and stripped organic cupric ion concentration and has a slope of $(O/A)^{-1}$ (Jergensen II, 1999). The resulting McCabe Theile diagram shows that one theoretical stage achieves the target raffinate and loaded organic concentrations (Figure III.C.3-2).

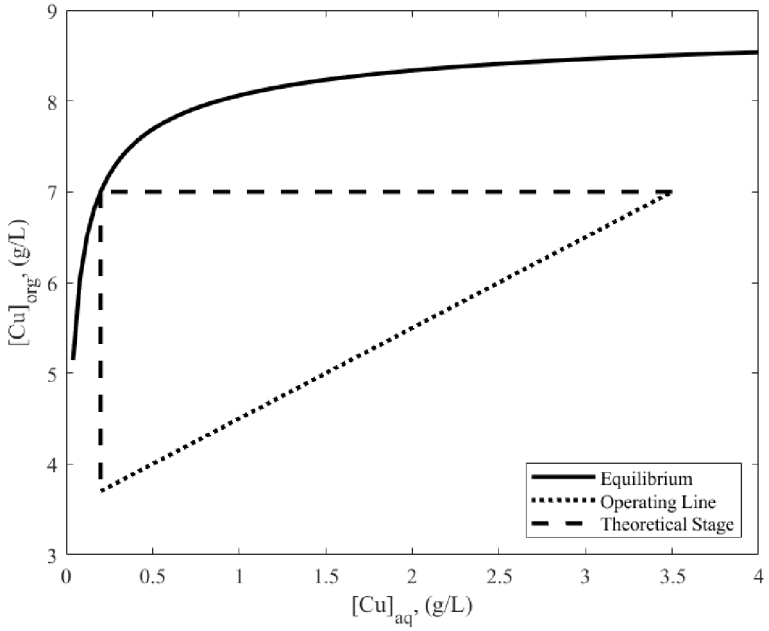

Figure III.C.3-2. McCabe Thiele Diagram for Cu^{2+} extraction from 5M HCl into 0.285 M Cyanex 921 in kerosene demonstrating one theoretical stage. The equilibrium line is given by Equation III.C.3.6 for 5 M HCl, [Cu] = 3.5g/L, $K = 0.0085$, 0.285 M Cyanex 921. The operating line is given by $(O/A)^{-1} = 1$.

Mixer-settler overview for copper extraction.

Mixer-settlers are used for Cu extraction and stripping as opposed to sieve-tray or packed columns or membrane contactors. Mixer-settlers suit processes with one or two theoretical stages, and so we designed for one theoretical stage (see Figure III.C.3-2) (Wankat, 2016). Mixer-settlers are flexible in handling wide solvent ratios, have high capacity, can handle high viscosity liquids, and have high stage-efficiency (Wankat, 2016). A schematic of a mixer-settler with two mixers is printed in Figure 16.3 in *Extractive Metallurgy of Copper (Fifth Edition)* by M.E. Schlesinger on page 329 (Schlesinger et al., 2011).

Copper extraction mixer design, R-202.

The mixer, R-202, disperses the organic and aqueous phases for good mass transfer without creating an emulsion. Both phases are fed to the bottom of the mixer and exit out of the top. Our mixer will run *organic continuous*, which means "that in the mixer there will be a matrix of organic and dispersed through it in small discrete bubbles will be the aqueous phase" (Jergensen II, 1999, p. 252). Organic continuous is favored by O/A ≥ 1 and is ensured by running the organic phase in 10% volume excess (Jergensen II, 1999). Running organic continuous risks aqueous entrainment in which some quantity of aqueous droplets remains in the organic phase exiting the settler. Aqueous ions, such as Fe ions, could reach electrowinning and contaminate the cathodes (Jergensen II, 1999). To avoid entrainment, mixer impeller tip speeds should not exceed 350 to 400 m/min (Schlesinger et al., 2011; Jergensen II, 1999). Alternatively, if the process were run *aqueous continuous*, organic entrainment could cause Cyanex 921 to leave in the raffinate. We prefer organic continuous because organic extractants are expensive and Cu loss is secondary to organic loss (Jergensen II, 1999).

The mixer's (R-202) effective volume is given by Equation III.C.3.8.

$$V_{R,eff} = Q_T \,/\, t_{R,mixer} \qquad (III.C.3.8)$$

where $V_{R,eff}$ is the mixer's effective volume in m^3, Q_T is the total volumetric throughput in m^3/h, and $t_{R,mixer}$ is the residence time in h. A typical residence time for extraction is 3 minutes (0.05 h) (Schlesinger et al., 2011). Our mixer must process 2000 m^3/h total; therefore, $V_{R,eff} = 100\ m^3$.

The mixer tank design is based on the geometric proportions suggested for a "standard" agitation system (Lepek et al., 2018). Assuming our tank is cylindrical, its effective volume is also given by Equation III.C.3.9.

$$V_{R,eff} = \pi\,(T_d / 2)^2 \times Z \qquad (III.C.3.9)$$

where T_d is the tank diameter in m, and Z is the tank height in m. We set T_d equal to Z, substituted T_d for Z in Equation III.C.3.9, and solved for T_d. Therefore, T_d and $Z = 5.03$ m, which we rounded up to 5.1 m. Thus, the reactor volume (V_R) is 104.2 m^3. The liquid height is given by Equation III.C.3.10.

$$H = V_{R,eff} \,/\, (\pi\,(T_d / 2)^2) \qquad (III.C.3.10)$$

where H is the liquid height in m. Based on the Xinhai tank design, the liquid height and tank diameter should scale similarly and have about 0.5 m headspace. If $V_{R,eff} = 100\ m^3$ and $T_d = 5.0$ m, and Z is scaled to 5.5 m, then $H = 5.1$ m, which leaves a headspace of 0.41 m. The other tank dimensions were set via the geometric proportions suggested by Lepek et al. (2018) and are given in Table III.C.3-2.

Table III.C.3-2. Copper Extraction Mixer, R-202, Dimensions

Part	Description	Geometric Proportion	Dimension (m)
T_d	Tank diameter		5.0
Z	Tank height		5.5
H	Liquid height		5.1
d_i	Impeller diameter	$d_i / T_d = 0.3$ to 0.5	1.6
C	Impeller clearance	$C / T_d = 1/3$	1.8
W	Impeller height	$W / d_i = 1/5$	0.32
J	Baffle width	$J / T_d = 1/12$	0.42

The Cu extraction mixer, R-202, is lined with cross-linked polyethylene (XLPE) because HCl vapor is corrosive (Eccles, n.d.). The mixer, R-202, uses a Lightnin A310, hydrofoil impeller because it provides axial flow at low shear and is efficient for liquid blending (Hemrajani & Tatterson, 2003). High shear would cause detrimental emulsions and entrainment. The impellers are lined with rubber to prevent corrosion (Xinhai, n.d.).

For an organic continuous process, the aqueous phase is dispersed in the organic phase. The volume fractions of the dispersed and continuous phases are determined experimentally with a shaker flask. Due to a lack of data, we set the continuous volume fraction to $\varphi_C = 0.70$ based on the rule of thumb that, for a given phase A, if $0.67 \leq \varphi_A$, then phase A is continuous (Wankat, 2016).

The density of the mixture in the mixer, R-202, is given by Equation III.C.3.11.

$$\rho_M = \varphi_D \rho_D + (1 - \varphi_D)\rho_C \qquad (III.C.3.11)$$

where ρ_M is the mixture density in kg/m^3, φ_D is the dispersed phase volume fraction in the mixer, ρ_D is the dispersed phase density, and ρ_C is the continuous phase density (Wankat, 2016).

The mixture viscosity is estimated with Equation III.C.3.12.

$$\mu_M = (\mu_C/\varphi_C) \times (1 + 1.5\mu_D\varphi_D / (\mu_C + \mu_D)) \qquad (III.C.3.12)$$

where μ_M is the mixture viscosity in Pa s, μ_D is the dispersed phase viscosity in Pa s, and μ_C is the continuous phase viscosity in Pa s (Wankat, 2016). Note that the mixture viscosity can be greater than either pure phase (Wankat, 2016).

The density of the continuous (organic) phase was estimated with Equation III.C.3.13, which is an alternate version of Equation III.C.3.11.

$$\rho_C = (V_{kerosene} / V_{organic}) \times \rho_{kerosene} + (V_{Cyanex\,921}/V_{organic}) \times \rho_{Cyanex\,921} \qquad (III.C.3.13)$$

where $V_{kerosene}$ is the volumetric flowrate of kerosene in the stripped organic in m^3/h, $V_{organic}$ is the total volumetric flowrate of the stripped organic in m^3/h, $\rho_{kerosene}$ is the density of kerosene (0.8 g/mL), $V_{Cyanex\,921}$ is the volumetric flowrate of Cyanex 921 in the stripped organic in m^3/h, and $\rho_{Cyanex\,921}$ is the density of Cyanex 921 (0.88 g/mL).

Due to a lack of data, the viscosity of the continuous phase was estimated using kerosene's viscosity (The Engineering Toolbox, n.d.-a). For the dispersed phase, the density of 15 wt% HCl solution is about 1.078 kg/L (Sunga, n.d.). We assumed the solution viscosity was approximately that of water at 20°C (Crittenden et al., 2012). The phase densities and viscosities are given in Table III.C.3-3.

Table III.C.3-3. Density and Viscosity of Continuous and Dispersed phases and Mixture in R-202

Property	Continuous (org)[1]	Dispersed (aq)[2]	Mixture
ρ, (kg/m^3)	810	1100	890
μ, (cP)	1.64	1.002	2.74

The mixture density and viscosity are used to find the dimensionless impeller Reynolds number, given by Equation III.C.2.12. For an impeller tip speed of 100 m/min, i.e., 0.33 RPS, *Re* is 2.76×10^5, which is in the turbulent regime. The dimensionless power number is given by Equation III.C.2.13. For a Lightnin A310 impeller under turbulent conditions with four standard baffles, $N_{Po} = 0.3$ (Hemrajani & Tatterson, 2003). Solving Equation III.C.2.13 for power yields 0.10 kW.

Copper extraction settler design, V-201.

After the Cu extraction, the solvents are pumped out of the top of the mixer, R-202, into the settler, V-201. The settler is a long, shallow basin in which the phases separate by gravity. Typically, settlers are built from HDPE-lined concrete and are 1 m deep with an organic phase depth of ~0.3 m and aqueous phase depth of ~0.5 m; these depths can be adjusted with weirs (Schlesinger et al., 2011). The organic phase (overflow) will float on the denser aqueous phase (underflow) (Jergensen II, 1999). The settling rate is given by Equation III.C.3.14.

$$v_c = Q / A_{set} \qquad (III.C.3.14)$$

where v_c is the settling rate in m^3 / (m^2 h), Q is the process flowrate in m^3/h, and A_{set} is the area of the settling zone in m^2 (Howe et al., 2012). Industrial settlers target a settling rate of $v_c = 4$ m^3/(m^2 h) (Schlesinger et al., 2011). Our throughput is 2000 m^3/h; therefore our settling zone is $A_{set} = 500$ m^2. For a square settler, this yields a 22.36 m × 22.36 m × 1 m, or 500 m^3 settler. This requires a 15 minute residence time for a 2000 m^3/h throughput.

The terminal settling velocity of the dispersed phase droplets is estimated by Stokes Law, given in Equation III.C.3.15.

$$u_{t,Stokes} = g\, d_d^{\,2}(\rho_C - \rho_D) / (18\, \mu_D) \qquad (III.C.3.15)$$

where $u_{t,Stokes}$ is the terminal settling velocity in m/s, g is acceleration due to gravity in m^2/s, and d_d is the dispersed phase drop diameter in m, often set empirically to 150 mm (Wankat, 2016). In an organic continuous operation, settling occurs downwards because $\rho_D > \rho_C$, indicated by a negative $u_{t,Stokes}$. To use Equation III.C.3.15, the Reynolds Number of the dispersed drop (Re_{drop}) must be sufficiently small and is given in Equation III.C.3.16.

$$Re_{drop} = d_d \, \rho_C \, u_{t,Stokes} / \mu_C \; < 0.3 \qquad (III.C.3.16)$$

For our process, we calculated $u_{t,Stokes}$ = - 0.003 m/s and Re_{drop} = 0.243 (Wankat, 2016). The distance traveled by a dispersed drop is given by Equation III.C.3.17.

$$h_{drop} = u_{t,Stokes} \times t_{R,set} \qquad (III.C.3.17)$$

where h_{drop} is the vertical distance traveled by the dispersed drop in m, and $t_{R,set}$ is the settler residence time of 900 s. Therefore, the dispersed drops would theoretically descend 2.9 m before reaching the end of the settler. The depth of the organic phase is only ~0.3 m, and so our settler is adequately large for phase separation. The excess length will help avoid aqueous entrainment.

III.C.4. Copper Stripping

Copper stripping chemistry.

Cu stripping is done in another mixer-settler similar to extraction except for that stripping is favored by a high acid concentration and a high O/A ratio (Schlesinger et al., 2011). Therefore, the spent electrolyte solution used for stripping is 180 g/L H_2SO_4 at 250 m^3/h (O/A = 4). The general stripping reaction is given by Equation III.C.4.1.

$$L_2\,Cu_{(org)} + 2H^+_{(aq)} \rightarrow Cu^{2+}{}_{(aq)} + 2RL \qquad (III.C.4.1)$$

where *L* refers to the organic extractant, Cyanex 921 (Jergensen II, 1999). Normally, a McCabe-Thiele method can be used for stripping where the operating line is O/A (Jergensen II, 1999); however, we lack equilibrium data for Cu transfer from Cyanex 921 into H_2SO_4 solution. The residence time for stripping is typically 3 minutes (Schlesinger et al., 2011). On the lab scale, nearly 100% of Cu was stripped from Cyanex 921 into 0.5 M H_2SO_4 after 3 minutes of shaking (Mishra & Devi, 2011).

In practice, the composition of input WEEE will vary, and the Cu concentration will be difficult to control. If the Cu concentration in the loaded organic is different than our target values, the O/A ratio can be adjusted to change the McCabe-Thiele, stripping operating line (Jergensen II, 1999). Alternatively, the electrolyte's acid concentration can be adjusted to change the stripping equilibrium (Jergensen II, 1999).

Copper stripping mixer design, R-203.

The mixer-settler design approach for Cu stripping is the same as for Cu extraction, except that the throughput is smaller due to the smaller electrolyte stream. The Cu stripping mixer, R-203, is built from HDPE-lined carbon steel. The throughput is 1250 m^3/h. Using Equation III.C.3.8 and t_R = 180 s, the effective volume of the mixer is $V_{R,eff}$ = 62.5 m^3. Again, we set the tank diameter, T_d equal to the tank height, *Z*, substituted T_d for *Z* in Equation III.C.3.9, and solved for T_d. Therefore, T_d and *Z* = 4.3 m, which we rounded up to 4.5 m. Thus, the reactor volume (V_R) is 71.6 m^3. Using Equation III.C.3.10, the liquid height, *H* = 3.93 m, which leaves a headspace of 0.57 m. The tank dimensions were set via the geometric proportions suggested by Lepek et al. (2018) and are given in Table III.C.4-1. A Lightnin A310 impeller is used for axial flow at low shear (Hemrajani & Tatterson, 2003).

Table III.C.4-1. Cu Stripping Mixer, R-203, Dimensions

Part	Description	Geometric Proportion	Dimension (m)
T_d	Tank diameter		4.3
Z	Tank height	$Z / T_d = 1$	4.3
H	Liquid height		3.93
d_i	Impeller diameter	d_i / T_d = 0.3 to 0.5	1.6
C	Impeller clearance	$C / T_d = 1/3$	1.5
W	Impeller height	$W / d_i = 1/5$	0.32
J	Baffle width	$J / T_d = 1/12$	0.375

We set the volumetric fractions equal to the feed fractions due to a lack of experimental data and because O/A > 1 (Wankat, 2016). Therefore, the stripper is in organic continuity with $\varphi_C = 0.8$.

The continuous phase's physical properties are the same as in extraction. The dispersed phase's density for 15 wt% H_2SO_4 at 20°C is given by the Engineering Toolbox (The Engineering Toolbox, n.d.-b). The dispersed phase's viscosity was estimated as water at 20°C (Crittenden et al., 2012). The mixer's densities and viscosities are given in Table III.C.4-2.

Table III.C.4-2. Density and Viscosity of Continuous and Dispersed phases and Mixture in R-203

Property	Continuous (org)	Dispersed (aq)	Mixture
ρ, (kg/m^3)	810	1106	870.0
μ, (cP)	1.64	1.002	2.7

Using Equation III.C.2.12, for an impeller tip speed of 100 m/min, i.e., 0.33 RPS, *Re* is 4.50×10^5, which is in the turbulent regime. Solving Equation III.C.2.13 yields a power of 0.10 kW, where $N_{Po} = 0.3$ for a Lightnin A310 impeller under turbulent conditions with four standard baffles (Hemrajani & Tatterson, 2003).

Copper stripping settler design, V-202.

The stripper's settler, V-202, is run in organic continuity because "organic entrainment entering the electrowinning creates very serious operational problems, is difficult to recover," and can degrade the organic (Jergensen II, 1999, p. 254). The settler, V-202 was designed just like V-201, except that $Q = 1250$ m^3/h. The settler, V-202, is built from HDPE-lined concrete (Schlesinger et al., 2011). Using the target $v_c = 4$ m^3/(m^2 h) and Equation III.C.3.14, the settling area is $A_{set} = 312.5$ m^2. For a square settler, this yields a 17.7 m × 17.7 m × 1 m, or 312.5 m^3 settler. This requires a 15 minute (900 s) residence time for a 1250 m^3/h throughput.

Using Equations III.C.3.15 and III.C.3.16, the terminal settling velocity is $u_{t,Stokes} = -13.0$ m/h and $Re_{drop} = 0.27$, and so Stokes' Law applies. Using Equation III.C.3.17, the dispersed drops would theoretically descend 1.99 m before reaching the end of the settler. The depth of the settler is only 1 m, and so our settler is adequately large for phase separation. The excess length will help avoid aqueous entrainment.

III.C.5. Copper Electrowinning, R-204

Copper electrowinning chemistry.

Cu electrowinning reduces cupric cations to Cu metal, which is recovered and then sold. Cu electrowinning, R-204, is done in a 35 g/L copper sulfate ($CuSO_4$) and 1.8 M (180 g/L) sulfuric acid (H_2SO_4) solution at 45°C.

The standard oxidation potential for the cathode reaction is given by Equation III.C.5.1.

$$Cu^{2+} \rightarrow Cu + 2e^- \qquad \Delta E^o = +0.34\ V \qquad (III.C.5.1)$$

At the anode, water is reduced to hydrogen ions and oxygen gas. The oxygen is vented from the process. The reduction reaction is given by Equation III.C.5.2.

$$H^+ + OH^- \rightarrow 0.5\ O_2 + 2H^+ + 2e^- \qquad \Delta E^o = -1.23\ V \qquad (III.C.5.2)$$

Copper electrowinning design.

Electrowinning takes place in a series of cells filled with the $CuSO_4$ and H_2SO_4 solution. Each cell is connected in series, and each electrode in parallel. The cells can continue to operate when cathodes are harvested. The cells are 8 m × 1.2 m × 1.5 m and constructed from HDPE-lined concrete to resist corrosion. These dimensions are based on industrial sizing (Schlesinger et al., 2011). The cathodes are stainless steel 1.2 m x 1.0 m x 0.003 m slabs, and anodes are 1.1 x 0.9 x 0.006 m slabs of Pb alloyed with 1.35 wt% Sn and 0.07 wt% Ca. These materials are typical for industrial Cu electrowinning (Schlesinger et al., 2011). We set the current density to 450 A/m^2, a standard value for electrowinning, and specified that both sides of the electrode could plate copper. Schlesinger et al., (2011) suggest an overvoltage of 0.05 V for the cathode, 0.5 V for the anode, 0.25 V for the potential drop across the electrolyte, and 0.3 V for the drop across other hardware, which totals the required voltage to nearly 2 V per cell.

The electroplating rate per cathode is given by Equation III.C.5.3.

$$m / t = (M_{Cu}\, I\, \zeta) / (n\, F) \qquad (III.C.5.3)$$

where m / t is the electroplating rate in kg/h, M_{Cu} is the molar mass of copper in g/mol, I is the total current in amperes, ζ is the current efficiency, n is the number of electrons exchanged per reaction (in this case 2), and F is Faraday's constant (98,500 C/mol). The current efficiency was calculated using an empirical correlation taken at 40°C (Khouraibchia & Moats, 2010). Our process runs at a slightly hotter temperature (45°C), but we assumed this correlation still held up to 2 significant figures. The correlation is given in Equation III.C.5.4.

$$\begin{aligned}\zeta(\%) = \; & 88.19 - 4.91[Fe^{3+}] + 0.52[Cu^{2+}] + 1.81 * 10^{-3}[Cu^{2+}]^2 \\ & + 0.028[Fe^{3+}][Cu^{2+}] + 4.015 * 10^{-3}\, j\, [Fe^{3+}]\end{aligned} \qquad (III.C.5.4)$$

The efficiency depends on the cupric and ferric ion concentrations in each cell, and *j* refers to current density, in this case 450 A/m^2. We assumed that no more than 1 g/L Fe^{3+} ions and 35 g/L Cu^{2+} ions were present, yielding a 97% efficiency.

The electroplating rate, given by Equation III.C.5.3, is 1.24 kg per hour. To plate 3300 kg Cu per hour, our design uses 32 cells of 84 electrode pairs, i.e., 2665 total electrode pairs.

The power for electrowinning is given by Equation III.C.5.5.

$$P = IV \qquad (III.C.5.5)$$

where P is power in watts, and V is voltage in volts. Because the cells are in parallel, current scales with the number of electrodes. Similarly, voltage scales with the number of cells. Therefore, the total power requirement is given by Equation III.C.5.6.

$$P = I_{electrodes/cell}\, n_{electrodes/cell} \times V_{cell}\, n_{cells} \qquad (III.C.5.6)$$

Therefore, the total power requirement is 3310 kW.

The enthalpy generated by the electrochemical reactions was calculated by relating the Nernst potential to the thermodynamic definition of Gibbs free energy (Equation III.C.5.7).

$$\Delta G_{rxn} = -nFE_{cell} = \Delta H_{rxn} - T\Delta S_{rxn} \qquad (III.C.5.7)$$

where ΔG_{rxn} stands for the reaction change in Gibbs free energy in J, E_{cell} stands for the cell potential in V, T stands for the cell temperature in Kelvin, ΔH_{rxn} stands for the reaction enthalpy in J, and ΔS_{rxn} stands for the total entropy change for both the anode and cathode reactions in J/K. ΔS_{rxn} was calculated via the change in formation entropies for each species. E_{cell} was calculated with Equation III.C.5.8 which accounts for nonidealities in the cell.

$$E_{cell} = E^{o}_{cell} - (RT / (nF)) \times \ln[Q_r] \qquad (III.C.5.8)$$

where E_{cell} and E^{o}_{cell} are the non-ideal and standard cell potentials respectively in V, R is the gas constant in J/(mol K), and Q_r is the reaction quotient at non-equilibrated conditions. In this case, the activity coefficients were neglected, and Q_r was assumed to change only with the product and reactant concentrations in the cells. Using Equations III.C.5.7 and III.C.5.8, ΔH_{rxn} was calculated to be 3020 kW.

III.C.6. Copper Recovery Heat Transfer Equipment

Heat transfer equipment is required to optimize the temperature of Cu electrowinning around 45°C, and then to cool the spent electrolyte which is sent back to the stripping mixer, R-203, to around 20°C. Temperatures significantly lower than 40°C result in efficiency losses; also, the correlation given in Equation III.C.5.4 was generated at 40°C. Furthermore, the equipment must withstand corrosion because of sulfuric acid in the Cu electrolyte.

Estimated thermal properties of copper electrolyte.

The thermal properties of the Cu electrolyte were estimated using the Wilson model in Aspen Plus for a 160 g/L aqueous solution of sulfuric acid and are given in Table III.C.6-1. The properties were taken at the average temperature between electrowinning and stripping, 33°C. The electrolyte stream's volumetric flowrate and estimated density were used to estimate a mass flowrate of 101.4 kg/s.

Table III.C.6-1. Properties of Cu Electrolyte Stream, 160 g/L H_2SO_4, Estimated with Aspen Plus at 33 °C

Property	Value
Heat Capacity (J / kg K)	2897
Density (kg / m^3)	1460
Viscosity (Pa s)	8.9×10^{-4}
Thermal Conductivity (W / m K)	0.53

Copper electrowinning heater, E-202.

Cu electrowinning generates 3020 kW of heat and raises the electrolyte temperature by 10.3°C. To raise the electrolyte temperature an additional 14.7°C to reach 45°C requires 4223 kW of additional heat. This heat is provided by resistive heating elements, E-202. This decision was based on the fact that there is a low demand for steam elsewhere in this process, and additional steam generation would require a large capital investment. Also, electrowinning already requires a large amount of electricity; additional demands from these heating elements are on the same order of magnitude. The heating elements will consist of a total length of 222 m of 22 mm diameter RW80 nichrome heating element wire. The heater's operating conditions are 2112 A and 2000 V, yielding a loading of 28.23 W/cm^2. These values were determined using loading guidelines for water immersed heating coils from Alloy Wire International Ltd. and their sizing calculation tool (*Alloy Wire International*, n.d.).

Copper spent electrolyte heat exchanger, E-201.

A countercurrent, shell and tube heat exchanger cools the spent electrolyte stream with cooling water. The shell side is made of carbon steel, and the tube side of 316 stainless steel to resist corrosion from sulfuric acid. The spent electrolyte flows on the tube size, which enables the shell to be carbon steel, reducing capital cost. Also, the spent electrolyte is more likely than water to cause fouling, and the tube side is easier to clean. Due to the spent electrolyte's large volumetric flowrate, the exchanger requires a heat transfer area of 599.6 m^2, estimated with Equations III.C.6.1, III.C.6.2, and III.C.6.3. This is achieved with one shell pass and one tube

pass with 500 tubes. Each tube is constructed of 0.25 in, schedule 40, 316 stainless steel pipe. These parameters yield an overall length of 27.8 m; however, due to structural constraints, this heat exchanger will be divided into five 6.0 m heat exchangers in series.

$$\dot{Q} = C_p \dot{m}(T_f - T_i) = U_0 A_0 \Delta T_{lm} F_c \qquad \textit{(III.C.6.1)}$$

$$\text{where } U_0 = \left(\frac{1}{h_i}\frac{r_o}{r_i} + \frac{r_o ln(r_o/r_i)}{k} + \frac{1}{h_o}\right)^{-1}, \qquad \textit{(III.C.6.2)}$$

$$\text{and } \Delta T_{lm} = \frac{(T_{h,1}-T_{c,1}) - (T_{h,2}-T_{c,2})}{ln\frac{(T_{h,1}-T_{c,1})}{(T_{h,2}-T_{c,2})}} \qquad \textit{(III.C.6.3)}$$

The heat transfer area, A_0, was determined using Equation III.C.6.1 where $\dot{Q}$ is heat flow in watts, C_P is the heat capacity in J/(kg K), $\dot{m}$ is the mass flowrate in kg/min, T_f is the outlet temperature and T_i is the inlet temperature in K, U_0 is the overall heat transfer coefficient in W/(m^2 K) given in Equation III.C.2, h_i and h_o are the inner and outer heat transfer coefficients respectfully in W/(m^2 K), ΔT_{lm} is the logarithmic mean temperature in K, defined in Equation III.C.6.3, and F_c is the correction factor for multiple shell and tube passes. F_c was assumed to be 1.0 because there is only one shell and one tube pass due to the relatively low temperature difference between the hot and cold sides. Equation III.C.6.2 was used to estimate U_0 to be 1697.8 W/(m^2 K), where h_o was estimated to be 5000 W/(m^2 K) as a moderate value of forced convection with water (Welty et al., 2008, p. 227), and h_i was estimated as 17298.2 W/(m^2 K) via the Dittus-Boelter correlation given in Equation III.C.6.4 (Welty et al., 2008, p. 335).

$$Nu = h D / \lambda = 0.023(Re)^{0.80}(Pr)^{0.33} \qquad \textit{(III.C.6.4)}$$

where Nu is the Nusselt number, h is the convective heat transfer coefficient in W/(m^2 K), D is the pipe diameter, λ is thermal conductivity in W/(m K), Re is the Reynolds number, and Pr is the Prandtl number. The operating conditions for E-201 are given in Table III.C.6-2.

Table III.C.6-2. Operating Conditions for Heat Exchanger, E-201

Operating Condition	Shell Side	Tube Side
Inlet Temperature (°C)	10	45
Outlet Temperature (°C)	40	20
Volumetric Flow Rate (m^3/h)	209.8	250

III.D. Block C: Gold Recovery

III.D.1. Gold Recovery Overview

Block C focuses on Au recovery via agitated leaching, adsorption, elution, and electrowinning. Au comprises 0.1 wt% of WEEE and is highly valuable; for instance, it constitutes ~65.4% of a PCB's intrinsic value (Park & Fray, 2009). Cu recovery must precede Au recovery because Cu complexes with TU, the lixiviant chosen for Au leaching (Torres & Lapidus, 2016). The Cu leach residue from R-201 in Block B is moved into an agitated leaching tank, R-301, in Block C. Au is leached out of the Cu leach residue for 6 hours by a 100 g/kg (1 mM) TU and 0.5 g/kg ferric sulphate solution at pH = 1, adjusted with H_2SO_4. Unlike Cu extraction, Au is removed from the PLS by selective adsorption in an activated carbon packed column, T-301. The Au is then eluted with a stripping solution, i.e., 6 g/L TU in 20% (v/v) isopropanol at pH = 1. Next, Au is electrowon onto cathodes consisting of polypropylene baskets packed with steel wool, R-302, and is harvested. The overall BFD for Block C is shown in Figure III.D.1-1. The mass flowrates represent the components of WEEE and do not include any solvents' mass flowrate. The volumetric flowrates represent the solvents.

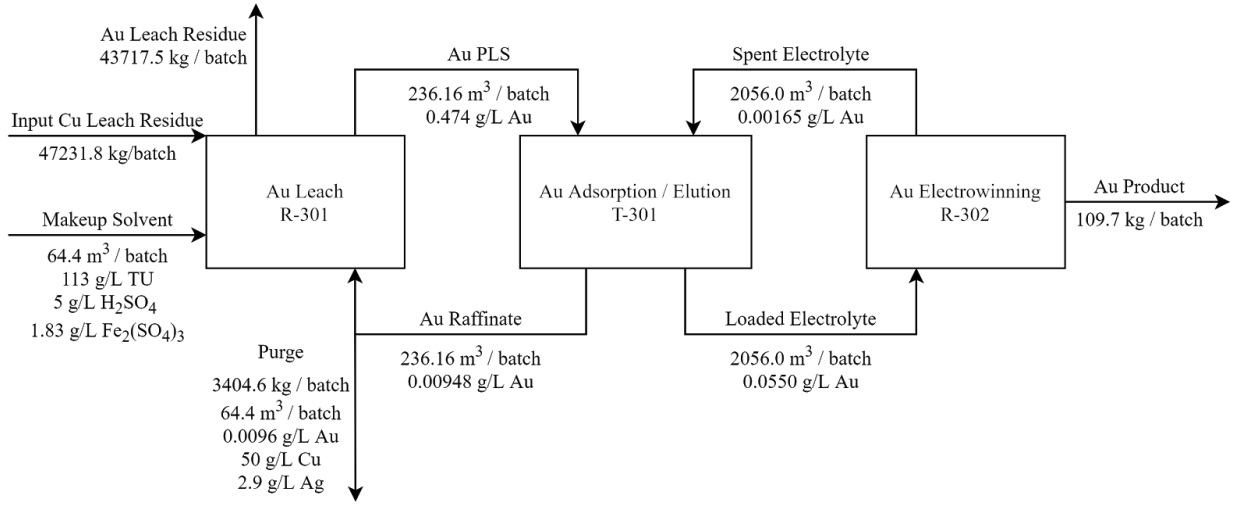

Figure III.D.1-1. Block C BFD.

Batch schedule.

One batch treats seven hours of accumulated Cu leach residue, and batches are staggered between trains. The residence time for the leaching is 6 hours, for adsorption is 1 hour, and for elution is 9 hours. This necessitates a semi-batch process with two trains. Each train has 21 elution columns. After leaching for 6 hours, the PLS will load the first train of 21 columns for 1 hour. The raffinate returns to the Au leaching agitation tank, R-301, and the next batch, which contains an accumulated seven hours of Cu leach residue, begins leaching while Au is eluted out of the first train for nine hours. The second batch will finish leaching before the first train finishes eluting, and so the PLS will be sent to the second train of 21 columns. Including electrowinning, each complete batch takes about 14 hours total.

III.D.2. Gold Leaching

Lixiviant selection: cyanide vs. thiourea.

Au is commonly leached with cyanide in an alkaline medium (pH > 10) with air sparging because cyanide can react with Au, the $Au(CN)_2^-$ ion is highly stable, and cyanide leaches Au and Ag more than other metals (Vignes, 2013). Drawbacks to cyanide are its environmental hazards and toxicity (Ahtiainen & Lundström, 2019). Also, cyanide leaching is slow, and other metal ions can interfere with Au recovery (Chen et al., 1980). Thiourea (TU) is a promising replacement for cyanide because it is more environmentally benign, easier to transport, has greater selectivity for Au, and leaches Au faster than cyanide (Ubaldini et al., 1998). TU is relatively non-toxic and even acts as a plant fertilizer. However, it is a suspected carcinogen and may dissolve heavy metals (Marsden & House, 2006). Drawbacks to TU are that it requires expensive, condensed-phase oxidizing agents (whereas cyanide uses air sparging) and is consumed faster than cyanide (Ubaldini et al., 1998; Schulze, 1984). Other potential lixiviants include thiosulfate and halides (Ahtiainen & Lundström, 2019).

Despite its drawbacks, TU leaching is promising for high-grade ore because of its vastly improved kinetics (Hiskey, 1984). In our process, Au is concentrated compared to traditional ore, and TU's faster leaching kinetics improve our throughput. Finally, TU's safety and environmental improvements over cyanide are important in a process that is already dangerous for workers. For these reasons, we chose TU as the lixiviant.

Gold leaching chemistry.

TU complexes with Cu such that excess Cu prevents Au from leaching in TU (Torres & Lapidus, 2016). Pretreatment of the crushed WEEE with HCl lixiviant in R-201 must precede Au leaching in R-301. In acidic conditions, Au and TU form a strong, cationic complex according to Equation III.D.2.1.

$$Au\,(s) \;+\; 2\,SC(NH_2)_2 \rightarrow Au(SC(NH_2)_2)_2^{+} \;+\; e^{-} \qquad (III.D.2.1)$$

where *Au* is solid gold, $SC(NH_2)_2$ is TU, $Au(SC(NH_2)_2)_2^{+}$ is the cationic complex, and e^- is an electron (Ubaldini et al., 1998). Oxidants, such as ferric sulphate, are required to drive this reaction. Thus, the overall reaction is described by Equation III.D.2.2.

$$Au\,(s) \;+ Fe^{3+} +\; 2\,SC(NH_2)_2 \rightarrow Au(SC(NH_2)_2)_2^{+} \;+\; Fe^{2+} \qquad (III.D.2.2)$$

where Fe^{3+} is ferric ion and Fe^{2+} is ferrous ion (Jing-ying et al., 2012). TU will also leach Ag according to Equation III.D.2.3.

$$Ag\,(s) \;+ Fe^{3+} +\; 3\,SC(NH_2)_2 \rightarrow Au(SC(NH_2)_2)_3^{+} \;+\; Fe^{2+} \qquad (III.D.2.3)$$

where *Ag* is solid silver, and $Au(SC(NH_2)_2)_3^+$ is the cationic complex between Ag and TU (Jing-ying et al., 2012). TU will also be oxidized by the ferric ion according to Equation III.D.2.4.

$$2\,SC(NH_2)_2 + 2Fe^{3+} + 3\,SC(NH_2)_2 \rightarrow (SCN_2H_3)_2 + 2\,Fe^{2+} + H^+ \qquad (III.D.2.4)$$

where $(SCN_2H_3)_2$ is formamidine disulfide (Jing-ying et al., 2012). Formamidine disulfide decomposes in acidic conditions according to Equation III.D.2.5.

$$(SCN_2H_3)_2 = CS(NH_2)_2 + NH_2CN + S \qquad (III.D.2.5)$$

where NH_2CN is cyanamide and *S* is elemental sulfur (Jing-ying et al., 2012). TU can be consumed by a ferric sulphate complex, given in Equation III.D.2.6.

$$Fe^{3+} + SO_4^{2-} + CS(NH_2)_2 = [FeSO_4 \cdot CS(NH_2)_2]^+ \qquad (III.D.2.6)$$

where $[FeSO_4 \cdot CS(NH_2)_2]^+$ is the ferric sulphate complex (Jing-ying et al., 2012).

Gold leaching data and kinetics.

The leaching of Au in TU versus time is given by Figure III.D.2-1 (Ubaldini et al., 1998).

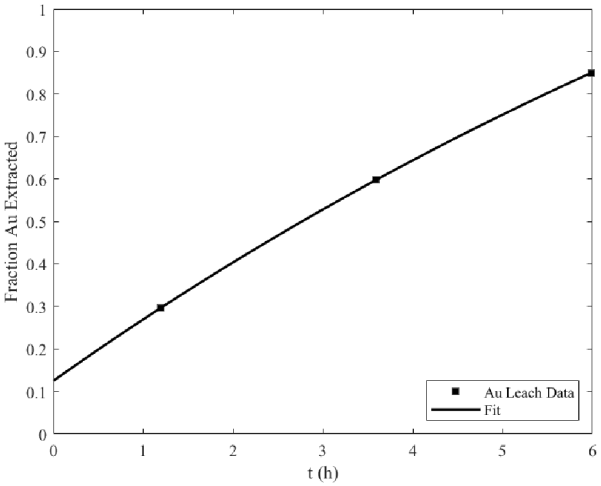

Figure III.D.2-1. Fraction of Au Leached vs. Time in 100 g/kg (1 mM) TU and 0.5 g/kg ferric sulphate solution at pH = 1, adjusted with H_2SO_4, at 20°C and 20% pulp density. Experimental data (squares) taken from Ubaldini et al. (1998); fit (line).

Parameters for the Au leaching data were empirically fit by minimizing the sum of squared errors (SSE) on the general expression $f(t) = a\exp(b\,t) + c$, given in Equation III.D.2.7.

$$E_{Au,C} = -2.0\, e^{(-0.07\, t)} + 2.15 \qquad (III.D.2.7)$$

where $E_{Au,C}$ is the fraction of Au leached in R-301, and t is the leach time in hours. Approximately 71.36% of Ag leaches based on an experiment with similar Au leaching. The original source was lost, but Hiskey (1984) reports a similar Ag leaching percentage of 75%. Copper will preferentially complex with TU before Au, and so we assumed 100% of Cu would leach before Au could (Torres & Lapidus, 2016; Zatko & Kratochvil, 1968). We assumed no other metals complex with TU.

Gold PLS, raffinate, purge, and recycle stream design.

The volume of the PLS achieves a 20% (w/v) pulp density of input solids (Ubaldini et al., 1998). We assumed no volume of the raffinate was lost to the adsorption column, T-301. The volume of the purge stream required to prevent Cu accumulation of is given by Equation III.D.2.8.

$$V_{P,C} = m_{Cu,C} E_{Cu,C} / C_{Cu,P,C} \qquad (III.D.2.8)$$

where $V_{P,C}$ is the volume of the purge stream in Block C in m^3/batch, $m_{Cu,C}$ is the input mass flowrate of Cu into Block C in g/batch, $E_{Cu,C}$ is the leach fraction of Cu in Block C, and $C_{Cu,P,C}$ is the concentration of Cu in the purge stream in g/L. $V_{P,C}$ is a function of $C_{Cu,P,C}$, shown in Figure III.D.2-2.

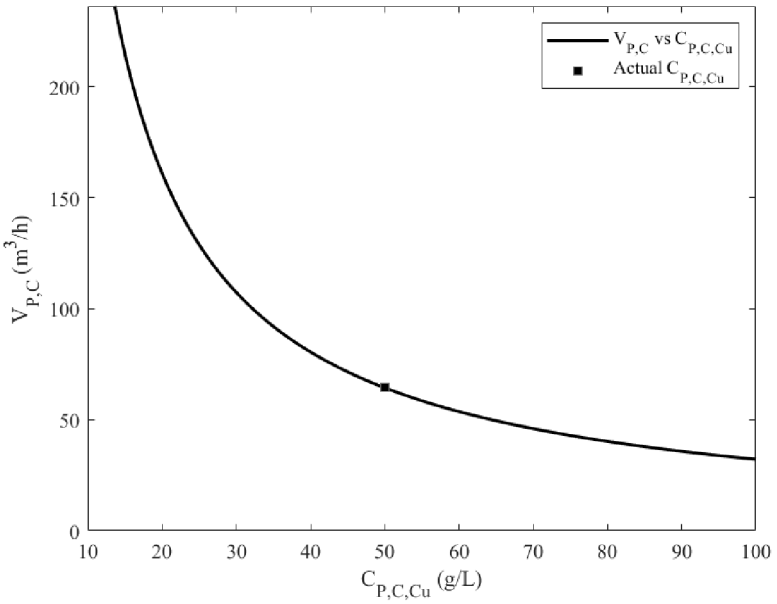

Figure III.D.2-2. Purge Volume vs. Purge Cu Concentration. Process conditions (square) are 50 g/L Cu and 64.4 m^3 purge per batch.

We chose $C_{Cu,P,C}$ to be 50 g/L because that concentration sits near the inflection point of the curve in Figure III.D.2-2 which allows for a minimized purge volume without excess Cu concentration. The concentration of Ag in the purge stream is given by Equation III.D.2.9.

$$C_{Ag,P,C} = m_{Ag,C}\, E_{Ag,C} \,/\, V_{P,C} \qquad (III.D.2.9)$$

where $C_{Ag,P,C}$ is the concentration of Ag in the purge stream in g/L, $m_{Ag,C}$ is the input mass flowrate of Ag into Block C in g/batch, $E_{Ag,C}$ is the leach fraction of Ag in the leaching agitation tank, R-301. The metal concentrations in the purge stream in Block C are given in Table III.D.2-1. Note that Au's purge concentration is based on adsorption in the column, T-301, and not a balance on accumulation.

Table III.D.2-1. Concentration of Metal ions in Purge Stream in Block C, where V_P = 64.4 m³/batch

Metal, *i*	Cu	Fe	Sn	Ni	Pb	Zn	Ag	Au	Pd
$C_{i,P,C}$ **(g/L)**	50	0	0	0	0	0	2.87	0.009	0

The volume of the recycle stream is simply the difference between the raffinate and purge volumes.

Gold leaching agitation tank design, R-301.

The Au leaching agitation tank, R-301, is a cylindrical, carbon steel tank, lined with XLPE to prevent corrosion due to sulfuric acid. The effective volume of the leaching agitation tank, R-301, and the PLS is 236.2 m³/batch to achieve a 20% pulp density. We set the tank diameter, T_d equal to the tank height, Z, substituted T_d for Z in Equation III.C.3.9, and solved for T_d. Therefore, T_d and Z = 6.7 m, which we rounded up to 7.0 m. Thus, the reactor volume (V_R) is 269.4 m³. Xinhai Mineral Processing EPC manufactures a Au leaching agitation tank with an effective volume of 269 m³, model SJ7.0X7.5 (Xinhai, n.d.). Therefore, only one tank is needed for Au leaching. We used the dimensions of model SJ7.0X7.5, which we assumed are optimized for Au leaching, for our leaching agitation tank, R-301, which are given in Table III.D.2-2.

Table III.D.2-2. Gold Leaching Agitation Tank, SJ7.0X7.5, by Xinhai Mineral Processing EPC Specifications

Part	**Description**	**Value**
V_{eff}	Effective volume	269 m³
T_d	Tank diameter	7.0 m
Z	Tank height	7.5 m
d_i	Impeller diameter	2.4 m
N	Impeller speed	21 RPM
P	Motor power	22 kW

The liquid height, H = 6.1 m, estimated with Equation III.C.3.10, leaves a headspace of 1.4 m. The unspecified tank dimensions were set via the geometric proportions suggested by Lepek et al., (2018) and are given in Table III.D.2-3.

Table III.D.2-3. Additional Au Leaching Agitation Tank, R-301, Dimensions

Part	Description	Geometric Proportion	Dimension
V_R	Reactor volume		288.6 m^3
H	Liquid height		6.1 m
C_{bot}	Bottom Impeller clearance	$C / T_d = 1/3$	2.3 m
C_{top}	Top Impeller clearance	$C / T_d = 2/3$	4.7 m
W	Impeller height	$W / d_i = 1/5$	0.48 m
J	Baffle width	$J / T_d = 1/12$	0.58 m

Two, 45° pitched-blade turbines (PBT) with four blades impellers were chosen for axial flow and solid suspension (Hemrajani & Tatterson, 2003). The impellers are coated with rubber to prevent corrosion (Xinhai, n.d.).

The Reynolds number is given by Equation III.C.2.12. The density of the lixiviant was estimated to be similar to water, i.e., 1077.6 kg/m. For an impeller speed of 21 RPM (i.e., 0.35 RPS), *Re* is 2.17×10^6, which is in the turbulent regime. For a 45° PBT, with four blades with four standard baffles, $N_{Po} = 1.27$ in the turbulent regime (Hemrajani & Tatterson, 2003). Therefore, solving Equation III.C.2.13 yields a power of 4.7 kW.

Solid-liquid separation.

After leaching, the solid residue must be separated from the PLS before entering the adsorption column, T-301 (Marsden & House, 2006). Typically, this is done with a counter-current decantation (CCD) circuit (Schlesinger et al., 2011). Due to the scope of our process, we did not design the CCD, but one is needed immediately after R-301. Designing the CCD would be a useful improvement to our process. Xinhai Mineral Processing EPC manufactures washing thickeners for Au-pregnant cyanide solutions.

III.D.3. Gold Adsorption in T-301

Gold adsorption background.

After leaching, Au is recovered by selective adsorption on activated carbon. Activated carbon refers to “highly porous carbonaceous materials" with massive surface area (1,000 m^2/g) not defined by a particular chemical structure (Rogans, 2012, p. 3). For Au adsorption, 1.19 - 3.36 mm particle sizes are typical (Rogans, 2012). Our process uses 2.38 mm activated carbon.

Industrially, Au adsorption is often done by carbon-in-pulp (CIP) or carbon-in-leach (CIL) processes (Rogans, 2012). Carbon-in-column (CIC) is also practiced (Denver Mineral Engineers, 2020). CIP is most prevalent, in which “carbon granules are added directly to the cyanide-ed pulp and moved counter-current to it. The gold-loaded carbon is later recovered by screening,” and “the carbon is returned to the adsorption circuit after suitable re-activation” (McDougall & Hancock, 1981, p. 138). CIP consists of a cascade of tanks in which the activated carbon and Au-pregnant cyanide move counter-currently. In CIL, activated carbon is added directly to the Au leach solution in leaching agitation tanks, and like CIP, the carbon moves counter-current to the cyanide solution (Wadnerkar et al., 2015). In CIL, Au simultaneously leaches into solution and adsorbs onto the activated carbon, whereas in CIP Au leaches and adsorbs in separate steps. In a CIC circuit, the Au-pregnant cyanide solution is pumped up through a series of fluidized-bed columns, often open-topped. CIC is prefered for heap leaching in which the PLS can have entrained solid residue (Denver Mineral Engineers, 2020).

After adsorption, Au desorbs from the activated carbon in an elution column (Rogans, 2012). Although not practiced industrially, we designed a single column to both adsorb and desorb Au instead of designing a CIP, CIL, or CIC circuit because we have the data and equations to describe column loading and elution and also to decrease the scope of our process. An improvement to our process would be to design a CIP, CIL, or CIC circuit but to retain the elution column.

Gold adsorption equilibrium onto activated carbon.

The adsorption of $AuTU_2^+$ onto activated carbon can be well-modeled by a Langmuir-Freundlich isotherm (H. Zhang et al., 2004). At high $AuTU_2^+$ concentrations, the adsorbed load approaches a limiting value, characteristic of a Langmuir isotherm. However, a Freundlich isotherm fits better at dilute $AuTU_2^+$ concentrations (H. Zhang et al., 2004). Adsorption data of $AuTU_2^+$ in 0.5 M TU onto 74 μm activated carbon is given in Figure III.D.3-1.

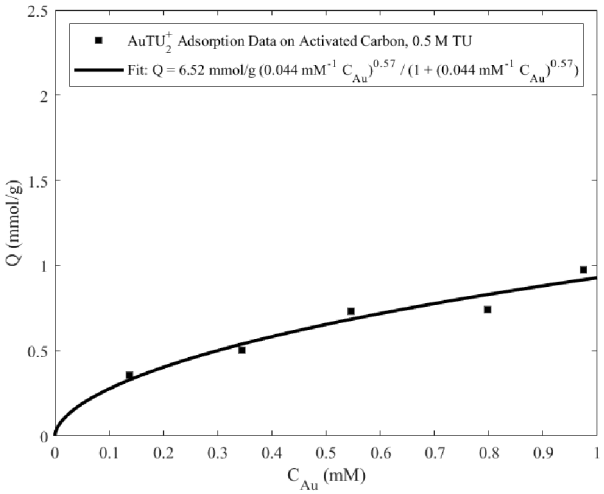

Figure III.D.3-1. Adsorption of $AuTU_2^{2+}$ on 74 µm Activated Carbon vs. $AuTU_2^{2+}$ Concentration in 0.5 M TU, pH 2.0 and 25°C. Experimental data (squares) taken from H. Zhang et al., (2004); fit (line).

Our PLS contains 1.2 M TU. Unfortunately, 0.5 M TU was the most concentrated data available, and so our calculations are not conservative. Also, our column uses 2.38 mm activated carbon, but the adsorption data was collected with 74 µm carbon. As much as 32% of TU can competitively adsorb onto the activated carbon which decreases adsorption efficiency and increases reagent consumption (H. Zhang et al., 2004).

A Langmuir-Freundlich isotherm is given by Equation III.D.3.1.

$$Q_{Au} = q_m(K\,C_{Au})^b \,/\, (1 + (K\,C_{Au})^b) \qquad (III.D.3.1)$$

where Q_{Au} is the adsorbed $AuTU_2^+$ concentration in mmol Au per g activated carbon, q_m is the maximum $AuTu_2^+$ adsorption capacity in mmol/g, K is the equilibrium constant for adsorption reaction in mM^{-1}, C_{Au} is the $AuTU_2^+$ concentration in solution in mM, and b is an empirical constant (Carta & Jungbauer, 2010). Minimizing a SSE cost function for Equation III.D.3.1 yields q_m = 6.52 mmol/g, K = 0.044 mM^{-1}, and b = 0.57. The fit is shown in Figure III.D.3-1.

Gold adsorption column design, T-301.

The adsorption column, T-301, was based on the elution columns designed for Ok Tedi Mine, a copper and gold mine in Papua New Guinea (Michaud, 2016). The column is made of rubber-lined mild steel and is rated to 350 kPa (Michaud, 2016). The column dimensions and operating conditions are given in Table III.D.3-1. The high column height-to-diameter ratio allows for even flow of the PLS without tunneling through the carbon (*Elution & Carbon Reactivation Resource Book*, n.d.).

Table III.D.3-1. Au Adsorption and Elution Column, T-301, Dimensions and Operating Conditions

Symbol	Description	Unit	Value
D_c	Column diameter	m	1.5
L_c	Column height	m	9
V_c	Column volume	m^3	15.9
Q_c	Column flowrate	L/min	150
T_{abs}	Adsorption temperature	°C	Ambient
P_{abs}	Adsorption pressure	bar	Ambient
T_{elute}	Elution temperature	°C	80
P_{elute}	Elution pressure	bar	Ambient
MOC	Material of construction		Rubber-lined mild steel
N_c	Number of columns in parallel		21
N_{trains}	Number of trains		2

Gold loading time in T-301, local equilibrium theory.

We described Au column loading using Au's adsorption isotherm (see Figure III.D.3-1) and local equilibrium theory, which is the ideal model of chromatography (Carta, 2019). In local equilibrium theory, the superficial velocity is described by Equation III.D.3.2.

$$u = Q_c / S \qquad (III.D.3.2)$$

where u is the superficial velocity in m/h, Q_c is the flowrate of the mobile phase in $m^{3/}h$, and S is the column's cross-sectional area in m^2 (Carta, 2019). The interstitial velocity is given by Equation III.D.3.3.

$$v = u / \varepsilon \qquad (III.D.3.3)$$

where v is the interstitial velocity in m/h, and ε is the interphase porosity (Carta, 2019). Typically, $\varepsilon \sim 0.3$ for spherical particles (Glover, 2012). The phase ratio is given by Equation III.D.3.4.

$$\Phi = (1 - \varepsilon) / \varepsilon \qquad (III.D.3.4)$$

where Φ is the phase ratio (Carta, 2019). The adsorbent moves down the column in a shockfront. The eluent is depleted of Au until the shockfront reaches the bottom of the column at the shock-time, t_s. The shockfront velocity is described by Equation III.D.3.6.

$$v_s = v / (1 + \Phi \, \overline{q}_F / C_F) \qquad (III.D.3.6)$$

where v_s is the shockfront velocity in m/h, $\bar{q}_F$ is the equilibrium amount of Au adsorbed at the feed concentration in mmol/g, and C_F is the feed Au concentration in mM (Carta, 2019). The shock-time is given by Equation III.D.3.7 (Carta, 2019).

$$t_s = L_c \,/\, v_s \qquad (III.D.3.7)$$

The mobile phase flowrate (Q_c) is 180 L/min, i.e., 10.8 m^3/h. Thus, the superficial and interstitial velocities are 6.11 m/h and 20.37 m/h respectively. Our feed Au concentration (C_F) is 0.474 g/L or 2.41 mM; therefore, using the fit Equation III.D.3.1, $\bar{q}_F$ = 1.41 mmol/g. The shockfront velocity is then v_s = 8.62 m/h (Equation III.D.3.6). Finally, the shock-time, i.e., the time required to load one column, is t_s = 1.04 h, or 63 minutes. The eluate volume is the product of the mobile phase flowrate and shock-time, and the number of column volumes (CV) required is the eluate volume divided by the column volume. Thus, 11.3 m^3 of eluate is required to load one column, which is 0.71 CV.

The amount of Au loaded per column is given by Equation III.D.3.8.

$$m_{Au,T-301} = Q_c t_s C_F \qquad (III.D.3.8)$$

where $m_{Au,T\text{-}301}$ is the amount of Au loaded in one T-301 column. Therefore, 5,343 g Au are loaded per column. To process 109,711 g Au per batch, 21 columns are needed in parallel.

The pressure drop across the column is given by the Kozeny–Carman equation for rigid particles and laminar flow in Equation III.D.3.9.

$$\Delta P = 150\,(1-\varepsilon)^2 \,/\, \varepsilon^3 \times \mu\, L_c\, u \,/\, {d_p}^2 \qquad (III.D.3.9)$$

where ΔP is the pressure drop in Pa, μ is the viscosity of the mobile phase in Pa s, u is the superficial velocity in m/s, and d_p is the packed particle diameter in m (Carta, 2019). The viscosity was estimated with pure water's viscosity. For d_p = 2.38 mm, the pressure drop across the column is $\Delta P = 7.30 \times 10^3$ Pa, or ΔP = 0.073 bar.

III.D.4. Gold Elution from T-301

Desorption, i.e., elution, occurs in the same column, T-301, as adsorption. Au is eluted with a 6 g/L (0.08 M) TU, 20% (v/v) isopropanol solution at 80 °C and a pH of 1, adjusted with H_2SO_4. The loaded electrolyte is sent to electrowinning and recycled for elution after the Au is plated.

Gold desorption equilibrium from activated carbon.

The Langmuir-Freundlich isotherm for Au adsorption (Equation III.D.3.1) depends on TU concentration which is more dilute in elution than in adsorption. The isotherm of $AuTU_2^+$ onto 74 μm activated carbon in 0.1 M TU solution is given in Figure III.D.4-1 which was used to approximate our operating condition of 0.08 M TU onto 2.38 mm carbon.

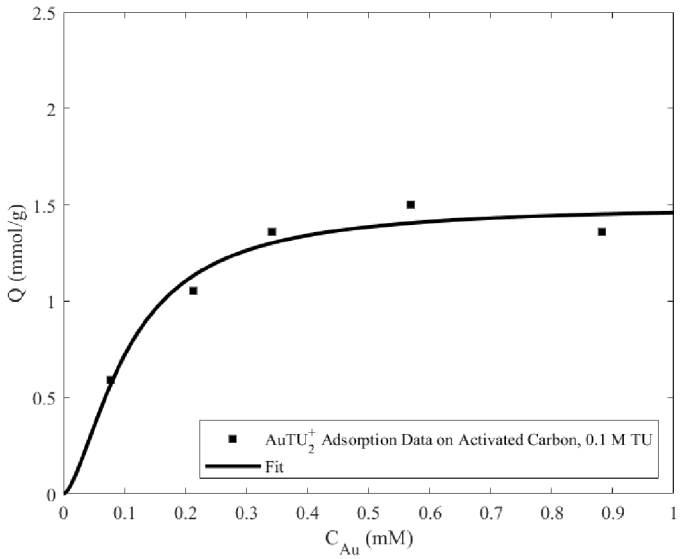

Figure III.D.4-1. Adsorption of $AuTU_2^{2+}$ on 74 μm Activated Carbon vs. $AuTU_2^+$ Concentration at 0.1 M TU, pH 2.0 and 25°C. Experimental data (squares) taken from H. Zhang et al., (2004); fit (line)

Minimizing a SSE cost function for Equation III.D.3.1 yields q_m = 1.499 mmol/g, K = 9.49 mM^{-1}, and b = 1.60. The fit Equation III.D.3.1 is shown in Figure III.D.4-1.

Gold elution time from T-301.

Adsorption and elution occur in one column, and so the column dimensions and flowrate are those given in Table III.D.3-1. The operating temperature increases to 80°C which aids Au desorption, but can also decompose TU, cause sulfur buildup, and hinder elution (Ubaldini et al., 1998).

The time required to elute a fully loaded column is described by local equilibrium theory. Chromatographic velocity describes how the adsorbent, e.g. Au, moves through the column with changing Au concentration and is given by Equation III.D.4.1.

$$v_{ch} = v \,/\, (1 + \Phi \frac{d\bar{q}}{dC_{Au}}) \qquad (III.D.4.1)$$

where v_{ch} is the chromatographic velocity in m/h, and $d\bar{q}/dC_{Au}$ is the differential change in $AuTU_2^+$ adsorption with $AuTU_2^+$ concentration, where $\bar{q}$ is the *total* amount of $AuTU_2^+$ adsorbed on the activated carbon in mmol/g (Carta, 2019). Differentiating a Langmuir-Freundlich isotherm (Equation III.D.3.1) yields Equation III.D.4.2.

$$\frac{d\bar{q}}{dC_{Au}} = (b\, k^b\, q_m\, C_{Au}^{(b-1)}) \,/\, (1 \;+\; (k\, C_{Au})^b)^2 \qquad (III.D.4.2)$$

The time required to elute the column is given by Equation III.D.4.3.

$$t_{elute} = L_c \,/\, v_{ch}(0) \qquad (III.D.4.3)$$

where $v_{ch}(0)$ is the chromatographic velocity at C_{Au} = 0 mM (Carta, 2019). In the case of a Langmuir isotherm, $d\bar{q}/dC_{Au}$ at C_{Au} = 0 mM is the isotherm's initial slope, which describes binding affinity. However, a Langmuir-Freundlich isotherm has an inflection point as C_{Au} approaches 0 mM because of the empirical constant, *b*. This causes the derivative to be zero. Therefore, we used C_{Au} = 0.05 mM, not 0 mM, in Equation III.D.4.3, to estimate the initial slope of the isotherm (see Figure III.D.4-1). At C_{Au} = 0.05 mM, $d\bar{q}/dC_{Au}$ = 8.57 L/g, and v_{ch} = 0.971 m/h. Thus, using Equation III.D.4.3, the elution time is t_{elute} = 9.3 h.

The total eluate volume is the product of the mobile phase flowrate (Q = 10.8 m^3/h) and elution time (t_{elute} = 9.3 h), and the CV of eluate required is the total eluate volume divided by the column volume. Thus, 100.1 m^3, or 6.3 CV, of eluate is required to desorb Au. This value is close to the industrially recommended 5 CV for Au elution which supports our method's plausibility (Michaud, 2016).

Carbon regeneration.

After elution, the activated carbon must be regenerated, usually via thermal regeneration (Rogans, 2012). Typically, thermal regeneration involves drying, vaporization of volatile species, and pyrolysis of non-volatile species in a kiln heated up to 700°C (Rogans, 2012). Due to the scope of our process, we did not design a kiln. However, regeneration is necessary to maintain adsorption efficiency. Regeneration can likely occur after some experimentally optimized number of batches.

III.D.5. Gold Electrowinning, R-302

Gold electrowinning design.

Au electrowinning reduces Au cations to metallic Au which is recovered and sold. Au electrowinning, R-302, occurs in 6 g/L TU and 20% (v/v) isopropanol at 60°C and a pH of 1, adjusted with H_2SO_4. The cell design is based on Cu electrowinning; this yields two HDPE-lined concrete cells of size 3.5 × 1.2 × 1.5 m^3, with 43 pairs of electrolytes each which can plate 21.9 kg Au/hour. Au electrowinning uses 0.5 m × 1 m × 0.003 m steel wool-packed polypropylene basket cathodes and 0.4 m × 0.9 m × 0.006 m stainless steel plate anodes (Conradie et al., 1995). These dimensions were chosen using the Cu cathode and anode dimensions as a basis due to a lack of data for Au. Electrowinning is run semi-batch for 5 hours per batch, which gives at least 2 hours of flex time to allow the rest of the process leading up to electrowinning to catch up. Au is harvested from the cathodes every 12 days.

Gold electrowinning chemistry.

The cathode reaction is given by Equation III.D.5.1.

$$Au(CS(NH_2)_2)_2^{+} + e^{-} \rightarrow Au + 2\,CS(NH_2)_2 \qquad \Delta E^o = 0.38\ V \qquad (III.D.5.1)$$

The anode reaction is given by Equation III.D.5.2, and is the same as in Cu electrowinning.

$$H^{+} + OH^{-} \rightarrow 0.5\,O_2 + 2H^{+} + 2e^{-} \qquad \Delta E^o = -1.23\ V \qquad (III.D.5.2)$$

The power requirement is the product of the required voltage and current. With an assumed 2 V requirement per cell and 2 cells, the total voltage required is 4 V. Assuming a current density of 500 A/m^2, the total required current for 43 electrode pairs is 21,500 A. Therefore, the total power requirement is 86 kW.

As in Cu electrowinning, the heat generation rate of the redox reactions was calculated to be 380 kW by relating the thermodynamic Gibbs free energy of reaction to the Nernst potential in Equations III.D.5.3 and III.D.5.4.

$$\Delta G_{rxn} = -nF E_{cell} = \Delta H_{rxn} - T\Delta S_{rxn} \qquad (III.D.5.3)$$

$$E_{cell} = E^o{}_{cell} - (RT / (nF)) \times \ln[Q_r] \qquad (III.D.5.4)$$

In the absence of a correlation to calculate current efficiency, we assumed an efficiency of around 7%, which reflects the low efficacy of the process per pass and is typical of reported Au electrowinning processes (Juarez & Dutra, 2000). Furthermore, in the absence of entropy and electrochemical potential data for the used TU complex, we approximated the data using Au^{2+} ion data instead.

III.D.6. Gold Recovery Heat Transfer Equipment

Heat transfer equipment is required to optimize the temperature of Au electrowinning around 60°C, and then to heat the spent electrolyte which is sent back to the elution column, T-301, to around 80°C. The equipment must withstand corrosion because of sulfuric acid in the electrolyte.

Estimated thermal properties of gold electrolyte.

The thermal properties of the Au electrolyte were estimated using the NRTL-HOC model in Aspen Plus for an 80:20 solution of water and isopropanol, given in Table III.D.6-1. Sulfuric acid was neglected. The properties were taken at the average temperature between electrowinning and elution, 53°C. The Au spent electrolyte stream's volumetric flowrate (10.8 m^3/h) and estimated density were used to estimate a mass flowrate of 3.6 kg/s.

Table III.D.6-1. Properties of Au Electrolyte Stream, 20% (v/v) Isopropanol, Estimated at 53 °C

Property	Value
Heat Capacity (J / kg K)	3110
Density (kg / m^3)	1200
Viscosity (Pa s)	7.0×10^{-4}
Thermal Conductivity (W / m K)	0.27

Gold advance electrolyte heat exchanger, E-301.

Cu electrowinning generates 380 kW of heat and raises the Au electrolyte temperature by 33.9°C. A countercurrent, shell and tube heat exchanger cools the advance electrolyte to 26.1°C with cooling water to achieve a final Au electrowinning cell temperature of 60°C. The shell side is carbon steel, and the tube side is 316 stainless steel because of sulfuric acid's corrosivity. The advance electrolyte flows on the tube side, which enables the shell to be carbon steel to reduce capital cost. Also, the advance electrolyte is more likely than water to cause fouling, and the tube side is easier to clean. The required heat transfer area was estimated to be 43.9 m^2 using Equations III.C.6.1-3. In order to keep overall length under 6.0 m, the heat exchanger has one shell pass and one tube pass with 175 tubes. Each tube will be constructed of 0.25 in, schedule 40, 316 stainless steel pipe. The overall estimated length is 5.8 m. All calculations were done using Equations III.C.6.1-4. The operating conditions are given in Tables III.D.6-2 and III.D.6-3.

Table III.D.6-2 Operating Conditions for Heat Exchanger, E-301

Operating Condition	Shell Side	Tube Side
Inlet Temperature (°C)	10	80
Outlet Temperature (°C)	30	26.1
Volumetric Flow Rate (m^3/h)	22.5	10.8

Table III.D.6-3 Calculated Values for Heat Exchanger, E-301

Variable	Value
ΔT_{lm} (K)	-32.1
Re Electrolyte	5892
Pr Electrolyte	8.06
Nu Electrolyte	47.5
h_i (W/m^2 K)	2021.6
h_o (W/m^2 K)	1000
U_o (W/m^2 K)	428.7
Velocity in tubes (m/s)	0.54
Heat duty (kW)	-603.9
Heat transfer area (m^2)	43.9
Length (m)	5.8

Au electrowinning heater, E-302.

A resistive heating element, E-302, within the piping is used to heat the Au spent electrolyte from 60°C to 80°C. The heat duty required is 223.9 kW and is provided by a total length of 80 m of 3.0 mm diameter RW80 nichrome heating element wire. The operating conditions for E-302 are 112 A and 2000 V, giving a loading of 29.87 W/cm^2. These values were determined using loading guidelines for water immersed heating coils from Alloy Wire International Ltd. and with their sizing calculation tool (*Alloy Wire International*, n.d.)

III.E. Block D: Syngas

III.E.1 Block D Overview

The design of Block D and syngas processing equipment is outside the scope of this project. Generally, the products of WEEE combustion and steam gasification in the MSR, R-101, consist of hydrogen gas, carbon monoxide, and gaseous hydrogen cyanide, which were estimated with Aspen Plus by feeding 5.1 kg/s (280 kmol/h) of H_2O and 1.4 kg/s (45 kmol/h) of O_2 to an RGIBBS reactor. According to Aspen Plus, these conditions did not produce CO_2 or NO_x, most likely because the molar amount of O_2 was too small. In a sensitivity study using Aspen Plus, increasing the O_2 flow rate to 200 kmol/hr produced CO_2. For the MSR, R-101, the syngas composition is mostly CO on a mass basis and mostly H_2 on a molar basis and is given in Table III.E.1-1.

Table III.E.1-1. Estimated Syngas Composition Exiting the MSR, R-101

Component	Weight Percentage (%)	Molar Percentage (%)
Hydrogen gas (H_2)	10	60
Carbon monoxide (CO)	86	38
Hydrogen cyanide (HCN)	4	2

Syngas can be fuel for a gas burner to produce heat. Assuming that each component fully combusts, that the gas burner has a 80% efficiency, and that the standard enthalpies of combustion are -143 kJ/g, -10.1 kJ/g, and -24.3 kJ/g for H_2, CO (Robinson, n.d.), and HCN (*Hydrogen Cyanide*, 1999) respectively, about 60,000 kW of thermal energy could be recovered. This energy is used to fully heat the MSR, R-101, and offsets energy costs. However, the MSR only requires 27,000 kW; thus, we plan to use the excess energy to generate electric power at a 30% efficiency. This offsets the process' electrical costs by 9,700 kW.

It may be more profitable to sell the syngas or use it as a chemical intermediate. Prior work has successfully removed HCN from H_2-rich syngas over Ni/Mg/Al catalysts (Kumagai et al., 2017). This cleaned syngas can be used as a chemical intermediate, for example in the Fischer-Tropsch process to convert the hydrogen and carbon monoxide into useful hydrocarbons. The productive use of CO would reduce carbon emissions. Future work should explore other uses for syngas and the economic, environmental, and safety ramifications.

III.F. Pump Design

Our process uses centrifugal pumps, which consume 384.8 kW in total. They were designed using the guidelines presented in the guide, *How to design a pump for CHE 4476*. The hydraulic power of each pump was found by multiplying the volumetric flowrate of each pumped stream by its differential pressure. The differential pressure was found using the actual change in pressure between the source and destination, the provided rules of thumb for frictional losses (0.5 atm for losses in pipes and through heat exchangers, and 1/3 the total frictional loss for a control valve), and the gravity head ($\rho g h$). The pump summary is given in Table III.F.1-1.

Table III.F.1-1. Pump Summary

Pump	Stream	Q (m^3/s)	ρ (kg/m^3)	Δh (m)	ΔP_{actual} (Pa)	$\Delta P_{frictional}$ (Pa)	ΔP_{head} (Pa)	ΔP_{total} (Pa)	P_{hyd} (kW)
P-201	Cu PLS	0.278	1,078	3.5	0	67,550	36,999	104,549	29.0
P-202	Cu Raffinate	0.278	1,078	8.0	0	67,550	84,570	152,120	42.3
P-203	Stripped Organic	0.278	810	4.5	0	67,550	35,757	103,307	28.7
P-204	Loaded Organic	0.278	810	3.3	0	67,550	26,222	93,772	26.0
P-205	Cu Spent Electrolyte	0.069	1,106	3.3	0	135,100	35,805	170,905	11.9
P-206	Cu Advance Electrolyte	0.069	1,106	3.3	0	135,100	35,805	170,905	11.9
P-301	Au PLS	0.066	1,078	1.5	0	67,550	15,857	83,407	5.5
P-302	Au Raffinate	0.066	1,078	7.5	0	67,550	79,284	146,834	9.6
P-303	Au Spent Electrolyte	0.571	1,200	8.0	0	135,100	94,176	229,276	130.9
P-304	Au Advance Electrolyte	0.571	1,200	1.0	7,343	135,100	11,772	154,215	88.1
								Total:	384.8

IV. ECONOMICS

The economic feasibility of this plant was determined by calculating the major expenses and revenues, and then analyzing the net present value of the cash flows and the discounted cash flow internal rate of return. The plant should operate over an 11-year period which is an appropriate lifespan for much industrial equipment. Major expenses include the raw material, waste disposal, and utility costs. Startup equipment costs are dwarfed by the annual manufacturing costs and revenue.

IV.A. Anticipated Annual Revenue

Table IV.A.1-1 shows the anticipated revenue from selling copper and gold, i.e., $7.4 billion per year.

Table IV.A.1-1 Anticipated Annual Revenue

Component	Amount Recovered (t/a)	Value (USD/t)	Revenue (USD/a)
Cu	31,886	4,340	138,387,420
Au	151	47,930,475	7,258,672,350
		Total:	$ 7,397,059,770

The metal values used to estimate revenue in Table IV.A.1-1 reflect their spot prices on March 30, 2020. We assumed that the values would not vary much over 11 years. Although only 0.5 wt% of the total product, Au accounts for 98% of the revenue; therefore, focus should be on optimizing Au recovery. Recovering other valuable metals such as silver and palladium could also be profitable.

IV.B. Purchased Equipment and Total Capital Plant Costs

The total purchased equipment cost is $3,262,000, and the total capital cost of the plant is $15,461,880. The cost breakdown is given in sections IV.B.1-4.

IV.B.1. Major Equipment Costs

Most of the equipment costs were estimated using CAPCOST 2017, a macro-enabled Microsoft Excel program. The Chemical Engineering Plant Cost Index (CEPCI), which accounts for inflation since 1957, is 596.1 as of November 2019 ("Economic Indicators," 2020). The cost of the concrete ponds (settler and electrowinning units) was estimated using the average cost to pour concrete, i.e., $110 per cubic yard, provided by HomeAdvisor, and by assuming a 0.25 m concrete thickness (HomeAdvisor, 2020). The shredders, X-103A/B, and magnetic separator, X-104, were priced with products sold on Alibaba (Changshu Shi Shouyu Machinery Co., Ltd., 2020; Gongyi Jinlong HengJi Heavy Industry Machinery Co., Ltd., 2020; Shijiazhuang Jiarun Technology Co., Ltd., 2020). The purchased equipment cost summary is given in Table IV.B.1-1.

Table IV.B.1-1. Purchased Equipment Cost Summary

Tag	Equipment Type	Base Equipment Cost (USD)	Purchased Equipment Costs (USD)	Number of units	Total cost (USD)
Block A					
R-101	MSR	22,300	22,300	1	22,300
X-101	Vessel	23,800	23,800	1	23,800
X-102	Dryer	13,300	13,300	1	13,300
X-103A	Shear Shredder	20,000	20,000	1	20,000
X-103B	Hammer Shredder	50,000	50,000	1	50,000
X-104	Magnetic Separator	9,800	9,800	4	39,200
Block B					
R-201	Agitation Tank	73,400	73,400	12	880,800
R-202	Mixer	32,900	32,900	1	32,900
V-201	Settling Pond	1,618	1,618	1	1,618
R-203	Mixer	32,900	32,900	1	32,900
V-202	Settling Pond	1,282	1,282	1	1,282
R-204	EW Cells	510	510	32	16,315
Block C					
R-301	Agitation Tank	32,900	32,900	1	32,900
T-301	Tower	23,300	23,300	42	978,600
R-302	EW Cells	510	510	2	1,020
				Total:	$ 2,138,935

IV.B.2. Pump Costs

The centrifugal pump costs were estimated with CAPCOST 2017, where the CEPCI is 596.1, and the MOC is stainless steel. The pump cost summary is given in Table IV.B.2-1.

Table VII.B.2-1. Purchased Pump Cost Summary

Tag	Stream	Base Equipment Cost (USD)	Purchased Pump Cost (USD)	Number of spares	Total Cost (USD)
P-201	Cu PLS	9,400	21,400	1	42,800
P-202	Cu Raffinate	11,500	26,200	1	52,400
P-203	Stripped Organic	9,350	21,300	1	42,600
P-204	Loaded Organic	8,900	20,300	1	40,600
P-205	Cu Spent Electrolyte	6,330	14,400	1	28,800
P-206	Cu Advance Electrolyte	6,330	14,400	1	28,800
P-301	Au PLS	4,900	11,200	1	22,400
P-302	Au Raffinate	5,850	13,300	1	26,600
P-303	Au Spent Electrolyte	22,200	53,300	1	106,600
P-304	Au Advance Electrolyte	17,700	40,700	1	81,400
				Total:	$ 473,000

IV.B.3. Heat Exchanger Costs

The shell and tube heat exchanger costs were estimated with CAPCOST 2017, where the CEPCI is 596.1. The RW80 resistive heating elements (E-202 and E-302) were roughly estimated by through hole, wirewound resistors sold by Vishay and TT Electronics (Vishay, 2020; TT Electronics, 2020). The heat exchanger cost summary is given in Table IV.B.3-1.

Table IV.B.3-1. Heat Exchanger Economic Cost Summary

Tag	Name	Base Equipment Cost (USD)	Purchased Cost (USD)
E-101	WEEE Heap	0	0
E-201	Cu Spent Electrolyte Heat Exchanger	383,000	347,000
E-202	Cu Electrolyte Heater	231,572	231,572
E-301	Au Loaded Electrolyte Heat Exchanger	37,100	67,200
E-302	Au Spent Electrolyte Heater	4,292	4,292
		Total:	$ 650,064

IV.B.4. Total Capital Cost of Plant

The Lang Factor method was used to estimate the total capital cost of the plant. Usually this method estimates the cost of an expansion to an existing plant, and so a better method may be required to accurately estimate the plant's total capital cost. From the Lang Factor method, the total capital cost is given by Equation IV.B.4.1.

$$C_{TM} = (F_{Lang}) \sum_{i=1}^{n} C_{E,i} \qquad (IV.B.4.1)$$

where C_{TM} is the plant's total capital cost, F_{Lang} is the Lang Factor, and $C_{E,i}$ is the purchased cost of each major piece of equipment (Turton et al., 2018). F_{Lang} for a fluid processing plant is 4.74, and the sum of purchased equipment costs is $3,262,000. Thus, the total capital cost is $15,461,880.

IV.C. Operating Costs

IV.C.1. Raw Materials

The usage, unit price, total annual costs, and startup costs for the plant's raw materials are given in Table IV.C.1-1. Price estimates for the metals were obtained from their spot prices on March 30, 2020, and prices for the other components were estimated from bulk chemical listings on Alibaba. The startup amount of each material was estimated as the amount needed to fill each reactor. We anticipate an annual expense of over one hundred million dollars, or $108,556,823, and startup expenses of over two million dollars, or $2,033,041. Note that the majority of annual expenses is the replenishment of LNK salt, and the majority of startup expenses is the Cyanex 921 and kerosene which we assumed to recycle perfectly. Acquiring and pretreating WEEE and discarding solder were assumed to be cost-free; however, transportation of solids would be expensive in practice.

Table IV.C.1-1. Raw Material Economic Cost Summary

Component	Steady-State Flow	Cost per Amount	Annual Cost (USD/a)	Startup Amount	Startup Cost (USD)
Block A					
Makeup Li_2CO_3	0.691 ton/hr	9070 $/ton	54,932,096	28560 kg	345,440
Makeup Na_2CO_3	0.691 ton/hr	200 $/ton	1,211,044	34544 kg	7,615
Makeup KCO_3	0.691 ton/hr	700 $/ton	4,238,654	33048 kg	26,700
99.5% O_2	1006.941 scm/hr	1.53 $/scm	13,511,506	--	
Block B					
5M HCl	0.648 ton/hr	100 $/ton	568,160	794 ton	79,428
0.28 M Cyanex 921	--	4.8 $/kg	--	110023 kg	528,109
Kerosene	--	0.49 $/L	--	874974 L	428,737
SS cathodes	1.131 ton/hr	2000 $/ton	19,828,131	81 ton	162,864
Pb anodes	--	1660 $/ton	--	198 ton	328,736
Block C					
Thiourea	1.01 ton/hr	1500 $/ton	13,330,226	30.7 ton	45,994
H_2SO_4	0.051 ton/hr	200 $/ton	88,868	1.471 ton	2949
Fe_2SO_4	0.019 ton/hr	300 $/ton	48,897	0.153 ton	46
Isopropanol	--	1000 $/ton	--	51.9 ton	51,864
Activated carbon	--	1000 $/ton	--	15.9 ton	15,900
NaOH (solid)	0.270 ton/hr	550 $/ton	1,294,556	--	--
Steel wool cathodes	0.004 ton/hr	3000 $/ton	102,575	1.12 ton	3,370
SS anodes	--	2000 $/ton	--	4.00 ton	7,988
		Total Annual Costs:	**$ 108,556,823**	Total Startup Costs:	**$ 2,033,041**

IV.C.2. Operating Labor

According to Turton et al., (2018), the technique used to best estimate operating labor requirements is given by Equation IV.C.2.1.

$$N_{OL} = (6.29 + 31.7P_{Px}{}^2 + 0.23N_{np})^{0.5} \qquad (IV.C.2.1)$$

where N_{OL} is the number of operators per shift, P_{Px} is the number of processing steps involving solid materials (e.g. transportation, distribution, particulate removal, etc.), and N_{np} is the number of nonparticulate processing steps. This equation is based on data obtained by five chemical companies and was correlated by Alkhayat and Gerrard. For this process, the number of solid-handling steps (P_{Px}) is 11, and the number of nanoparticulate steps (N_{np}) is 19. Therefore, the number of operators per shift is 62.

Several assumptions were made to estimate the operator labor cost per year, e.g., on average, an operator works five, 8-hour shifts per week for 49 weeks per year, and the chemical plant operates 24 hours per day (Turton et al., 2018). This requires 245 shifts per operator, and 1,095 shifts per year, yielding about 4.5 operators for each operator position required. Thus, 279 total operators are needed. According to the Bureau of Labor Statistics, the average salary of a chemical plant and systems operator in 2010 was $61,820/a (*Overview of BLS Wage Data by Area and Occupation*, n.d.). Thus, the total operating labor cost is about $17,247,780 per year.

IV.C.3. Utilities

Standard pricing for major utilities is given in Table IV.C.3-1, adapted from Table 8.3 in Turton et al. (2018).

Table IV.C.3-1. Standard Pricing for Major Utilities

Waste Stream	Price (USD)	Per Unit
Electrical Substation (mixer, pumps)	0.0674	/ kWh
Pressurized air supply (add 20% for instrument air)	0.50	/ 100 std m^3
Process steam	4.22	/ 1000 kg
Cooling Water	15.70	/ 1000 m^3

The total utility costs per year were estimated via the standard prices in Table IV.C.3-1, and are given in Table IV.C.3-2. The syngas generated from the MSR, R-101, can be burned to supply more than enough power to sustain the MSR. The remaining syngas is converted to electrical power for other utilities. This is represented as a negative utility. The total utilities cost is $904,160 per year.

Table IV.C.3-2. Utility Cost Summary and Total Cost Estimates

Equipment Tag	Utility Stream	Amount / a		Total Cost (USD) / a
R-101	O_2 feed	8,820	L	0.05
R-101	Electricity from MSR syngas	-84,409,011	kWh	-5,689,170
R-101	Steam	44,353,460	kg	187,170
R-201	Air Sparging	630	m^3	3.15
R-201	Cu Agitation tank Mixing (85% eff)	161,800	kWh	10,905
R-202	Cu Mixer (70% eff)	1,250	kWh	84
R-203	Cu Mixer (70% eff)	1,250	kWh	84
R-204	Cu Electrowinning (total)	50,808,000	kWh	3,424,460
E-201	Cooling water	1,837,850	kWh	28,850
E-202	Heating of Cu (resistance)	36,993,480	kWh	2,493,360
P-201	Cu PLS pump (88% eff)	288,680	kWh	19,460
P-202	Cu Raffinate pump (88% eff)	421,080	kWh	28,380
P-203	Stripped Organic Pump (88% eff)	285,700	kWh	19,255
P-204	Loaded Organic Pump (88% eff)	258,820	kWh	17,440
P-205	Cu Loaded Electrolyte Pump (85% eff)	122,640	kWh	8,265
P-206	Cu Spent Electrolyte Pump (85% eff)	122,640	kWh	8,265
R-301	Au Agitation Tank (80% eff)	51,465	kWh	3,470
R-302	Au Electrowinning	753,360	kWh	50,780
E-301	Cooling water	197,100	m^3	3,090
E-302	Resistive heating for Au Elec	1,961,360	kWh	132,195
P-301	Au PLS pump (80% eff)	60,225	kWh	4,060
P-302	Au Raff Pump (85% eff)	98,940	kWh	6,670
P-303	Au Spent Electrolyte (90% eff)	1,274,090	kWh	85,870
P-304	Au Spent Electrolyte (90% eff)	907,950	kWh	61,195
			Total	**$ 904,160**

IV.C.4. Waste

According to Turton et al., (2018), waste disposal costs can be estimated with industry standards. Standard waste pricing is $36 per tonne for non hazardous solid and liquid waste, $1,000 per tonne for hazardous solid and liquid waste, and $41 per 100 m^3 for primary water filtration (Turton et al., 2018). The plant's waste costs are summarized in Table IV.C.4-1. The total waste costs are $73,722,700 per year.

Table IV.C.4-1. Waste Stream Summary and Total Cost Estimates

Equipment Tag	Waste Stream	Amount/a	Total Cost/a (USD)
X-101	Waste Rinse Bath Water	334,282 m^3	13,705,550
R-201	Cu Purge	5,308 tonnes	5,307,860
R-301	Au Leach Residue, Solid Waste	54,708 tonnes	54,709,290
		Total:	$ 73,722,700

IV.C.5. Standard Cost of Manufacturing

The cost of manufacturing (C_{OM}) is equal to the sum of several factors related to direct manufacturing costs (e.g. raw materials, waste treatment, and utilities), fixed costs (e.g. local taxes and plant overhead), and general expenses (e.g. administration costs, distribution costs, and research and development). Although many factors must be considered, C_{OM} can be estimated with the fixed capital investment (FCI), and the cost of operating labor, utilities, waste treatment, and raw materials. The FCI was estimated as the sum of the purchased equipment costs and startup raw materials costs. A summary of estimations and a breakdown of C_{OM} is given in Table IV.C.5-1.

Table IV.C.5-1. Cost of Manufacturing Breakdown and Estimation Summary

Cost Type	Cost Item	Estimation	Total Cost/a (USD)
Direct Costs	Raw materials	C_{RM}	108,556,800
	Waste treatment	C_{WT}	73,722,700
	Utilities	C_{UT}	904,160
	Operating labor	C_{OL}	17,247,780
	Direct supervision and clerical labor	0.18 C_{OL}	3,104,600
	Maintenance and repairs	0.06 FCI	1,049,700
	Operating supplies	0.009 FCI	157,450
	Laboratory charges	0.15 C_{OL}	2,587,170
	Patents and royalties	0.03 C_{OM}	8,267,690
Fixed Costs	Local taxes and insurance	0.032 FCI	559,840
	Plant overhead	0.708 Co_{OL}+ 0.036 FCI	12,284,618
General Manufacturing Expenses	Administration costs	0.177 C_{OL} + 0.009 FCI	3,052,860
	Distribution and selling costs	0.11 C_{OM}	30,314,870
	Research and development	0.05 C_{OM}	13,779,490
			$ 275,589,740

IV.D. Cash Flow Analysis

IV.D.1. Working Capital

Working capital is "the amount of capital required to start up the plant and finance the first few months of operation before revenue from the process starts" (Turton et al., 2018, p. 297). Working capital is fully recoverable and cannot be depreciated. For this project, the working capital was conservatively estimated as six months of raw materials and utility costs, totalling $54,730,490, which should cover workers' salaries and all raw material inventories and should serve as a contingency for downtime and start-up delays.

IV.D.2. Depreciation

Our plant uses a variety of equipment without known salvage values, and so a double declining balance depreciation method (DDB), which does not not require salvage values, was used to estimate the equipments' depreciation. According to Turton et al., (2018), the formula for estimating the depreciation allowance is given by Equation IV.D.2.1.

$$d_k^{DDB} = (2/n)\,[FCI_L - \sum_{j=0}^{j=k-1} d_j] \qquad (IV.D.2.1)$$

The DDB method is an example of accelerated depreciation schemes which are more economically favorable. This is because, under this depreciation scheme, the earlier years of a plant's life have the greatest cash flow which is worth more than later cash flows due to the time value of money.

IV.D.3. Taxes

Taxation rates depend on plant location and local laws. A 2016 federal tax rate provided by Turton et al., (2018) was used to estimate the plant's taxation. The plant's net taxable income is on the order of billions of dollars, and so it qualifies for the highest taxation rate which is 35% of the net taxable income. Additional state, city, and local taxes could increase the overall taxation rate to as high as 50%, and so this value was used to conservatively estimate our plant's taxes.

IV.D.4. Non-discounted Cash Flow

A cash flow analysis helps determine if the plant is economically viable. The analysis assumes a typical schedule for plant startup, i.e., that construction takes 18 months, and startup takes over 6 months, and so the first year of full operation generates half of the normally expected gross revenue. The analysis period includes 9.5 years of operational time and 11 years total because most plant equipment has about a 9.5 year class life with no salvage value. The non-discounted cash flow summary is given in Table IV.D.4-1, and a graphical representation of it is given in Figure IV.D.4-1.

Table IV.D.4-1. Non-Discounted Cash Flow Summary

Year	Expenses (USD)	Depreciation (USD)	Revenue (USD)	Income Taxes (USD)	Non-Discounted Cash Flow (USD)
0	-17,490,000	0	0	0	-17,490,000
1	-324,810,000	-3,500,000	3,624,200,000	-1,647,900,000	1,647,990,000
2	-270,000,000	-2,800,000	7,248,400,000	-3,487,800,000	3,487,800,000
3	-270,000,000	-2,200,000	7,248,400,000	-3,488,100,000	3,488,100,000
4	-270,000,000	-1,800,000	7,248,400,000	-3,488,300,000	3,488,300,000
5	-270,000,000	-1,400,000	7,248,400,000	-3,488,500,000	3,488,500,000
6	-270,000,000	-1,200,000	7,248,400,000	-3,488,600,000	3,488,600,000
7	-270,000,000	-900,000	7,248,400,000	-3,488,800,000	3,488,700,000
8	-270,000,000	-700,000	7,248,400,000	-3,488,900,000	3,488,800,000
9	-270,000,000	-600,000	7,248,400,000	-3,488,900,000	3,488,900,000
10	-270,000,000	-500,000	7,248,400,000	-3,489,000,000	3,488,900,000

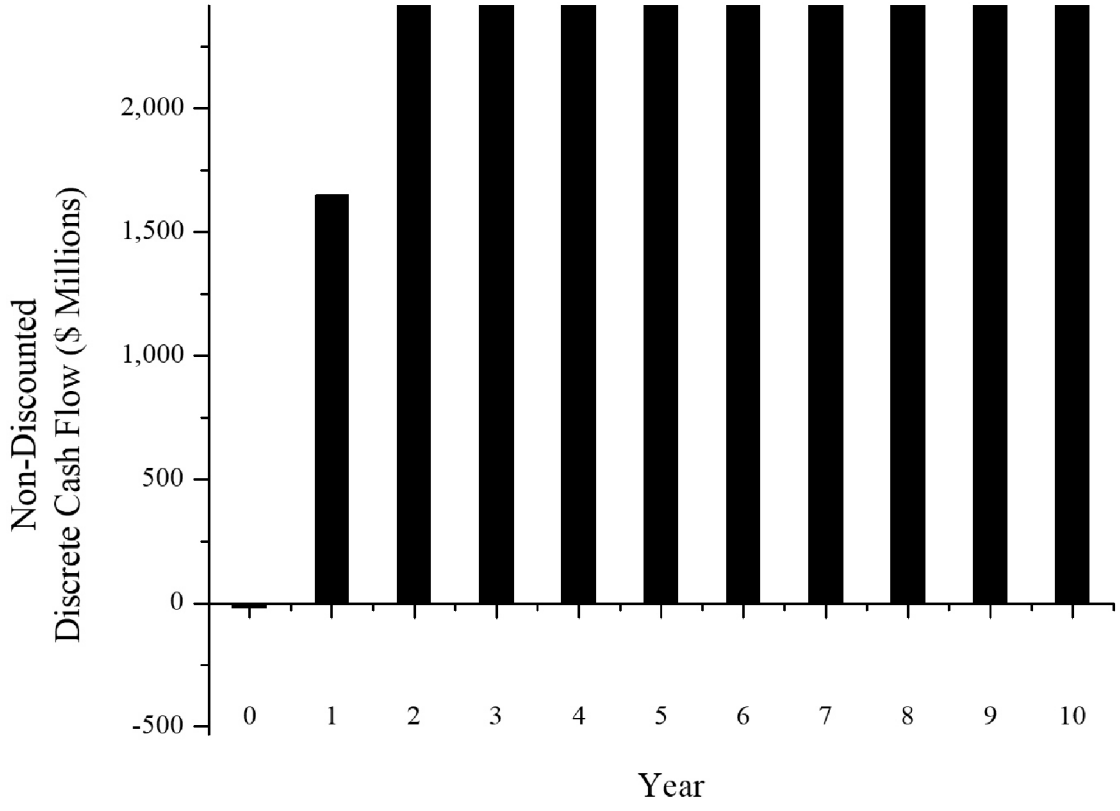

Figure IV.D.4-1: Non-discounted cash flow over the first 11 years of the plant.

IV.E. Profitability Analysis

The discounted cash flow rate determines if the plant is economically viable. The basis for profitability can either be time, cash, or interest rate. In this case, the internal rate of return (IRR) was calculated to determine profitability. The IRR is the interest rate at which the net present value (NPV) of all the cash flows equals zero and is given in Equation IV.E.1.

$$0 = NPV = \sum_{t=0}^{n} \left(\frac{CF_t}{(1+r)^t} \right) \qquad (IV.E.1)$$

where NPV is the net present value in dollars, CF_t is cash flow at year t, and r is the IRR.

We used Microsoft Excel's Goal Seek function to calculate the IRR which was more than 9,500% over an 11 year period. This is considered an extremely opportunistic investment. Plants rarely have IRRs this high, and in this case, is likely due to the plant's extremely high annual revenue compared to its relatively low fixed capital costs.

IV.F. Economic Summary

This plant is economically feasible and incredibly profitable from selling Cu and Au. The non-discounted cash flow rate indicates profit gains within as little as one year after plant construction. Although this does not consider interest rates, the IRR over an 11-year period is well over 9,500%, indicating that our process is a very good investment.

V. ENVIRONMENTAL CONSIDERATIONS

Currently, the vast majority of WEEE is either sent to landfills or exported to less developed countries, and so any solution that can both recover resources from WEEE and put less strain on conventional disposal routes would be a benefit to the environment. The steam gasification of WEEE in a MSR should greatly reduce the output of toxic gases and also produce syngas, a fuel or useful chemical intermediate. The syngas produced in this process is burned to heat the MSR, R-101, which reduces additional energy consumption and environmental impact.

This plant's estimated carbon footprint is 45,900 tons per year. The metal recovery produces a considerable amount of hazardous waste. However, all hazardous streams are disposed of by licensed professionals following environmental guidelines. Instead of electronic devices crowding landfills, their useful components can be recovered and their hazardous components can be concentrated and disposed of more effectively.

V.A. Block A: MSR and Metal Processing Environmental Considerations

V.A.1. Solder

The MSR's high operating temperature produces a phase of molten metals which are removed as a waste stream. These metals, i.e., lead, zinc, and tin, come from the soldered connections in the WEEE and can be reused as solder with minimal post-processing. The solder is saleable and has minimal negative environmental impacts because we expect to recover 99% of the input solder. Trace amounts of tin, lead, and zinc not recovered in this stream will be safely disposed of with the leach residue waste out of Block C, Au Recovery.

V.A.2. Saltwater

The Rinse Bath, X-101, elutes 3,600 L/h of water containing 21.1 g/L of LNK salt, i.e., 272.7 kg/h of potassium carbonate, sodium carbonate, and lithium carbonate each, and trace amounts of bromine, and needs to be disposed of properly. According to their MSDS sheets, potassium carbonate and sodium carbonate are both classified as having little to no risk to the environment, low toxicity to aquatic marine organisms, and no bioaccumulation (*Potassium Carbonate Safety Data Sheet*, 2004; *Sodium Carbonate Safety Data Sheet*, 2013). However, their disposal methods require licensed disposal contractors, and they must be treated as hazardous. Also, state and local regulations must be followed, depending on facility siting. Lithium carbonate is listed as moderately toxic to aquatic life, and its disposal also requires licenced disposal contractors (*Lithium Carbonate Safety Data Sheet*, 2001). To reduce this waste stream's volume and to save on material costs, a salt recovery unit which could either evaporate the wash water or use a filtration system to recover the salt should be considered.

V.B. Block B: Copper Recovery Environmental Considerations

V.B.1. Copper Purge Stream

The Cu recovery purge stream contains many heavy metals not suitable for the environment. These metals include iron, tin, zinc, lead, gold, nickel, and palladium, in

descending order of concentration, and are dissolved in 5M HCl. The concentrations of valuable metals should be small, and so we considered this stream to be worthless. The HCl needs to be neutralized with an equimolar amount of NaOH and disposed of by a licenced disposal contractor.

We assumed the solvents used for Cu extraction in R-202 and V-201 are immiscible, but organic entrainment could cause trace Cyanex 921 and kerosene to be in the purge stream. Cyanex 921 is an acute and chronic hazard to aquatic life. Kerosene is toxic to aquatic life with long lasting effects.

V.B.2. HCl and Hydrogen Gas

Both HCl vapor and H_2 gas evolve from the Cu leaching agitation tank, R-201, and need to be vented. The amount of gases produced was not estimated due to a lack of data on the multitude of reactions that occur during leaching. Experimentation on pilot scale leaching agitation tanks is needed to characterize gas production. If substantial amounts of HCl are generated, a gas scrubber must remove the HCl from the H_2 gas so that it can be neutralized and discarded. If a small amount of H_2 gas is produced, it can be sent to a flare to be burned. If a substantial amount of H_2 gas is generated, it may be worth combining it with the syngas stream for additional energy recovery.

V.C. Block C: Gold Recovery Environmental Considerations

V.C.1. Solid Waste

The solid, leach residue waste stream removed from the leaching agitation tank, R-301, contains all of the glass, refractory oxides, and char which were not gasified in the MSR, R-101. Also, all of the metals not leached or recovered will end up in this stream, making this the metaphorical “bottoms” of the process. This stream includes iron, nickel, tin, zinc, lead, silver, gold, palladium, and trace amounts of copper. The stream retains some thiourea and H_2SO_4. This stream may have value because it contains precious metals; however, due to the toxic nature of being the bottoms waste of the entire process, this stream is considered hazardous waste and needs to be disposed of by licenced disposal contractors, most likely by deep welling.

V.C.2. Gold Purge Stream

The Au purge stream has the majority of the silver from WEEE, as well as some gold and copper. These metals are dissolved in a solution of thiourea, ferric sulfate, and sulfuric acid. Silver recovery would branch off from this stream as the next expansion to this plant which we recommend as an area of improvement. This stream has clear intrinsic value, and it would be wasteful to discard it. We imagine that a company specializing in silver recovery would be willing to buy this stream. However, because the purge stream’s value is difficult to determine, we will conservatively estimate its value to be zero for our economic analysis.

V.D. Block D: Syngas Stream Environmental Considerations

V.D.1 Gas Waste

Gaseous products from the MSR, R-101, result from the gasification and combustion of the plastic components of WEEE. This stream was expected to contain CO, CO_2, H_2, and HCN, but Aspen Plus predicted that only CO, H_2, and HCN were present. We believe that this is due to a small oxygen flowrate.

The gases can be further combusted to heat MSR, R-101. Complete combustion of these gases, at stoichiometric conditions, will yield CO_2, NO_x, and water vapor, which are the same gases that evolve from any hydrocarbon combustion and are common industrial and tailpipe emissions. We expect a carbon footprint of 45,900 tons of CO_2 to be produced per year. NO_x and CO concentrations should be carefully measured to control how much air is provided for combustion. Any CO indicates that not enough air is provided, and too much NO_x indicates that too much air is provided. Therefore, the ideal amount of air produces the least amount of NO_x while also minimizing CO. NO_x production should be minimized because it contributes to photochemical smog and acid rain. CO should be minimized because it also contributes to photochemical smog and increases levels of direct greenhouse gases, such as methane.

VI. SAFETY CONSIDERATIONS

VI.A. Upstream Safety: Explosion, Burn, and Mechanical Hazards

VI.A.1. Explosion and Burn Hazards

Explosion hazards.

The high operating temperatures and explosion potential of the MSR, R-101, are critical safety considerations. The high temperatures necessitate proper PPE and safety training for anyone working near the MSR. All entrained moisture must be removed from the WEEE before entering into the MSR, R-101. Even small amounts of trapped water are dangerous. OSHA reported an incident in which an operator dipped a used towing bar into a molten salt dip tank, and the water entrained in the towing bar's welded tube sections vaporized and caused an explosion. This ruptured the dip tank, violently killed the operator, and injured two other operators (OSHA, 2010).

The combustion of plastic to produce syngas can be hazardous within a pressurized vessel, and so the oxygen flowrate into the MSR needs to be monitored. A runaway reaction is unlikely because the oxygen supply can be controlled, but in that unlikely event, an emergency stop should cut off the steam and air supply to the MSR, and an installed explosion vent should prevent unwanted pressure buildup.

Burn hazards.

Contact with the molten salt would cause third degree burns. Dumping WEEE into the MSR, R-101, should not pose a splashing hazard of molten liquid because of the proposed lock hopper mechanism and closed reactor design. However, if the reactor were to rupture, the molten salt would be dangerous. The MSR should be equipped with pressure relief safeties and reinforced to mitigate the chance of a leak or explosion. Burn treatment kits should be provided on-site.

VI.A.2. Mechanical Hazards

The metal processing equipment in Block A poses physical and mechanical hazards. The WEEE is moved on a conveyor belt, which is a pinching hazard. Loose clothing could become caught in the moving belt. The dryer, X-102, operates at high temperatures and could cause burns. The crusher, X-103A/B, is a pinching hazard and moving equipment hazard. Proper guards must be installed to prevent anyone from reaching any moving parts or blades while the crusher is running. Proper lock-out-tag-out procedures must be followed for all equipment.

VI.B. Downstream Safety: Chemical and Electrical Hazards

Most of the downstream process operates at ambient temperatures and pressures, and so the remaining safety considerations involve chemical and electrical hazards.

VI.B.1. Chemical Hazards

Acidic hazards.

Acidic solutions are used to recover copper and gold. Copper is leached in a 5M HCl lixiviant, which can cause severe skin burns and eye damage. Similarly, gold is leached in an acidic solution (pH = 1), adjusted by H_2SO_4, which can cause severe skin burns. Both electrowinning steps require concentrated H_2SO_4. Emergency eyewash and shower stations should be placed throughout the entirety of the plant. Proper training and PPE are required, including corrosion-resistant outerwear and footwear, goggles, face masks, and resistant gloves. We do not anticipate handling fuming acids, and so respiratory protection should not be needed, but the plant should be well-ventilated to prevent the gradual buildup of fumes.

Organic hazards.

Thiourea, used in gold leaching, has several safety benefits over cyanide, but it is a suspected carcinogen (Marsden & House, 2006). Cyanex 921, i.e., trioctylphosphine oxide, causes skin irritation and serious eye damage (*Trioctylphosphine Oxide Safety Data Sheet*, 2020). Kerosene is combustible, may be fatal if swallowed or enters airways, causes skin irritation, and may cause drowsiness or dizziness (*Kerosene Safety Data Sheet*, 2020).

Gaseous hazards.

Gaseous H_2 and HCl vapor may exit the Cu Agitated Leaching Tank, R-201. H_2 gas is flammable and poses an explosion hazard. HCl vapor is corrosive and could destroy equipment and injure workers.

VI.B.2. Electrical Hazards

There are two electrowinning units: one for copper and one for gold. Both operate at a high electrical current: 90,720 A for copper, and 21,500 A for gold. Contact with 20 mA of current can be fatal, and so precautions must be taken when operating around these devices (Fish & Geddes, 2009). Only trained professionals should be allowed to operate directly on electrical equipment. These individuals must wear insulating protective equipment such as rubber gloves and boots, non-conductive clothing, and protective equipment. Additional considerations include disallowing metal jewelry, and potentially allowing for eye, face, and hearing protection if arc flash explosions are possible (*Electrical Personal Protective Equipment*, n.d.).

VII. SOCIAL CONSIDERATIONS

VII.A. Political and Social Impacts

As the global abundance of electronic devices grows, so too does the amount discarded in landfills. Unfortunately, only 20% of WEEE is properly recycled, with the other 80% reported to be improperly discarded. Substandard recycling practices are becoming more problematic in less developed countries. East Africa in particular has become a dumping ground for WEEE. In addition to the exported waste from more developed countries, rising wages and increased accessibility to electronic devices has increased WEEE recycling jobs in areas like East Africa (Nkinzingabo, 2019). However, working conditions are extremely poor, and environmental damage is immense. For example, the preferred method to recover copper from WEEE in Ghana is to burn insulated wires on open fires to remove the insulation which produces smoke containing dioxin, heavy metals, and other highly toxic pollutants (Minter, 2016). Computers and cellphones are dismantled and circuit boards are "cooked," often within domestic housing, exposing families to dioxin and heavy metals (Mansell & Raboy, 2011). Lead-acid batteries are cut open with machetes and the battery acid dumped onto the ground by hand, polluting the groundwater (Nkinzingabo, 2019). Excess waste beyond what can be processed by hand merely sits in open dumping grounds, leaching more chemicals into the groundwater.

The adoption of a systematic, industrial-scale process for recycling WEEE would not stop these unregulated practices, but would reduce the accumulation of waste exported by the United States. This could reduce local groundwater pollution and may encourage safer handling and disposal methods. Also, our process' molten LNK salt breaks down hazardous chemicals like dioxin. Furthermore, by making WEEE disposal a regulated process, communities make a positive impact on the environment. If more plants like this one were built, especially in areas where unsafe and risky metal recovery from dumped WEEE is rampant, then those communities may reap benefits from environmental health, safety, and profit.

This plant may find support and collaboration with local communities and governments because it would create jobs and benefit the environment. Social and political factors could affect the plant. For instance, governmental policies and local attitudes toward recycling may affect the price, quality, and abundance of input WEEE. Carbon emission regulations may restrict the burning of syngas. If more environmentally sustainable practices were adopted worldwide, perhaps landfilling, open dumping, and improper handling of WEEE could become a thing of the past.

VII.B. Plant Siting

In deciding where to site the plant, it is imperative to consider both technical and socioeconomic factors. With regards to technology, we prefer an area with a lower ambient temperature because the WEEE Heap, E-101, involves cooling solids with ambient air. More importantly, we prefer a location that will allow for a greater temperature differential for the Cu spent electrolyte heat exchanger, E-202, which cools a 45°C liquid stream to 20°C. To efficiently achieve this, the cooling water must be colder than 20°C, which is easier to achieve in areas with dry air and lower dew points.

Logistically and socially, it would be best to site somewhere that produces an abundance of WEEE and that already incentivizes WEEE recycling. Thus, California is a prime state for siting. Not only is it one of the largest producers of WEEE in the United States, but also California has passed several laws regarding proper e-waste recycling, such as the *Electronic Waste Recycling Act of 2003*, which places a fee on most electronic devices and funds state efforts to collect and treat WEEE (*California's E-Waste Disposal Crisis*, 2015; CalRecycle, 2020). California even has a fee associated with not recycling e-waste (*Electronic Waste Recycling*, n.d.). Furthermore, locating somewhere that already has established WEEE handling systems helps our design which does not handle pretreatment. Our economic analysis assumes that it costs nothing to acquire a large amount of WEEE which is likely unrealistic. Siting near a community of frequent recyclers could ease WEEE procurement.

Economically, we hope to site somewhere with abundant and cheap land. Locating near a city is expensive and unlikely to be allowed under plant siting ordinances. Therefore, the plant must be located somewhere more rural.

We propose siting on the eastside of northern California. The rural areas surrounding Adin, CA may be ideal because Adin's average dew point is near 8°C in July (*Adin, CA Climate*, 2020). Potential downsides include high taxes and stricter carbon emission regulations. Also, Adin is far from any urban center, e.g., is about 300 miles from San Francisco, and so it may be difficult to hire skilled workers.

VIII. FINAL RECOMMENDED DESIGN

VIII.A. Overall Design Specifications

Every major piece of purchased equipment is given in Table VIII.A.1-1.

Table VIII.A.1-1. Equipment Summary for Entire Process

Equipment ID	Name	Equipment Type
Block A		
R-101	Molten Salt Reactor	Reactor
E-101	WEEE Heap	Heat Exchanger
X-101	Rinse Bath	Vessel
X-102	Dryer	Dryer
X-103	Crusher	Crusher
X-104	Magnetic Separator	Magnetic Separator
Block B		
R-201	Cu Agitated Leaching Tank	Reactor
R-202	Cu Extraction Mixer	Mixer
V-201	Cu Extraction Settler	Settling Pond
R-203	Cu Stripping Mixer	Mixer
V-202	Cu Stripping Settler	Settling Pond
R-204	Cu Electrowinning Cells	EW Cells
E-201	Cu Spent Electrolyte Heat Exchanger	Heat Exchanger
E-202	Cu Electrowinning Heat Exchanger	Heat Exchanger
P-201	Cu PLS Pump	Centrifugal Pump
P-202	Cu Raffinate Pump	Centrifugal Pump
P-203	Cu Stripped Organic Pump	Centrifugal Pump
P-204	Cu Loaded Organic Pump	Centrifugal Pump
P-205	Cu Spent Electrolyte Pump	Centrifugal Pump
P-206	Cu Loaded Electrolyte Pump	Centrifugal Pump
Block C		
R-301	Au Agitated Leaching Tank	Reactor
T-301	Au Adsorption / Elution Column	Tower
R-302	Au Electrowinning Cells	EW Cells
E-301	Au Advance Electrolyte HE	Heat Exchanger
E-302	Au Electrowinning HE	Heat Exchanger
P-301	Au PLS Pump	Centrifugal Pump
P-302	Au Raffinate Pump	Centrifugal Pump
P-303	Au Spent Electrolyte Pump	Centrifugal Pump
P-304	Au Loaded Electrolyte Pump	Centrifugal Pump

VIII.B. Block A: MSR and Metal Processing Design Specifications

VIII.1. Block A Equipment Summary

Block A requires a MSR, heat exchanger, rinse bath, cusher, dryer, and magnetic separator. The equipment summary for Block A is given in Table VIII.B.1-1.

Table VIII.B.1-1. Equipment Summary for Molten Salt Reactor, R-101, and Preliminary Metal Processing

Equipment ID	Name	Equipment Type	Design Specification
R-101	Molten Salt Reactor (MSR)	Reactor	MOC: Hastelloy C276 Temperature 675 °C Pressure 2 bar Solid input 10,089 kg/h Residence time 30 min Capacity 480 ft^3 13.6 m^3 Dimensions 4′ × 20′ × 6′
E-101	WEEE Heap	Heat Exchanger	WEEE is cooled in a heap by convection
X-101	Rinse Bath	Vessel	MOC: Polyethylene Temperature ambient Pressure ambient Vol. flow rate 10 L/s Capacity 19,000 L Dimensions 211″ × 102″ × 96″ Make Norwesco Model 44877
X-102	Dryer	Dryer	Temperature 250 °C Pressure ambient Length 12 ft
X-103A	Shear Shredder	Crusher	Shear shredder, particle size: 10mm, surface Gauss, 700 G Make SOYU Model SYU80300 Dimension 8300×2900×4200 mm Motor Power 2×225 kW
X-103B	Hammer Shredder	Crusher	Swing hammer, particle size: 5mm, surface Gauss, 3,000 G Make HJ brand Model PSJ-750 Motor Power 6000 kW
X-104	Magnetic Separator	Magnetic Separator	Four (4) cross-belt magnetic separators Temperature ambient Pressure ambient Loading 10-15 TPH 3,000 G Motor Power 7.5 kW

VIII.C. Block B: Copper Recovery Design Specifications

VIII.1. Copper Recovery Equipment Overview

Block B requires 12 leaching agitation tanks in parallel, two mixer-settlers, and an electrowinning unit. Additionally, it requires six pumps (not including spares) and two heat exchangers.

VIII.2. Copper Leaching Equipment Summary

The equipment summary for Cu leaching is given in Table VIII.C.2-1.

Table VIII.C.2-1. Equipment Summary for Copper Leaching

Equipment ID	Name	Equipment Type	Design Specification	
R-201	Cu Agitated Leaching Tank	Agitation Tank	MOC: XLPE-lined carbon steel	
			Impellers: (2) 45° PBT	
			Temperature	ambient
			Pressure	ambient
			Volumetric flow rate	1000 m^3/h
			Solid input	10,089 kg/h
			Make	Xinhai
			Model	SJ8.5X9.0
			Number of tanks (parallel)	12
			Capacity	480 m^3
			Diameter	8.5 m
			Height	9.0 m
			Bottom impeller clearance	2.8 m
			Top impeller clearance	5.7 m
			Impeller diameter	3.3 m
			Impeller height	0.66 m
			Baffle width	0.71 m
			Number of baffles	4
			Impeller speed	18.5 RPM
			Power	15.7 kW

VIII.3. Copper Extraction Equipment Summary

The equipment summary for Cu extraction is given in Table VIII.C.3-1.

Table VIII.C.3-1. Equipment Summary for Copper Extraction

Equipment ID	Name	Equipment Type	Design Specification
R-202	Cu Extraction Mixer	Mixer	MOC: XLPE-lined carbon steel Impeller: (1) Lightnin A310 Temperature ambient Pressure ambient Flowrate 2000 m^3/h Capacity 100 m^3 Diameter 5.0 m Height 5.5 m Impeller clearance 1.83 m Impeller diameter 1.6 m Impeller height 0.32 m Baffle width 0.42 m Number of baffles 4 Impeller speed 19.9 RPM Power 0.10 kW
V-201	Cu Extraction Settler	Settling Pond	MOC: HDPE-lined concrete Temperature ambient Pressure ambient Flowrate 2000 m^3/h Settling rate 4 m^3 / m^2 h Settling velocity 7.2 m/h Residence time 0.25 h Length, Width 22.36 m Depth 1.0 m
P-201	Cu PLS pump	Centrifugal Pump	1000 m^3/h, 1.05 bar pressure drop, 29.0 kW
P-202	Cu Raffinate pump	Centrifugal Pump	1000 m^3/h, 1.52 bar pressure drop, 42.3 kW

VIII.4. Copper Stripping Equipment Summary

The equipment summary for Cu stripping is given in Table VIII.C.4-1.

Table VIII.C.4-1. Equipment Summary for Copper Stripping

Equipment ID	Name	Equipment Type	Design Specification
R-203	Cu Stripping Mixer	Mixer	MOC: XLPE-lined carbon steel Impeller: (1) Lightnin A310 Temperature ambient Pressure ambient Flowrate 1250 m^3/h Capacity 100 m^3 Diameter 4.3 m Height 4.3 m Impeller clearance 1.5 m Impeller diameter 1.6 m Impeller height 0.32 m Baffle width 0.375 m Number of baffles 4 Impeller speed 19.9 RPM Power 0.10 kW
V-202	Cu Stripping Settler	Settling Pond	MOC: HDPE-lined concrete Temperature ambient Pressure ambient Flowrate 1250 m^3/h Settling rate 4 m^3 / m^2 h Settling velocity 7.96 m/h Residence time 0.25 h Length, Width 17.7 m Depth 1.0 m
P-203	Cu Stripped Organic Pump	Centrifugal Pump	1000 m^3/h, 1.03 bar pressure drop, 28.7 kW
P-204	Cu Loaded Organic Pump	Centrifugal Pump	1000 m^3/h, 0.94 bar pressure drop, 26.0 kW

VIII.5. Copper Electrowinning Equipment Summary

The equipment summary for Cu electrowinning is given in Table VIII.C.5-1.

Table VIII.C.5-1. Equipment Summary for Copper Electrowinning

Equipment ID	Name	Equipment Type	Design Specification
R-204	Cu Electrowinning	EW Cells	MOC: HDPE-lined concrete 2665 electrode pairs, 84 pairs/cell, 32 cells 2.4 m^2 SS cathodes, 1.98 m^2 Pb anodes 14.4 m^3 cells filled with $CuSO_4 + H_2SO_4$ Harvest one third of cathodes per day Temperature 45 °C Pressure ambient Flowrate 250 m^3/h Residence time 0.058 h Current density 450 A/m^2 Efficiency 97 % Power 5800 kW Cells 32
P-205	Cu Loaded Electrolyte Pump	Centrifugal Pump	250 m^3/h, 1.71 bar pressure drop, 11.9 kW
P-206	Cu Spent Electrolyte Pump	Centrifugal Pump	250 m^3/h, 1.71 bar pressure drop, 11.9 kW
E-201	Cu Spent Electrolyte Heat Exchanger	Countercurrent Shell and Tube Heat Exchanger	MOC: carbon steel shell; 0.25in, schedule 40, 316 stainless steel tubes; 1 shell pass, 1 tube pass; cooling water in shell. 6 HE in series. Total length 27.8 m Number of tubes 500 Heat transfer area 599.6 m^2 Water flowrate 209.6m^3/h Electrolyte flowrate 250 m^3/h Water inlet temperature 10°C Water outlet temperature 40°C Electrolyte inlet temperature 45°C Electrolyte outlet temperature 20°C
E-202	Cu Electrolyte Heater	Resistive Heating Element	MOC: RW80 nichrome heating element wire, 22mm diameter, 222m length, coiled inside the perimeter of EW tank Temperature 700°C Pressure ambient Flowrate 250 m^3/h Voltage 2000 V Current 2112 A Loading 28.23 W/cm^2 Temperature change 14.7°C

VIII.D. Block C: Gold Recovery Design Specifications

VIII.D.1. Gold Recovery Equipment Overview

Block C requires one leaching agitation tank, two trains of 21, activated carbon packed columns, and an electrowinning unit. Additionally, it requires four pumps and two heat exchangers.

VIII.D.2. Gold Leaching Equipment Summary

The equipment summary for Au leaching is given in Table VIII.D.2-1.

Table VIII.D.2-1. Equipment Summary for Gold Leaching

Equipment ID	Name	Equipment Type	Design Specification		
R-301	Au Agitated Leaching Tank	Agitation Tank	MOC: XLPE-lined carbon steel		
			Impellers: (2) 45° PBT		
			Temperature	ambient	
			Pressure	ambient	
			Batch time	7	h
			Batch volume	236.16	m^3
			Solids input per batch	47232	kg
			Make	Xinhai	
			Model	SJ7.0X7.5	
			Capacity	269	m^3
			Diameter	7.0	m
			Height	7.5	m
			Bottom impeller clearance	2.3	m
			Top impeller clearance	4.7	m
			Impeller diameter	2.4	m
			Impeller height	0.48	m
			Baffle width	0.58	m
			Number of baffles	4	
			Impeller speed	21	RPM
			Power	4.7	kW
P-301	Au PLS Pump	Centrifugal Pump	236 m^3/h, 0.83 bar pressure drop, 5.5 kW		
P-302	Au Raffinate Pump	Centrifugal Pump	236 m^3/h, 1.47 bar pressure drop, 9.6 kW		

VIII.D.3. Gold Adsorption, Elution, and Electrowinning Equipment Summary

The equipment summary for Au adsorption, elution, and electrowinning is given in Table VIII.D.3-1.

Table VIII.D.3-1. Equipment Summary for Gold Adsorption, Elution, and Electrowinning

Equipment ID	Name	Equipment Type	Design Specification
T-301	Au Adsorption & Elution Column	Tower	MOC: rubber-lined mild steel Packing: 2.38 mm activated carbon Volume 15.9 m^3 Diameter 1.5 m Height 9 m Flowrate 10.8 m^3/h Number of columns 21 Number of trains 2 Pressure drop 0.073 bar **Adsorption** Temperature ambient Pressure ambient Load time 1.04 h Load volume 0.71 CV **Elution** Temperature 80 °C Pressure ambient Elution time 9.3 h Eluate volume 6.3 CV
R-302	Au Electrowinning	EW Cells	MOC: HDPE-lined concrete 86 electrode pairs, 43 pairs/cell, 2 cells 0.5 × 1 × 0.003 m steel wool cathodes 0.4 × 0.9 × 0.006 m stainless steel anodes 14.4 m^3 cells filled with $CuSO_4$ & H_2SO_4 Harvest cathodes every 12 days. Temperature 45 °C Pressure ambient Flowrate 250 m^3/h Residence time 5 h Current density 500 A/m^2 Efficiency 7 % Power 86 kW
P-303	Au Spent Electrolyte Pump	Centrifugal Pump	2,056 m^3/h, 2.14 bar pressure drop, 122 kW
P-304	Au Advance Electrolyte Pump	Centrifugal Pump	2,056 m^3/h, 1.52 bar pressure drop, 87.0 kW

Table VIII.D.3-1. Equipment Summary for Gold Adsorption, Elution, and Electrowinning Continued

Equipment ID	Name	Equipment Type	Design Specification
E-301	Au Loaded Electrolyte Heat Exchanger	Countercurrent Shell and Tube Heat Exchange	MOC: carbon steel shell; 1in, schedule 40, 316 stainless steel tubes; 1 shell pass, 1 tube pass; cooling water in shell. Length 5.8 m Number of tubes 175 Heat transfer area 94.3 m^2 Water flowrate 39.8 m^3/h Electrolyte flowrate 10.8 m^3/h Water inlet temperature 17 °C Water outlet temperature 30 °C Electrolyte inlet temperature 80 °C Electrolyte outlet temperature 26.1 °C
E-302	Au Spent Electrolyte Heater	Resistive Heating Element	MOC: RW80 nichrome heating element wire, 3.0mm diameter, 80m length, coiled inside the return piping to the stripping column. Temperature 700 °C Pressure ambient Flowrate 10.8 m^3/h Voltage 2000 V Current 112 A Loading 29.87 W/cm^2 Temperature change 20 °C

IX. CONCLUSIONS AND RECOMMENDATIONS

IX.A. Conclusions

A total of 181.5 kt/a (18,800 kg/h) of WEEE is fed to the process, and 31.9 kt/a Cu and 0.151 kt/a Au are recovered, which would otherwise be lost to landfills. The process requires upwards of 1,160 kW of additional power. The projected startup costs of this process total more than $17 million, with a yearly non-discounted cash flow of about $3.4 billion, and an IRR over 11 years of over 9,500%. The process is both profitable and environmentally conscious.

Based on the economic analysis, we recommend building this process. The base revenue from selling copper and gold alone is $7.4 billion per year. Gold constitutes almost all of the revenue despite accounting for a small fraction (i.e., <1%) by mass of the processed material.

We suggest siting the plant somewhere with a low dew point, relatively low, average ambient temperatures, and with abundant access to WEEE. Therefore, we suggest siting near Adin, CA.

Significant safety and environmental concerns are posed by this process. The MSR, R-101, must be carefully pressure-controlled to reduce the risk of rupture or explosion. Dangerous solvents are used, including carcinogenic organic solvents and highly corrosive acids. Safety must be stressed, especially during disposal.

Most of the direct annual costs come from waste disposal. Toxic waste streams should be deep-welled or otherwise properly treated if this process is to have a net positive environmental impact. Because waste disposal is expensive, future work should minimize waste production.

We assumed that the input WEEE has a constant composition and flowrate and can be acquired for free, with no cost of pretreatment. The latter two are especially poor assumptions; we expect transporting solids to have substantial costs, and electronic devices may someday be manufactured with less precious metals. We also assumed that the value of gold and copper would not change for the next 11 years. Most of this design's data was taken from lab-scale studies, but when possible we used conservative estimates for unknown values.

Other design challenges that engineers must address include the MSR's lock hopper design. We did not explicitly design a mechanism that would allow solids to be removed from the MSR. Indeed, this design may be extremely challenging to build on a large-scale.

This process is a great investment in terms of projected revenue and has many potential environmental and societal benefits. We offer our highest recommendation to build this process.

IX.B. Recommendations

IX.B.1. Overall Process Recommendations

We recommend exploring the recovery of other precious metals, such as silver and palladium. For example, the Au raffinate stream is silver-rich, but all of the silver is lost to the purge stream or to the solid waste. Also, the physical properties of each mixture stream should be found or estimated more accurately. For example, the density of isopropanol in water as a function of temperature has been estimated experimentally by Lebo (1921).

IX.B.2. Block A, MSR and WEEE Treatment Recommendations

We recommend designing a salt recovery unit to recycle the LNK salt leaving with the saltwater eluting from the Rinse Bath, X-101, back into the MSR, R-101. This would reduce raw material costs. We considered evaporating the water to recover the salt; however, this method was too energy intensive. To achieve salt recovery, a filtration system may be necessary.

IX.B.3. Block B, Copper Recovery Recommendations

For Cu leaching, we assumed the other metals' leach fractions and concentrations were trivial. Kinetic leaching data for each metal in 5M HCl with air sparging should be collected to optimize this design. A CCD also must be designed to separate the solid leach residue from the PLS. For Cu extraction, the *selective* extraction of cupric ions into Cyanex 921 likely depends on pH. Cyanex 921 can also extract Fe. We recommend that the pH of our PLS be optimized for cupric ion selectivity with additional data.

IX.B.4. Block C, Gold Recovery Recommendations

For Au leaching, a CCD must be designed to separate the solid leach residue from the PLS. Xinhai Mineral Processing EPC manufactures Washing Thickeners for Au-pregnant cyanide solutions. For Au adsorption, a CIP, CIL, or CIC circuit should be designed. An acid wash should be added before the elution column, T-301. Data for Au adsorption onto activated carbon at the specified operating conditions (e.g. TU concentration and carbon particle size) would improve the column design.

IX.B.5. Block D, Syngas Recommendations

We recommend designing Block D, which we black-boxed to reduce our process' scope. The needed equipment depends on the intended use for syngas. If the syngas is to be burned, we recommend optimizing the operating conditions of the MSR, R-101, to produce the best syngas composition and designing a turbine. If the syngas is to be a chemical intermediate, then we recommend designing a gas scrubber to remove HCl from the gas stream. Syngas can be converted into useful hydrocarbons via the Fischer-Tropsch process. Both an economic and environmental analysis should assess what should be pursued for Block D.

X. ACKNOWLEDGEMENTS

We would like to thank Professor Eric W. Anderson of the Department of Chemical Engineering at the University of Virginia for his guidance and insight throughout the entirety of the project.

XI. TABLE OF NOMENCLATURE

Symbol	unit	Description
ε	-	Interphase porosity
ζ	-	Current efficiency
λ	W / m K	Thermal conductivity
μ	Pa s	Viscosity
μ_C	Pa s	Continuous phase viscosity in mixer-settler mixer
μ_D	Pa s	Dispersed phase viscosity in mixer-settler mixer
μ_M	Pa s	Mixture viscosity in mixer-settler mixer
ρ	kg/m^3	Density
ρ_C	kg/m^3	Continuous phase density in mixer-settler mixer
ρ_D	kg/m^3	Dispersed phase density in mixer-settler mixer
ρ_i	kg/m^3	Density of species *i*
ρ_M	kg/m^3	Mixture density in mixer-settler mixer
τ	s	Space time
φ_C	-	Continuous phase volume fraction in mixer-settler mixer
φ_D	-	Dispersed phase volume fraction in mixer-settler mixer
Φ	-	Phase ratio in packed column
A	min^{-1}	Pre-exponential factor
A_0	m^2	Heat transfer area
A_{set}	m^2	Settling zone area
Ag	-	Silver
Au	-	Gold
b	-	Empirical constant for a Langmuir-Freundlich isotherm
C	m	Impeller clearance
C_{Au}	mM	$AuTU_2^+$ concentration in activated carbon packed column, T-301
C_F	g/L	Column feed concentration
$C_{E,i}$	USD	Purchased cost of equipment *i*
$C_{i,P,\mathrm{X}}$	g/L	Concentration of species *i* in purge stream in Block *X*
$C_{i,PLS,\mathrm{X}}$	g/L	Concentration of species *i* in PLS in Block *X*
$C_{i,R,\mathrm{X}}$	g/L	Concentration of species *i* in recycle stream in Block *X*
$C_{i,Raff,\mathrm{X}}$	g/L	Concentration of species *i* in raffinate in Block *X*
$C_{i,\mathrm{X}}$	g/L	Concentration of species *i* in Block *X*, all streams
Cl^-	-	Chloride ion
$C_{P,i}$	J/K	Heat capacity of species *i*
Cu	-	Copper
Cu^{2+}	-	Cupric ion

$CuCl_2^-$	-	Cupric chloride
C_{TM}	USD	Total capital plant cost
d_d	m	Dispersed droplet diameter
d_i	m	Impeller diameter
d_p	m	Column packing particle diameter
D	m	Diameter
D_c	m	Column diameter
e^-	-	Electron
E	J	Reaction activation energy
ΔE^o	J/C	Standard Cell Potential
E_{cell}	J/C	Cell Potential
$E_{i,\mathrm{X}}$	-	Fraction of metal *i* leached in Block *X*
$f_{mag,i}$	-	Fraction of metal *i* removed by magnetic separation, X-104
F	C mol^{-1}	Faraday's Constant
F_c	-	Correction factor for multiple shell and tube passes
Fe	-	Iron
Fe_{in}	kg/s	Mass flow of iron into magnetic separation
Fe_{out}	kg/s	Mass flow of iron out of magnetic separation
F_{Lang}	-	Lang Factor constant
g	m/s^2	Gravitational acceleration
g_c	m/s^2	Gravitation constant
G_{rxn}	kg / m^2 s^2	Gibbs Free Energy of a reaction
h	W / m^2 K	Convective heat transfer coefficient
h_{drop}	m	Vertical distance traveled by a dispersed drop
h_i	W / m^2 K	Inner heat transfer coefficient
h_o	W / m^2 K	Outer heat transfer coefficient
H	m	Tank liquid height
H^+	-	Hydrogen ion
H_2O	-	Water
$H_{fus,i}$	kg / m^2 s	Heat of fusion of species *i*
ΔH_{rxn}	kg / m^2 s	Change in enthalpy of a reaction
I	A	Electrical current
J	m	Baffle width
k	min^{-1}	Reaction rate constant
K	-	Reaction equilibrium constant
L	-	Cyanex 921, organic extractant
L_c	m	Column height
$m_{au,T\text{-}301}$	kg	Amount of Au loaded in one T-301 column
$\dot{m}_i$	kg/h	Mass flowrate of species *i* through MSR

$m_{i,X}$	kg/h	Mass flowrate of species *i* in Block *X*
$m_{i,in,X}$	kg/h	Input mass flowrate of species *i* in Block *X*
m/t	kg/h	Electroplating rate
m_{WEEE}	g/h	Input mass flowrate of WEEE into MSR
M_{Cu}	g/mol	Molecular mass of copper
MOC	-	Material of construction
M^{n+}	-	Metal cation
n	-	Number of items
N	s^{-1}	Impeller revolutions per second (RPS)
N_c	-	Number of columns in parallel
N_{np}	-	Number of nonparticulate processing steps
N_{OL}	-	Number of operators per shift
N_{Po}	-	Dimensionless Power Number
N_{trains}	-	Number of trains
Nu	-	Nusselt number
O_2	-	Oxygen gas
O/A	-	Volumetric ratio of spent organic solution to aqueous PLS in a mixer-settler
OH^{-1}	-	Hydroxide ion
P	W	Power
ΔP	Pa	Pressure drop
P_{abs}	bar	Column adsorption pressure
P_{elute}	bar	Column elution pressure
P_{Px}	-	Number of processing steps involving solid materials
Pr	-	Prandtl number
$\bar{q}_F$	mm/g	Equilibrium amount of $AuTU_2^+$ adsorbed at the feed concentration
q_m	mmol/g	Maximum $AuTu_2^+$ adsorption capacity on activated carbon
$\dot{Q}$	W	Heat duty
Q_c	m^3/h	Column flowrate
Q_1	W	Heat duty of MSR estimated by Aspen Plus
Q_{Au}	mmol/g	Adsorbed $AuTU_2^+$ per gram of activated carbon
Q	m^3/h	Volumetric throughput through settler
Q_r	-	Reaction quotient at non-equilibrated conditions
$\dot{Q}_{tot}$	W	Total heat duty of MSR
Q_T	m^3/h	Volumetric throughput through mixer
R	J / mol K	Gas constant
Re	-	Dimensionless Impeller Reynolds Number
Re_{drop}	-	Dimensionless Reynolds Number of the dispersed drop
S	m^2	Column cross-sectional area
ΔS_{rxn}	J / K	Change in entropy of a reaction

t	h	Time
t_{elute}	h	Time required to elute a column
$t_{R,X}$	h	Residence time for process X
t_s	h	Shock time
T	K	Temperature
T_{abs}	K	Column adsorption temperature
T_d	m	Tank diameter
T_{elute}	K	Column elution temperature
T_f	K	Outlet temperature
T_i	K	Inlet temperature
ΔT_{lm}	K	Logarithmic mean temperature
TU	-	Thiourea
u	m/h	Superficial velocity
U_0	W / m^2 K	Overall heat transfer coefficient
$u_{t,Stokes}$	m/s	Terminal velocity of dispersed phase droplet
v	m/h	Interstitial velocity
v_c	m^3 / m^2 h	Settling rate
v_{ch}	m/h	Chromatographic velocity
v_s	m^3/h	Shockfront velocity
V	J/C	Voltage
V_c	m^3	Column volume
V_{eff}	m^3	Effective volume
V_i	m^3/h	Volumetric flowrate of species i
$V_{P,X}$	L/h	Volumetric flowrate of purge stream in Block X
$V_{PLS,X}$	L/h	Volumetric flowrate of PLS stream in Block X
$V_{R,eff}$	m^3	Effective volume of cylindrical tank
$V_{R,X}$	L/h	Volumetric flowrate of recycle stream in Block X
$V_{Raff,X}$	L/h	Volumetric flowrate of raffinate stream in Block X
V_{tot}	L/s	Total volumetric flowrate through washer
V_w	L	Washer volume
W	m	Impeller height
x_i	-	Weight fraction of species i in WEEE
X^{-1}	-	Anion
Z	m	Tank height

XII. REFERENCES

Adin, CA Climate. (2020). http://myforecast.co/bin/climate.m?city=513490&metric=false

Ahtiainen, R., & Lundström, M. (2019). Cyanide-free gold leaching in exceptionally mild chloride solutions. *Journal of Cleaner Production*, *234*, 9–17. https://doi.org/10.1016/j.jclepro.2019.06.197

Alloy Wire International. (n.d.). Retrieved March 23, 2020, from https://www.alloywire.us.com/electrical-resistance-wire-hot-cutting-wire/heating-element-design/overview-heating-element-design-calculation/

Baldé, C. P., Forti, V., Gray, V., Kuehr, R., & Stegmann, P. (2017). *The Global E-waste Monitor*. United Nations University.

Brems, A., Dewil, R., Baeyens, J., & Zhang, R. (2013). *Gasification of plastic waste as waste-to-energy or waste-to-syngas recovery route*. https://doi.org/10.4236/ns.2013.56086

Bunting Electro Crossbelt Magnets. (n.d.). Retrieved March 22, 2020, from https://buymagnets.com/

CalRecycle. (2020, January 9). *Retailer Information & Covered Electronic Waste Recycling Fee*. CA.Gov. https://www.calrecycle.ca.gov/electronics/retailer

Carling, R. W., & Mar, R. W. (1981). *Industrial use of molten nitrate/nitrite salts* (SAND-81-8020, 5257229; p. SAND-81-8020, 5257229). https://doi.org/10.2172/5257229

Carta, G. (2019). *5d. Local equilibrium theory* [Powerpoint Slides].

Changshu Shi Shouyu Machinery Co., Ltd. (2020). *Two shaft shredder (SYU50 Series}*. https://www.shredder3e.com/two-shaft-shredder-syu50-series-p00024p1.html

Chen, C. K., Lung, T. N., & Wan, C. C. (1980). A study of the leaching of gold and silver by acidothioureation. *Hydrometallurgy*, *5*(2–3), 207–212. https://doi.org/10.1016/0304-386X(80)90039-0

Conradie, P. J., Johns, M. W., & Fowles, R. J. (1995). Elution and electrowinning of gold from gold-selective strong-base resins. *Hydrometallurgy*, *37*(3), 349–366. https://doi.org/10.1016/0304-386X(94)00032-X

Crittenden, J. C., Trussell, R. R., Hand, D. W., Howe, K. J., & Tchobanoglous, G. (2012). Appendix C: Physical Properties of Water. In *MWH's Water Treatment* (pp. 1861–1862). John Wiley & Sons, Inc. https://doi.org/10.1002/9781118131473.app3

Denver Mineral Engineers. (2020). *The Basic Processes of Gold Recovery*. https://www.denvermineral.com/gold-mining-process-development/

Diplas, A., R Garrett, Lutton, K., Marlowe, D., McGarth, M., & Tramblian, A. (2015). *Recycling of Printed Circuit Boards from Electronic Waste: A Hydrometallurgical Process.* University of Virginia School of Engineering and Applied Science.

Dziwinski, E., & Szymanowski, J. (1998). Composition of Cyanex® 923, Cyanex® 925, Cyanex® 921 and Topo. *Solvent Extraction and Ion Exchange*, *16*(6), 1515–1525. https://doi.org/10.1080/07366299808934592

Eccles, A. (n.d.). *Hydrochloric Acid Storage Tanks & HCl Specifications*. ProTank. Retrieved February 20, 2020, from https://www.protank.com/hydrochloric-acid

Economic Indicators. (2020). *Chemical Engineering; New York*, *127*(2), 56.

Electrical Personal Protective Equipment. (n.d.). North Carolina State University Environmental Health & Safety. Retrieved April 6, 2020, from https://ehs.ncsu.edu/health-safety/occupational-health/electrical-personal-protective-equipment-ppe/

Electronic waste. (n.d.). WHO. Retrieved December 4, 2019, from http://www.who.int/ceh/risks/ewaste/en/

Fish, R. M., & Geddes, L. A. (2009). Conduction of Electrical Current to and Through the Human Body: A Review. *Eplasty*, *9*. https://www.ncbi.nlm.nih.gov/pmc/articles/PMC2763825/

Flandinet, L., Tedjar, F., Ghetta, V., & Fouletier, J. (2012). Metals recovering from waste printed circuit boards (WPCBs) using molten salts. *Journal of Hazardous Materials*, *213–214*, 485–490. https://doi.org/10.1016/j.jhazmat.2012.02.037

Glover, P. (2012). Porosity. In *Petrophysics MSc Course Notes* (pp. 10–20). http://homepages.see.leeds.ac.uk/~earpwjg/PG_EN/CD%20Contents/GGL-66565%20Petrophysics%20English/Chapter%202.PDF

Gongyi Jinlong HengJi Heavy Industry Machinery Co., Ltd. (2020). *Best selling scrap metal shredder machine for recycling*. https://www.alibaba.com/product-detail/Best-selling-scrap-metal-shredder-machine_62151876612.html?spm=a2700.details.deiletai6.2.5a30JGpwJGpwBt

Hemrajani, R. R., & Tatterson, G. B. (2003). Mechanically Stirred Vessels. In E. L. Paul, V. A. Atiemo-Obeng, & S. M. Kresta (Eds.), *Handbook of Industrial Mixing* (pp. 345–390). John Wiley & Sons, Inc. https://doi.org/10.1002/0471451452.ch6

Hiskey, J. B. (1984). Thiourea Leaching of Gold and Silver—Technology Update and Additional Applications. *Mining, Metallurgy & Exploration*, *1*(3), 173–179. https://doi.org/10.1007/BF03402573

HomeAdvisor. (2020). *2020 Concrete Slab Cost Per Square Foot*. HomeAdvisor. https://www.homeadvisor.com/cost/outdoor-living/concrete-slab/#thickness

Hosseini, S. A., Khalilzadeh, M. A., & Jamshidi, A. (2012). Kinetic Study of Spent Nickel Catalyst Dissolution in HCl and Aqua Regia Medium. *Chemical Engineering & Technology*, *35*(4), 729–734. https://doi.org/10.1002/ceat.201000536

Hydrogen Cyanide. (1999). Cameo Chemicals. https://webcache.googleusercontent.com/search?q=cache:sJI-1MGV7U8J:https://cameochemicals.noaa.gov/chris/HCN.pdf+&cd=9&hl=en&ct=clnk&gl=us

Jadhav, U., & Hocheng, H. (2015). Hydrometallurgical Recovery of Metals from Large Printed Circuit Board Pieces. *Scientific Reports*, *5*. https://doi.org/10.1038/srep14574

Janz, G. J., & Lorenz, M. R. (1961). Solid-Liquid Phase Equilibria for Mixtures of Lithium, Sodium, and Potassium Carbonates. *Journal of Chemical & Engineering Data*, *6*(3), 321–323. https://doi.org/10.1021/je00103a001

Jergensen II, G. (1999). *Copper Leaching, Solvent Extraction, and Electrowinning Technology*. Society for Mining, Metallurgy, and Exploration (SME). https://app.knovel.com/web/toc.v/cid:kpCLSEET03/viewerType:toc/

Juarez, C. M., & Dutra, A. J. B. (2000). Gold electrowinning from thiourea solutions. *Minerals Engineering*, *13*(10), 1083–1096. https://doi.org/10.1016/S0892-6875(00)00092-3

Kanai, Y., Fukunaga, K., Terasaka, K., & Fujioka, S. (2013). Mass transfer in molten salt and suspended molten salt in bubble column. *Chemical Engineering Science*, *100*, 153–159. https://doi.org/10.1016/j.ces.2012.11.029

Kerosene Safety Data Sheet. (2020). Millipore Sigma.

Khouraibchia, Y., & Moats, M. S. (2010). *Evaluation of the Effect of Copper Electrowinning Parameters on Current Efficiency and Energy Consumption Using Surface Response Methodology*. 295–306. https://doi.org/10.1149/1.3367922

Kumagai, S., Hosaka, T., Kameda, T., & Yoshioka, T. (2017). Removal of toxic HCN and recovery of H2-rich syngas via catalytic reforming of product gas from gasification of polyimide over Ni/Mg/Al catalysts. *Journal of Analytical and Applied Pyrolysis*, *123*, 330–339.

Larmer, B. (2018, July 5). E-Waste Offers an Economic Opportunity as Well as Toxicity. *The New York Times*. https://www.nytimes.com/2018/07/05/magazine/e-waste-offers-an-economic-opportunity-as-well-as-toxicity.html

Lebo, R. B. (1921). PROPERTIES OF MIXTURES OF ISOPROPYL ALCOHOL AND WATER. *Journal of the American Chemical Society*, *43*(5), 1005–1011. https://doi.org/10.1021/ja01438a004

Lepek, D., Geankoplis, C., & Hersel, A. A. (2018). *Transport Processes and Separation Process Principles, Fifth Edition*. Prentice Hall.

Lithium Carbonate Safety Data Sheet. (2001). FMCLithium. https://webcache.googleusercontent.com/search?q=cache:yCP1A52RxNUJ:https://www.conncoll.edu/media/website-media/offices/ehs/envhealthdocs/Lithium_Carbonate.pdf+&cd=3&hl=en&ct=clnk&gl=us

Liu, T., Xu, X., Liu, W., & Zhuang, X. (2019). Corrosion of alloys in high temperature molten-salt heat transfer fluids with air as the cover gas. *Solar Energy*, *191*, 435–448. https://doi.org/10.1016/j.solener.2019.09.015

Lu, Y., & Xu, Z. (2016). Precious metals recovery from waste printed circuit boards: A review for current status and perspective. *Resources, Conservation and Recycling*, *113*, 28–39. https://doi.org/10.1016/j.resconrec.2016.05.007

Magdi Abadir. (n.d.). Unit Operations. In *Chapter 4: Size reduction* (pp. 39–55). Retrieved April 8, 2020, from https://scholar.cu.edu.eg/?q=magdi/files/chapter_4_updated.pdf

Mansell, R., & Raboy, M. (Eds.). (2011). *The Handbook of Global Media and Communication Policy*. Wiley-Blackwell.

Marsden, J., & House, I. (2006). *The Chemistry of Gold Extraction* (2nd ed). Society for Mining, Metallurgy, and Exploration.

McDougall, G., & Hancock, R. (1981). Gold Complexes and Activated Carbon. *Gold Bulletin*, *14*, 138–153. https://doi.org/10.1007/BF03216558

Michaud, D. (2016, March 31). AARL Carbon Stripping System Operation: Elution & Electrowinning. *911Metallurgist*. https://www.911metallurgist.com/blog/carbon-stripping-system-operation

Minter, A. (2016, January 13). The Burning Truth Behind an E-Waste Dump in Africa. *Smithsonian Magazine*. https://www.smithsonianmag.com/science-nature/burning-truth-behind-e-waste-dump-africa-180957597/

Mishra, S., & Devi, N. (2011). Extraction of copper(II) from hydrochloric acid solution by Cyanex 921. *Hydrometallurgy*, *107*(1), 29–33. https://doi.org/10.1016/j.hydromet.2010.12.016

Nkinzingabo, J. (2019, May 12). Electronic Marvels Turn Into Dangerous Trash in East Africa—The New York Times. *The New York Times*. https://www.nytimes.com/2019/05/12/climate/electronic-marvels-turn-into-dangerous-trash-in-east-africa.html

Olympic Games. (2019). *Tokyo 2020 Medals*. https://www.olympic.org/tokyo-2020-medals

OSHA. (2010). *Accident: 200651685—Employee Is Killed, Two Are Burned In Dip Tank Explosion*. https://www.osha.gov/pls/imis/accidentsearch.accident_detail?id=200651685

Overview of Wage Data by Area and Occupation. (n.d.). Retrieved April 8, 2020, from https://www.bls.gov/bls/blswage.htm

Park, Y. J., & Fray, D. J. (2009). Recovery of high purity precious metals from printed circuit boards. *Journal of Hazardous Materials*, *164*(2), 1152–1158. https://doi.org/10.1016/j.jhazmat.2008.09.043

Piyush Sabharwall, Matt Ebner, Manohar Sohal, & Phil Sharpe. (2010). *Molten Salts for High Temperature Reactors: University of Wisconsin Molten Salt Corrosion and Flow Loop Experiments -- Issues Identified and Path Forward* (INL/EXT-10-18090, 980798; p. INL/EXT-10-18090, 980798). https://doi.org/10.2172/980798

Potassium Carbonate Safety Data Sheet. (2004). Baker Hughes.

PubChem. (2020). https://pubchem.ncbi.nlm.nih.gov/

Quan, C., Li, A., & Gao, N. (2013). Combustion and Pyrolysis of Electronic Waste: Thermogravimetric Analysis and Kinetic Model. *Procedia Environmental Sciences*, *18*, 776–782. https://doi.org/10.1016/j.proenv.2013.04.104

Reddy, R. G. (2011). Molten Salts: Thermal Energy Storage and Heat Transfer Media. *Journal of Phase Equilibria and Diffusion*, *32*(4), 269. https://doi.org/10.1007/s11669-011-9904-z

Riedewald, F., Goode, K., Sexton, A., & Sousa-Gallagher, M. J. (2016). Scrap tyre recycling process with molten zinc as direct heat transfer and solids separation fluid: A new reactor concept. *MethodsX*, *3*, 399–406. https://doi.org/10.1016/j.mex.2016.05.003

Riedewald, F., & Sousa-Gallagher, M. (2015). Novel waste printed circuit board recycling process with molten salt. *MethodsX*, *2*, 100–106. https://doi.org/10.1016/j.mex.2015.02.010

Robinson, T. (n.d.). *UTILIZING CYANIDE RECOVERY TECHNIQUES IN THE CESL GOLD-SILVER PROCESS*. 12.

Rogans, J. (2012). *Activated Carbon in Gold Recovery*.

Salbidegoitia, J. A., Fuentes-Ordóñez, E. G., González-Marcos, M. P., González-Velasco, J. R., Bhaskar, T., & Kamo, T. (2015). Steam gasification of printed circuit board from e-waste: Effect of coexisting nickel to hydrogen production. *Fuel Processing Technology*, *133*, 69–74. https://doi.org/10.1016/j.fuproc.2015.01.006

Schlesinger, M., King, M., Sole, K., & Davenport, W. (2011). *Extractive Metallurgy of Copper*. Elsevier. https://doi.org/10.1016/C2010-0-64841-3

Schulze, R. G. (1984). New Aspects in Thiourea Leaching of Precious Metals. *JOM*, *36*(6), 62–65. https://doi.org/10.1007/BF03338478

Semuels, A. (2019, May 23). The World Has an E-Waste Problem. *Time*. https://time.com/5594380/world-electronic-waste-problem/

Shijiazhuang Jiarun Technology Co., Ltd. (2020). *Crossbelt Magnetic Separator Ferrous Metal Separation Sorting*. https://www.alibaba.com/product-detail/Crossbelt-Magnetic-Separator-Ferrous-Metal-Separation_62362528965.html?spm=a2700.galleryofferlist.0.0.47c4a3a2rdJkBQ

Sodium Carbonate Safety Data Sheet. (2013). OCI. http://webcache.googleusercontent.com/search?q=cache:ZhC9eQEQhVIJ:www.rigchem.com/_literature_108323/SDS_-_Soda_Ash_Dense_Natural+&cd=1&hl=en&ct=clnk&gl=us

Sunga, R. (n.d.). *The Complete Aqueous Hydrochloric Acid Solutions Density-Concentration Calculator*. HandyMath.Com. Retrieved February 28, 2020, from https://handymath.com/cgi-bin/hcltble3.cgi?submit=Entry

Tantalum Price 2020 [Updated Daily]. (n.d.). *Metalary*. Retrieved March 21, 2020, from http://www.metalary.com/tantalum-price/

The Engineering Toolbox. (n.d.-a). *Dynamic Viscosity of common Liquids*. The Engineering Toolbox. Retrieved February 28, 2020, from https://www.engineeringtoolbox.com/absolute-viscosity-liquids-d_1259.html

The Engineering Toolbox. (n.d.-b). *Sulfuric Acid—Density*. Retrieved February 28, 2020, from https://www.engineeringtoolbox.com/indsulfuric-acid-density-d_2163.html

Torres, R., & Lapidus, G. T. (2016). Copper leaching from electronic waste for the improvement of gold recycling. *Waste Management*, *57*, 131–139. https://doi.org/10.1016/j.wasman.2016.03.010

Trioctylphosphine Oxide Safety Data Sheet. (2020). Millipore Sigma.

TT Electronics. (2020). *AS1CR050HLF IRC by TT Electronics*. Mouser Electronics. https://www.mouser.com/ProductDetail/66-AS1CR050HLF

Turton, R., Shaeiwitz, J. A., Bhattacharyya, D., & Whiting, W. B. (2018). *Analysis, Synthesis, and Design of Chemical Processes, Fifth Edition* (5th ed.). Prentice Hall. https://proquest.safaribooksonline.com/9780134177502

Ubaldini, S., Fornari, P., Massidda, R., & Abbruzzese, C. (1998). An innovative thiourea gold leaching process. *Hydrometallurgy*, *48*(1), 113–124. https://doi.org/10.1016/S0304-386X(97)00076-5

Vignes, A. (2013). Hydrometallurgical Extraction Processes. In *Extractive Metallurgy 2: Metallurgical Reaction Processes* (pp. 1–86). John Wiley & Sons, Ltd. https://doi.org/10.1002/9781118616932.ch1

Vishay. (2020). *C52TF1001JB by Vishay*. Arrow.Com. https://www.arrow.com/en/products/c52tf1001jb/vishay

Wadnerkar, D., Tade, M. O., Pareek, V. K., & Utikar, R. P. (2015). Modeling and optimization of Carbon in leach (CIL) circuit for gold recovery. *Minerals Engineering*, *83*, 136–148. https://doi.org/10.1016/j.mineng.2015.09.001

Wall, B. P., Parkin, J. E., & Sunderland, V. B. (1985). Intrinsic dissolution of lithium carbonate in aqueous solutions. *Journal of Pharmacy and Pharmacology*, *37*(5), 338–340. https://doi.org/10.1111/j.2042-7158.1985.tb05077.x

Wankat, P. (2016). *Separation Process Engineering: Includes Mass Transfer Analysis, Fourth Edition* (4th ed.). Prentice Hall.

Welty, J. R., Wicks, C. E., Rorrer, G. L., & Wilson, R. E. (2008). *Fundamentals of Momentum, Heat, and Mass Transfer* (5th ed). Wiley.

Xinhai. (n.d.). *Leaching Agitation Tank*. Xinhai. Retrieved February 6, 2020, from https://www.xinhaimining.com/product/gold/leaching-agitation-tank

Yoo, J.-M., Jeong, J., Yoo, K., Lee, J.-C., & Kim, W. (2009). Enrichment of the metallic components from waste printed circuit boards by a mechanical separation process using a stamp mill. *Waste Management (New York, N.Y.)*, *29*(3), 1132–1137. https://doi.org/10.1016/j.wasman.2008.06.035

Zatko, D. A., & Kratochvil, Byron. (1968). Copper(II) oxidation of thioureas in acetonitrile. *Analytical Chemistry*, *40*(14), 2120–2123. https://doi.org/10.1021/ac50158a031

Zhang, H., Ritchie, I. M., & La Brooy, S. R. (2004). The adsorption of gold thiourea complex onto activated carbon. *Hydrometallurgy*, *72*(3), 291–301. https://doi.org/10.1016/S0304-386X(03)00182-8

Zhang, S., Yoshikawa, K., Nakagome, H., & Kamo, T. (2013). Kinetics of the steam gasification of a phenolic circuit board in the presence of carbonates. *Applied Energy*, *101*, 815–821. https://doi.org/10.1016/j.apenergy.2012.08.030

Zhang, Y., Liu, S., Xie, H., Zeng, X., & Li, J. (2012). Current Status on Leaching Precious Metals from Waste Printed Circuit Boards. *Procedia Environmental Sciences*, *16*, 560–568. https://doi.org/10.1016/j.proenv.2012.10.077

XIII. APPENDIX

The *Appendix* includes stream tables (Section A) and sample calculations (Section B).

XIII.A. Stream Tables

XIII.A.1 Block A, MSR and WEEE Treatment, Stream Summary

The stream table for Block A: MSR and WEEE treatment is given in Table XIII.A.1-1. The stream tags are labeled on the PFD, i.e., Figure III.A.1-1.

Table XIII.A.1-1. Block A: MSR and WEEE Treatment

Stream Number	**A1**	**A2**	**A3**	**A4**	**A5**	**A7**	**A8**	**A10**	**A11**	**A12**	**A14**	**A15**	**A16**
Description	WEEE Feed	LNK Makeup	Steam Feed	O_2/air feed	Syngas Mixture	Solder	MSR Output	Wash Water In	Wash Water Out	Dryer input	Crusher Input	Magnetic Separator Input	Fe/Ni Output
Temperature (°C)	25	25	100	25	675	675	675	25	25	25	25	25	25
Pressure (kPa)	101	101	101	202	202	101	101	101	101	101	101	101	101
Vapor mole fraction	0	0	1	1	1	0	0	0	0	0	0	0	0
Volumetric flowrate (m^3/h)	-	-					-			-	-	-	-
Mass flowrate (kg/h)	18,800	1880	5060	1440	12140	1303	13736	36000	37880	11,856	11,856	11,856	1767
Component flowrates (kg/h)													
Cu	3760	0	0	0	0	0	3760	0	0	3760	3760	3760	0
Fe	1504	0	0	0	0	0	1504	0	0	1504	1504	1504	1414
Sn	752	0	0	0	0	744	8	0	0	8	8	8	0
Ni	376	0	0	0	0	0	376	0	0	376	376	376	0
Pb	376	0	0	0	0	372	4	0	0	4	4	4	353
Zn	188	0	0	0	0	186	2	0	0	2	2	2	0
Ag	38	0	0	0	0	0	38	0	0	38	38	38	0
Au	19	0	0	0	0	0	19	0	0	19	19	19	0
Pd	1	0	0	0	0	0	1	0	0	1	1	1	0
Misc. metal	506	0	0	0	0	0	506	0	0	506	506	506	0
R.O	5640	0	0	0	0	0	5640	0	0	5640	5640	5640	0
Plastic	5640	0	0	0	0	0	0	0	0	0	0	0	0
LNK	0	1880	0	0	0	0	1880	0	1880	0	0	0	0
H_2O	0	0	5060	0	0	0	0	36000	36000	0	0	0	0
O_2	0	0	0	1440	0	0	0	0	0	0	0	0	0
H_2	0	0	0	0	1102	0	0	0	0	0	0	0	0
HCN	0	0	0	0	430	0	0	0	0	0	0	0	0
CO	0	0	0	0	9888	0	0	0	0	0	0	0	0

XIII.A.2. Block B, Copper Recovery, Stream Summary

The stream table for Block B: Cu recovery is given in Table XIII.B.2-1. The stream tags are labeled on the PFD, i.e., Figure III.A.1-1.

Table XIII.B.2-1. Block B: Copper Recovery Stream Table

Stream Number	**B1**	**C1**	**B2**	**B5**	**B9**	**B7**	**B8**	**B11**	**B9**	**B13**	**B10**	**B12**
Description	Solids in	Solids out	Makeup Solvent	PLS	Raffinate	Purge	Recycle	Spent Organic	Loaded Organic	Spent Electrolyte	Advance Electrolyte	Copper Product
Temperature (°C)	25	25	25	25	25	25	25	25	25	25	25	45
Pressure (kPa)	101	101	101	101	101	101	101	101	101	101	101	101
Vapor mole fraction	0	0	0	0	0	0	0	0	0	0	0	0
Volumetric flowrate (m^3/h)	-	-	0.56	1000	1000	0.56	999.44	1000	1000	250	250	-
Mass flowrate (kg/h)	10089	6747	666	1259426	1256126	708	1255419	919689	922989	303750	307050	3300
Component flowrates (kg/h)												
Cu	3,760.0	459.9	0	3,500	200	0.11	200	3,700	7,000	8750	12050	3300
Fe	90.2	63.2	0	48,113	48,113	27.07	48,086	0	0	0	0	0
Sn	7.52	0	0	13,365	13,365	7.52	13,357	0	0	0	0	0
Ni	22.6	22.2	0	600	600	0.34	599.7	0	0	0	0	0
Pb	3.76	0	0	6,682	6,682	3.76	6,679	0	0	0	0	0
Zn	1.88	0	0	3,341	3,341	1.88	3,339	0	0	0	0	0
Ag	37.6	37.0	0	1,000	1,000	0.56	999	0	0	0	0	0
Au	18.8	18.5	0	500	500	0.28	499.7	0	0	0	0	0
Pd	0.94	0.93	0	25	25	0.01	24.99	0	0	0	0	0
Misc. metal	505.7	505.7	0	0	0	0	0	0	0	0	0	0
R.O	5,640.0	5,640.0	0	0	0	0	0	0	0	0	0	0
H_2O	0	0	563	1000000	1000000	563	999437	0	0	250000	250000	0
HCl	0	0	103	182300	182300	103	182197	0	0	0	0	0
Kerosene	0	0	0	0	0	0	0	800000	800000	0	0	0
Cyanex 921	0	0	0	0	0	0	0	115989	115989	0	0	0
H_2SO_4	0	0	0	0	0	0	0	0	0	45000	45000	0

XIII.A.3. Block C, Gold Recovery, Stream Summary

The stream table for Block C: Au recovery is given in Table XIII.A.3-1. The stream tags are labeled on the PFD, i.e., Figure III.A.1-1.

Table XIII.A.3-1. Block B: Gold Recovery Stream Table

Stream Number	C1	C3	C2	C5	C7	C4	C6	C9	C8	C10
Description	Solids in	Solids out	Makeup Solvent	PLS	Raffinate	Purge	Recycle	Spent Electrolyte	Advance Electrolyte	Gold Product
Temperature (°C)	25	25	25	25	25	25	25	85	85	60
Pressure (kPa)	101	101	101	101	101	101	101	101	101	101
Vapor mole fraction	0	0	0	0	0	0	0	0	0	0
Volumetric flowrate (m^3/h)	-	-	39.2	33.7	33.7	9.2	124.5	294.9	294.9	-
Mass flowrate (kg/h)	6747	6245	189219	380834.7	262740.024	71626.4	191113.7	1651733231	1651733247	15.87
Component flowrates (kg/h)										
Cu	459.9	0	0	1686.8	1686.8	459.9	1227	0	0	0
Fe	63.2	63.2	0	0	0	0	0	0	0	0
Sn	0	0	0	0	0	0	0	0	0	0
Ni	22.2	22.2	0	0	0	0	0	0	0	0
Pb	0	0	0	0	0	0	0	0	0	0
Zn	0	0	0	0	0	0	0	0	0	0
Ag	37.0	10.6	0	96.9	96.9	26.4	70.5	0	0	0
Au	18.5	2.8	0	16.0	0.324	0.088	0.2363	0.491	16.36	15.87
Pd	0.926	0.926	0	0	0	0	0	0	0	0
Misc. metal	505.7	505.7	0	0	0	0	0	0	0	0
R.O	5640	5640	0	0	0	0	0	0	0	0
H_2O	0	0	64380	236159	236159	64380	171779	1651386028	1651386028	0
Thiourea	0		6438	23616	23616	6438	17178	12385	12385	0
Ferric Sulfate	0	0	118079	118079	0	0	0	0	0	0
H_2SO_4	0	0	322	1181	1181	322	859	10321	10321	0
Isopropanol	0	0	0	0	0	0	0	324497	324497	0

XIII.B. Sample Calculations

XIII.B.1. Molten Salt Reactor, R-101, Sample Calculations

Heat duty of MSR, R-101.

The total heat duty of the MSR, R-101, is given by **Equation III.B.3.2**.

$Q_1 = 3.965 * 10^6 cal/sec = 16589.56\ kW$ (combustion/steam gasification, in Aspen)

$Q_2 = \sum_{i=1}^{n} \dot{m}_i\ C_{P,i,avg} \Delta T$ *n = number of components that heat up* (components heating up in MSR)

$Q_3 = \sum_{i=1}^{k} \dot{m}_i \Delta H_{fus,i}$ *k = number of components that melt* (components melting in MSR)

For example, Q_3 includes all of the solder (Pb, Zn, Sn) which melt

$\Delta H_{fus,\,Pb} = 23.02\ kJ/kg$ $\quad \dot{m}_{Pb} = 0.104\ kg/s$

$\Delta H_{fus,\,Zn} = 111.96\ kJ/kg$ $\quad \dot{m}_{Zn} = 0.052\ kg/s$

$\Delta H_{fus,\,Sn} = 59.22\ kJ/kg$ $\quad \dot{m}_{Sn} = 0.207\ kg/s$

$Q_3 = (23.02\ \frac{kJ}{kg})(0.104\ \frac{kg}{s}) + (111.96\ \frac{kJ}{kg})(0.052\frac{kg}{s}) + (59.22\ \frac{kJ}{kg})(0.207\frac{kg}{s}) = 20.47kW$

Thus, $Q_{tot} = Q_1 + Q_2 + Q_3 = 16589.56\ kW + 8,795.04\ kW + 20.47kW = 25,400kW$

Kinetics of WEEE combustion and pyrolysis.

The Arrhenius rate equation used is **Equation III.B.3.1**.

$k = Aexp(-E/RT)$

$n_i = n_{i,0} exp(-kt) \rightarrow t = ln(\frac{n_i}{n_{i,0}})/-k$

The parameters from Quan et al. (2013), assuming that stage 2 of the reaction is the rate limiting step (RLS):

$A = 9.24 * 10^3 min^{-1}$

$E = 1.08 * 10^2 kJ/mol$

$k = 9.24 * 10^3 min^{-1} exp((-1.08 * 10^2 kJ/mol)/(8.34 * 10^{-3} kJ/mol\ K * 948\ K)$

$= 1.03 * 10^{-2} min^{-1}$

Aiming for 20% of the carbon char to remain for steam gasification, and assuming the prior pyrolysis and combustion was the RLS:

$t = ln(0.2)/1.03 * 10^{-2} min^{-1} = 27.44$ min

XIII.B.2. Heat Transfer Equipment Sample Calculations

WEEE Heap, E-101, sample calculations.

The WEEE Heap, E-101, cools the solid MSR output by convection. The dimensionless Biot number is given by **Equation III.B4.1**

$$Bi = \frac{h}{k}L = \frac{50\ W/(m^2K)}{102.2\ W/(m\ K)} * 0.1m = 0.049$$

The time for the waste to cool to 25℃ is given by **Equation III.B4.3**

$$t = \frac{d\ \rho\ Cp(T_i - T_f)}{h(T_i - T_\infty)} = \frac{(0.1m)(5807.9\ kg/m^3)(593204\ J/kg)}{(50\ W/(m^2K))(948K - 293K)} = 10519.9\ s = 2.9\ h$$

which is derived from **Equation III.B4.2**

$$\dot{Q} = Cp\ \dot{m}(T_i - T_f) = A\ h(T_i - T_\infty)$$

$$\dot{m} = L \times W \times d \times \rho/t$$
$$A = L \times W$$
$$Cp\ (L \times W \times d \times \rho/t)(T_i - T_f) = (L \times W)h(T_i - T_\infty)$$
$$t = \frac{d\ \rho\ Cp(T_i - T_f)}{h(T_i - T_\infty)}\ ;\ d = depth\ of\ solids$$

Countercurrent shell and tube heat exchanger sample calculations.

The countercurrent, shell and tube heat exchangers E-201 and E-301 were designed using the following equations. **Equation III.C.6.1** was used to determine the heat transfer area.

$$\dot{Q} = C_p\ \dot{m}(T_f - T_i) = U_0 A_0 \Delta T_{lm} F_c$$

$$A_0 = \frac{C_p\ \dot{m}(T_f - T_i)}{U_0 \Delta T_{lm} F_c} = \frac{(2897\ J/kg)(101.4\ kg/s)(318K - 293K)}{(1697.8\ W/(m^2\ K))(7.2\ K)(1)} = 599.6\ m^2$$

The overall heat transfer coefficient is given by **Equation III.C.6.2.**

$$U_0 = \left(\frac{1}{h_i}\frac{r_o}{r_i} + \frac{r_o ln(r_o/r_i)}{k} + \frac{1}{h_o}\right)^{-1} = \left(\frac{1}{17289.2\ W/(m^2K)}\frac{0.0069m}{0.0032m} + \frac{(0.0069m)ln(\frac{0.0069m}{0.0032m})}{20\ W/(m\ K)} + \frac{1}{5000W/(m^2K)}\right)^{-1}$$
$$U_0 = 1697.8\ W/(m^2K)$$

The logarithmic mean temperature difference is given by **Equation III.C.6.3.**

$$\Delta T_{lm} = \frac{(T_{h,1} - T_{c,1}) - (T_{h,2} - T_{c,2})}{ln\frac{(T_{h,1} - T_{c,1})}{(T_{h,2} - T_{c,2})}} = \frac{(293 - 283) - (318 - 313)}{ln\frac{(293 - 283)}{(318 - 313)}} = 7.2\ \ all\ units\ are\ Kelvin$$

The tube side heat transfer coefficient is given by **Equation III.C.6.4.**

$$Nu = h\,D\,/\,k = 0.023(Re)^{0.80}(Pr)^{0.33}$$

$$h = (k/D)\ 0.023(Re)^{0.80}(Pr)^{0.33} = \frac{0.53\ W/(m\,K)}{0.0064\ m}\ 0.023(45684.3)^{0.80}(4.86)^{0.33} = 17289.2\ W/(m^2\,K)$$

XIII.B.3. Rinse Bath Sample Calculations

The volume required for a given residence time and volumetric flowrate

$$V_w = \tau V_{tot} = (0.5\ h)(3600\ s/h)(10.64\ L/s) = 19147\ L$$

XIII.B.4. Magnetic Separation Sample Calculations

The amount of iron recovered from magnetic metal separation is given by:

$$Fe_{out} = f_{Ni,mag} \times Fe_{in} = 0.94 \times 1504\ kg/h = 1414\ kg/h$$

XIII.B.5. Copper Leaching Sample Calculations

Cu leach fraction sample calculations.

Copper leaching occurs in an agitated leaching tank, R-201. The fraction of Cu leached in six hours is given by **Equation III.C.2.3**.

$$E_{Cu,B} = -2.7\ e^{(-1.62\ t)} + 0.88 = -2.7\ e^{(-1.62\ 6\ h)} + 0.88 = 0.878$$

The percentage of Ni leached in six hours is given by **Equation III.C.2.4**.

$$1 - (1 - E_{Ni,B})^{2/3} = 0.0011\ t - 0.023$$

Isolating $E_{Ni,B}$ yields

$$E_{Ni,B} = (\ 1000000 + 11 \times \sqrt{11} \times \sqrt{(-(t - 930)^3}\ )\ /\ 1000000$$

Plugging in t = 6h and solving yields

$$E_{Ni,B} = (\ 1000000 + 11 \times \sqrt{11} \times \sqrt{(-(6h - 930)^3}\ )\ /\ 1000000 = 1.50\% = 0.0150$$

Stream design for Cu leaching.

The concentration of each metal in the purge stream required to prevent accumulation is given by **Equation III.C.2.9.**

$$C_{i,P,B} = m_{i,in,B} \times E_{i,B} \,/\, V_{P,B}$$

For example, for Ag, $m_{i,in,Ag}$ = 37.6 kg/h, $E_{Ag,B}$ = 0.015 (see Table III.C.1-1), and $V_{P,B}$ = 0.56 m^3/h (see Equation III.C.2.8 and Figure III.C.2-2). Therefore, the concentration of Ag in the purge stream required to prevent accumulation is:

$$C_{Ag,P,B} = 37.6\ kg/h \times 0.015 \,/\, 0.56\ m^3/h\ \times (1000 g/kg \times 1\ m^3/1000\ L)$$
$$C_{Ag,P,B} = 1.0\ g/L$$

For Cu leaching, the effective volume of lixiviant required is given by **Equation III.C.2.10.** The input of WEEE into R-101 is m_{WEEE} = 18,799,848 g/h.

$$V_{eff} = 6\ h \times (m_{WEEE} \,/\, 20\ g\ WEEE\ /L) \times 1\ m^3/1000L = 5640\ m^3$$

Tank design for Cu leaching.

The liquid height of a cylindrical, agitation tank is given by **Equation III.C.2.11**. For example, if the effective volume $V_{R,eff}$ = 480 m^3 and T = 8.5 m, then

$$H = V_{R,eff} \,/\, (\pi\ (\ T\ /\ 2)^2) = 480\ m^3\ /\ (\pi\ (\ 8.5\ m\ /\ 2)^2) = 8.5$$

The tank headspace is given by the tank height minus the liquid volume, so for Z = 9 m, the headspace is 0.50 m.

The dimensionless, impeller Reynolds number is given by **Equation III.C.2.12.** For an impeller diameter of 3.3 m, impeller speed of 18.5 RPM (0.31 RPS), fluid density of 1077.6 kg/m^3, and fluid viscosity of 1 cP, the Impeller Reynolds number is

$$Re = d_i^2 N\rho\ /\mu\ = (3.3\ m)^2\ 0.31\ RPS \times 1077.6\ kg/m^3\ /\ 0.001\ Pa\ s = 3.62 \times 10^6$$

The dimensionless Power Number is given by **Equation III.C.2.13**. Power can be isolated and solved for. For a 45° PBT, with four blades with four standard baffles, N_{Po} = 1.27 in the turbulent regime (Hemrajani & Tatterson, 2003). Therefore, the power is given by

$$P = N_{Po}\rho\ N^3\ d_i^5\ /\ g_c = 1.27 \times 1077.6\ kg/m^3 \times (0.31\ RPS)^3 \times (3.3\ m)^5\ /\ 1\ m/s^2$$
$$P = 15.7\ kW$$

XIII.B.6. Copper Extraction Sample Calculations

Mixer design for Cu extraction.

A mixer's effective volume is given by **Equation III.C.3.8.** For a residence time of t_R = 0.05 h, and volumetric throughput of Q_T = 2000 m^3/h total, V_R is given by

$$V_{R,eff} = Q_T \,/\, t_R = 2000\ m^3/h \,/\, 0.05\ h = 100\ m^3$$

A cylindrical, agitation tank's effective volume is also given by **Equation III.C.3.9**. We set T_d equal to Z and solved for T_d. Therefore, T_d and Z are given by

$$T_d = Z = (4\ V_{R,eff} \,/\, \pi)^{1/3} = (4\ \times 100\ m^3 \,/\, \pi)^{1/3} = 5.03\ m$$

The liquid height is approximated the same as for the Cu leaching agitation tank.

The density of the liquid mixture is given by equation Equation III.C.3.11. For a continuous phase density of 810 kg/m^3 and a dispersed phase density of 1078 kg/m^3 and volumetric fraction of 0.3, the mixture density is given by

$$\rho_M = \varphi_D \rho_D + (1 - \varphi_D)\rho_C = 0.3 \times 1078\ kg/m^3 + (1 - 0.3) \times 810\ kg/m^3 = 890\ kg/m^3$$

The mixture viscosity is estimated with **Equation III.C.3.12**. For a dispersed phase viscosity of 1.002 cP and a continuous phase viscosity of 1.64 cP, the mixture viscosity is given by

$$\mu_M = (\mu_C/\varphi_C) \times (1 + 1.5\mu_D\varphi_D \,/\, (\mu_C + \mu_D))$$
$$\mu_M = (1.64\ cP/0.7) \times (1 + 1.5(1.002)0.3 \,/\, (1.64\ cP + 1.002\ cP)) = 2.74\ cP$$

The density of the continuous (organic) phase was estimated using **Equation III.C.3.13.** If $V_{kerosene}$ = 875 m^3/h, $V_{organic}$ = 1000 m^3/h, $\rho_{kerosene}$ = 800 kg/m^3, $V_{Cyanex\ 921}$ = 125 m^3/h, and $\rho_{Cyanex\ 921}$ = 880 kg/m^3 , then the continuous phase density is given by

$$\rho_C = (V_{kerosene} \,/\, V_{organic}) \times \rho_{kerosene} + (V_{Cyanex\ 921}/V_{organic}) \times \rho_{Cyanex\ 921}$$
$$\rho_C = (875\ m^3/h \,/\, 1000\ m^3/h) \times 800\ kg/m^3 + (125\ m^3/h \,/\, 1000\ m^3/h) \times 800\ kg/m^3$$
$$\rho_C = 810\ kg/m^3$$

The impeller Reynolds number and the power were calculated the same way as for Cu leaching.

Settler design for Cu extraction.

The settler's settling zone area is calculated with **Equation III.C.3.14**. For a settling rate of 4 m^3 / m^2 h and throughput of 2000 m^3/h, the settling area is given by

$$A_{set} = Q \,/\, v_c = (2000\ m^3/h) \,/\, (4\ m^3 \,/\, m^2\ h) = 500\ m^2$$

If the settler is square, the length and width are the square root of A_{set} , i.e.,

$$L = W = \sqrt{A_{set}} = 22.36\ m$$

Settlers are typically 1 m deep; therefore, the volume of settler is

$$V = LWh = 22.36\ m \times 22.36\ m \times 1\ m = 500\ m^3$$

The settling velocity of a dispersed phase droplet is given by **Equation III.C.3.15**. The dispersed phase drop diameter in m, often set empirically to 150 mm. Therefore, the settling velocity is given by

$$u_{t,Stokes} = g\, d_d^{\,2}(\rho_C - \rho_D) / (18\ \mu_D)$$
$$u_{t,Stokes} = 9.81\ m/s^2 \times (1.5 \times 10^{-4}\ m)^2(810\ kg/m^3 - 1078\ kg/m^3)/(18 \times 0.001\ Pa\ s)$$
$$u_{t,Stokes} = -0.003\ m/s = -11.\ m/h$$

where the negative sign indicates descent. The Reynolds number of the dispersed drop is given in **Equation III.C.3.16**, and must be less than 0.3 to use Equation II.C.3.15.

$$Re_{drop} = d_d\, \rho_C\, u_{t,Stokes} / \mu_C = 1.5 \times 10^{-4} \times 1078\ kg/m^3 \times 0.003\ m/s / 0.001\ Pa\ s$$
$$Re_{drop} = 0.243$$

The theoretical, vertical distance traveled by the drop is given by Equation III.C.3.17. If the residence time of the settler is 900 s, then the vertical distance is given by

$$h_{drop} = u_{t,Stokes} \times t_{R,set} = -0.003\ m/s \times 900\ s = -2.9\ m$$

where the negative sign indicates descent.

XIII.B.7. Copper Stripping Sample Calculations

The mixer-settler for Cu stripping was designed with the same equations as for Cu extraction.

XIII.B.8. Copper Electrowinning Sample Calculations

Equation III.C.5.8 calculates the cell potential based on the departure from standard cell potential conditions.

$$E_{cell} = E^o{}_{cell} - (RT / (nF)) \times \ln[Q_r] = -0.89 \frac{V}{mol} - \frac{8.314\ \frac{J}{mol\,K} \cdot 318\ K}{2 * 96500\ \frac{J}{V}} ln[\frac{3.66}{0.55}] = -0.916\ \frac{V}{mol}$$

This can be combined with **Equation III.C.5.7** to calculate the enthalpy of reaction:

$$\Delta G_{rxn} = -nF E_{cell} = \Delta H_{rxn} - T\Delta S_{rxn}$$

The entropy of reaction is calculated using the change in entropy from both the anode and cathode reactions, tabulated in literature. The above equation is rearranged:

$$\Delta H_{rxn} = -nF E_{cell} + T\Delta S_{rxn} = -2 * 96500\ \frac{J}{V}(-0.916\ V) + 318\ K\ *\ 165.4\ \frac{J}{mol\,K}$$
$$= 1.24\ kW \quad \text{per electrode.}$$

Since there are 2665 electrode pairs, we multiply this by 2665 to yield 3300 kW.

XIII.B.9. Gold Leaching Sample Calculations

Au Leach fraction sample calculations.

Au leaching occurs in the Agitated Leaching Tank, R-301. The fraction of Au leached in six hours is given by **Equation III.D.2.7**.

$$E_{Au,C} = -2.0\, e^{(-0.07\, t)} + 2.15 = -2.0\, e^{(-0.07\, 6h)} + 2.15 = 0.851$$

Stream design for Au leaching.

The concentration of Ag in the purge stream is given by **Equation III.D.2.9**. Therefore, for an Ag input of 259,259 g/batch, an Ag leach fraction of 0.7136, and a purge volume of 64.4 m^3/batch, the Ag purge concentration is given by

$$C_{P,C,Ag} = m_{Ag,C}\, E_{Ag,C} \,/\, V_{P,C} = 259,259\ g/batch \times 0.7136/64.4\ m^3/batch = 2.87\ g/L$$

The Au leaching agitation tank, R-301, was designed with the same equations as the Cu leaching agitation tank, R-201.

XIII.B.10. Gold Adsorption Sample Calculations

The superficial velocity of the adsorption column, T-301, is given by **Equation III.D.3.2**. For a mobile phase flowrate of 10.8 m^3/h and a cross-sectional area of 1.77 m^2, the superficial velocity is given by

$$u = Q_c \,/\, S = (10.8\ m^3/h) \,/\, (1.77\ m^2) = 6.11\ m/h$$

The column's interstitial velocity is given by **Equation III.D.3.3**. If the interphase porosity is 0.3, then the interstitial velocity is given by

$$v = u \,/\, \varepsilon = (6.11\ m/h\ ) \,/\, 0.3 = 20.37\ m/h$$

The phase ratio is given by **Equation III.D.3.4**.

$$\varphi = (1 - \varepsilon) \,/\, \varepsilon = (1 - 0.3) \,/\, 0.3 = 2.33$$

The shockfront velocity is described by **Equation III.D.3.6**. For a feed, Au concentration (C_F) of 0.47 g/L or 2.41 mM and Q_F = 1.41 mmol/g, the shockfront velocity is given by

$$v_s = v \,/\, (1 + \varphi\, \overline{q}_F \,/\, C_F) = 20.37\ m/h \,/\, (1 + 2.33 \times 1.41\ mmol/g \,/\, 2.41\ mM) = 8.62\ m/h$$

The shock time is given by **Equation III.D.3.7**. For a 9 m tall column, the shock time is given by

$$t_s = L_c/v_s = 10\ m\ /\ 8.62\ m/h = 1.04\ h$$

The amount of Au loaded per column is given by **Equation III.D.3.8**. The amount of Au loaded in T-301 is given by

$$m_{Au,T-301} = Q_c t_s C_F = 10.8\ m^3/h \times 1.04\ h \times 0.47\ g/L \times 1000\ L/m^3 = 5343\ g\ Au$$

The pressure drop across the column is given by the Kozeny–Carman equation for rigid particles and laminar flow in **Equation III.D.3.9**. For 2.38 mm activated carbon, the pressure drop is given by

$$\Delta P = 150\ (1 - \varepsilon)^2\ /\ \varepsilon^3 \times \mu\ L_c\ u\ /\ {d_p}^2$$
$$\Delta P = 150\ (1 - 0.3)^2\ /\ 0.3^3 \times (0.001\ Pa\ s)(9\ m)(6.11\ m/h)\ /\ (0.00238)^2 = 7.30 \times 10^3\ Pa$$

XIII.B.11. Gold Elution Sample Calculations

The chromatographic velocity is given by Equation III.D.4.1. When C_{Au} = 0.05 mM, q_m = 1.5 mmol/g, K =9.49 mM^{-1}, and b = 1.6, the chromatographic velocity is given by

$$v_c = v\ /\ (1 + \varphi \frac{d\overline{q}}{dC_{Au}})\ = v\ /\ (1 + \varphi\ (\ (b\ k^b\ q_m\ {C_{Au}}^{(b-1)})\ /\ (1\ +\ (k\ C_{Au})^b)^2\ )\ )$$
$$v_c = 20.37\ /\ (1 + 2.33\ (\ (1.6\ (9.49)^{1.6}\ 1.5\ (0.05)^{(1.6-1)})\ /\ (1\ +\ (9.49\ (0.05))^{1.6})^2\ )\ )$$
$$v_c = 0.971\ m/h$$

XIII.B.12. Gold Electrowinning Sample Calculations

Gold electrowinning calculations were done using the same method as in copper electrowinning.